MONTE CARLO STUDY OF THE TWO-DIMENSIONAL DIPOLAR ISING MODEL

ALLAN B. MacISAAC

MONTE CARLO STUDY OF THE TWO-DIMENSIONAL DIPOLAR ISING MODEL

By

©Allan B. MacIsaac

B. Sc. Hons., St. Francis Xavier University,

Antigonish, Nova Scotia, Canada

A THESIS SUBMITTED TO THE SCHOOL OF GRADUATE STUDIES IN PARTIAL FULFILLMENT OF THE REQUIREMENTS FOR THE DEGREE OF MASTERS OF SCIENCE

DEPARTMENT OF PHYSICS

MEMORIAL UNIVERSITY OF NEWFOUNDLAND

OCTOBER, 1992

ST. JOHN'S NEWFOUNDLAND

ISBN 0-315-82598-7

Table of Contents

List of Tables

List of Figures

Abstract

The two-dimensional Ising model with a dipolar and superexchange interaction will be examined. This model will be studied using Monte Carlo simulations. The results of this study will be discussed in two ways. First, the results will be analysed treating the system as a possible model for the rare earth ordering in the compounds $REBa_2Cu_4O_7$, where RE one of the Kramers rare earth ions. A comparison between the Néel temperature of a pure dipolar system and the experimental Néel temperature of these compounds will be done. As well, the results will be analysed in terms of what may be learned about dipolar systems in general. In particular, the Néel temperature and the static critical exponents will be discussed.

Chapter 1

Introduction

In this work we will be interested in examining the magnetic interactions between the rare earth ions in a class of superconductors based on the compound $YBa_2Cu_3O_{7-\delta}$ discovered by Maw-Kuen Wu and Ching-Wu Chu in 1987.[1] In the compounds of interest, the yttrium ions will be replaced with the rare earth Kramers ions from the lanthanide series, which may be found in the periodic table beginning with cerium (Ce) and ending with ytterbium (Yb). Interest in these compounds is very high, not simply due to the superconducting properties of the materials, but also because of the novel magnetic properties they possess. The coexistence of superconductivity and magnetic ordering make these compounds even more intriguing as they are ideal systems for the study of the interplay between superconductivity and magnetism in layered systems.

In this introduction we will look at some of the experimental work which has been done on many of the rare earth compounds. In particular we will look at neutron scattering and specific heat experiments, since these experiments yield information concerning the magnetic properties of the material under study. The interpretation of the information provided by neutron scattering and specific heat experiments, unfortunately, can be difficult and sometimes inconclusive. Therefore claims made in experimental papers must always be treated carefully, as one will see in the following discussion. From these experiments, we will develop a picture of the properties which a successful model of these compounds must reproduce. Chapter 2 discusses the fundamental theory behind Monte Carlo simulations. In chapter 3 we will discuss our implementation and study of our

model using Monte Carlo simulations. Chapter 4 will present the results of our investigation and a discussion of the success and applicability of our model. In chapter 5 we will summarise the results of our computer simulations, and discuss further work which will be carried out. Reports containing some of this work have appeared elsewhere.[2][3]

1.1 Experimental Survey

The first of the high temperature superconductors was $La_{2-x}Ba_xCuO_4$,discovered by K. Alex Müller and George Bednorz in 1986. Maw-Kuen Wu and Ching-Wu Chu began experimenting with the substitution of the lanthanum ions in $La_{2-x}Ba_xCuO_4$ with the rare earth element yttrium. They were able to create a compound which had a superconducting transition temperature above 77 Kelvin, the temperature of liquid nitrogen, making difficult to handle and expensive liquid helium unnecessary to achieve the superconducting temperature. The chemical composition of the resulting compound was determined by Robert M. Hazen *et al.* at the Geophysical Laboratory of the Carnegie Institution of Washington. [4] The chemical formula of this new superconductor is $YBa_2Cu_3O_{7-\delta}$, and figure 1.1 shows the positions of the various ions.

Note that the rare earth ion is located in the center cube of a quasi-perovskite structure. The rare earth ion has a copper-oxygen plane located directly above and below. It is thought that the existence of these planes is essential to the superconductivity of these compounds. In the rare earth sublattice, one finds that the a and b lattice vectors, both parallel to the copper-oxygen planes, are approximately equal and about three times smaller than the c lattice vector. Typically ones finds a and b to be approximately 4 Å and c equal to about 12 Å. Thus one will have an anisotropic system and, in particular, one has a layered system. Experiments discussed below will support this observation.

One notes that the oxygen content of $YBa_2Cu_3O_{7-\delta}$ is generally noted as $O_{7-\delta}$. The

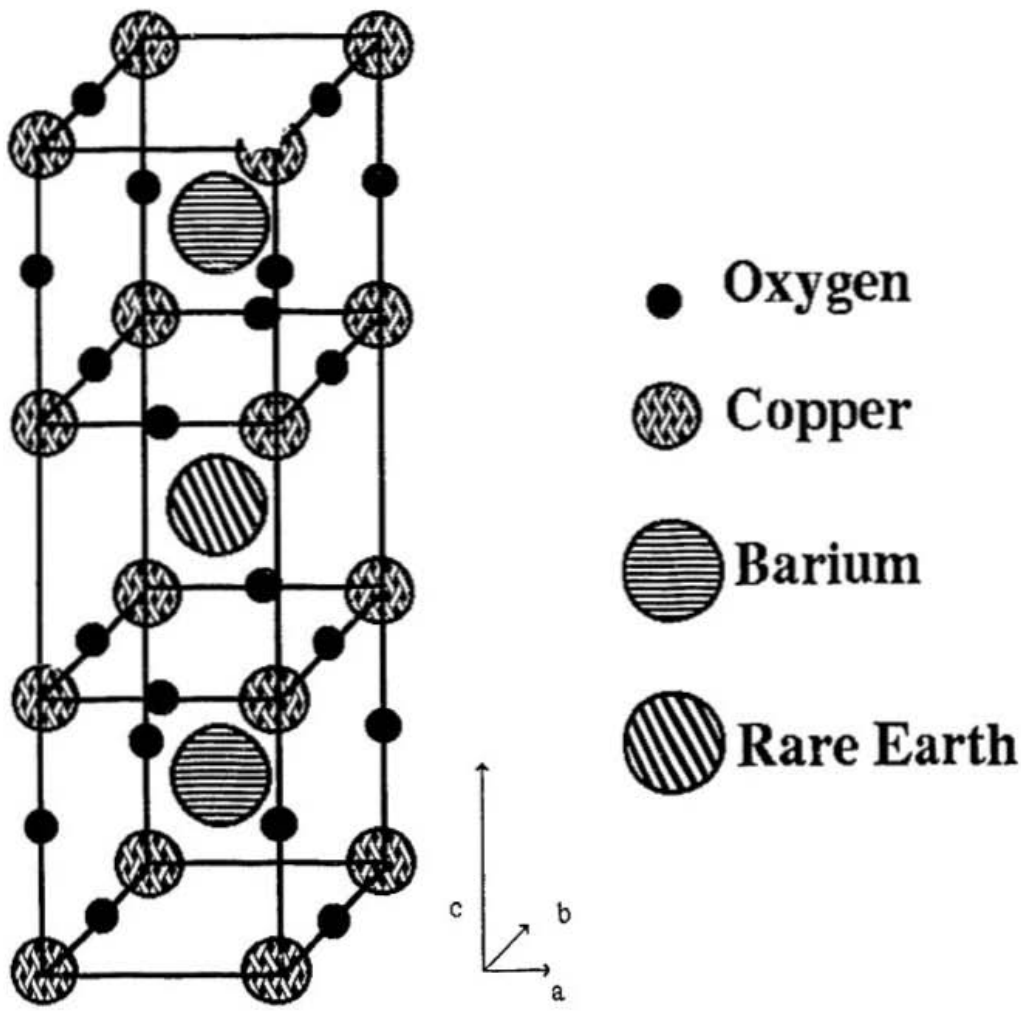

Figure 1.1: Chemical unit cell of $YBa_2Cu_3O_{7-\delta}$

oxygen deficiency, δ, is a critical parameter in determining the crystal structure and the superconducting properties. The fully oxygenated compound, $\delta = 0$, is a superconductor and forms an orthorombic phase. As δ increases there is a transition from the superconducting, orthorombic phase to a tetragonal, semi conducting phase. To illustrate we include an approximate phase diagram of $YBa_2Cu_3O_{7-\delta}$ in figure 1.2. We are not gen-

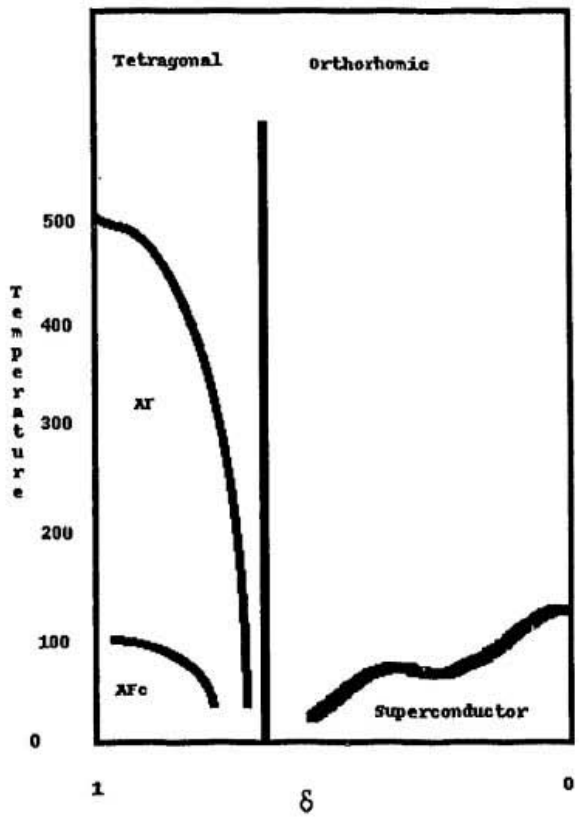

Figure 1.2: Phase diagram for $YBa_2Cu_3O_{7-\delta}$ as a function of oxygen concentration

erally interested in the variation of the crystal properties due to oxygen content at this point, but later in this work we will make use of this information. In all cases we will be referring to the fully or near fully oxygenated compound (compounds where $\delta \approx 0$)

unless otherwise stated.

In most known conventional superconductors a small percentage of magnetic impurities will either destroy the superconductivity or suppress T_c, the superconducting transition temperature. The compound $YBa_2Cu_3O_7$ has a superconducting transition temperature of about 90 K.[5] When the yttrium is replaced by certain magnetic rare earth ions from the lanthanide series, the superconducting transition temperature does not change significantly from 90 K. The exceptions are Ce, Pr, Pm, and Tb, which destroy the superconducting state at sufficient concentrations.[5] In certain compounds, where we have full substitution of the yttrium, there is also a transition, at low temperature, to a phase where the rare earth ions are ordered. Thus for some rare earth ions one has a magnetically ordered phase coexisting with the superconducting state. This is similar to the behaviour found in the rare earth ternary compounds such as $(RE)Rh_4B_4$, $(RE)Mo_6Se_8$, and $(RE)Mo_6S_8$.[6] We will be interested in understanding the magnetic ordering in the compounds where yttrium has been replaced with the Kramers ions, Nd^{3+}, Sm^{3+}, Gd^{3+}, Dy^{3+}, Er^{3+}.

The first neutron scattering experiments carried out on $REBa_2Cu_3O_{7-\delta}$ compounds were done on $ErBa_2Cu_3O_{7-\delta}$. There has been controversy and contradiction in the analysis of the results ever since. The initial work of Shelton *et al.* [7], and Lynn *et al.* [8] established that there is a transition from a magnetically disordered to a magnetically ordered state around 0.5 Kelvin. At this transition, both Shelton *et al.* and Lynn *et al.* found that the magnetic moments of the rare earth ions become ordered within each of the planes determined by the a and b lattice vectors, (the a-b plane). Within the a-b plane the spins are arranged as in figure 1.3a (ferromagnetically ordered in the b direction, and anti-ferromagnetically ordered in the a direction) with the spins orientated so as to lie along the b axis. We will refer to this as AF ordering. Both Shelton *et al.* and Lynn *et al.* found no ordering in the c direction. While their results showing

two-dimensional behaviour were not completely unexpected due to the layered nature of these compounds, the long range nature of the dipole interaction, thought to be important in this temperature range, meant the result was not obvious. Because $c \approx 3a$ and a≈b, the dipolar interaction between layers will be much smaller than within a layer. Both Lynn *et al.* and Shelton *et al.* described the $ErBa_2Cu_3O_{7-\delta}$'s rare earth sub-system as two-dimensional.

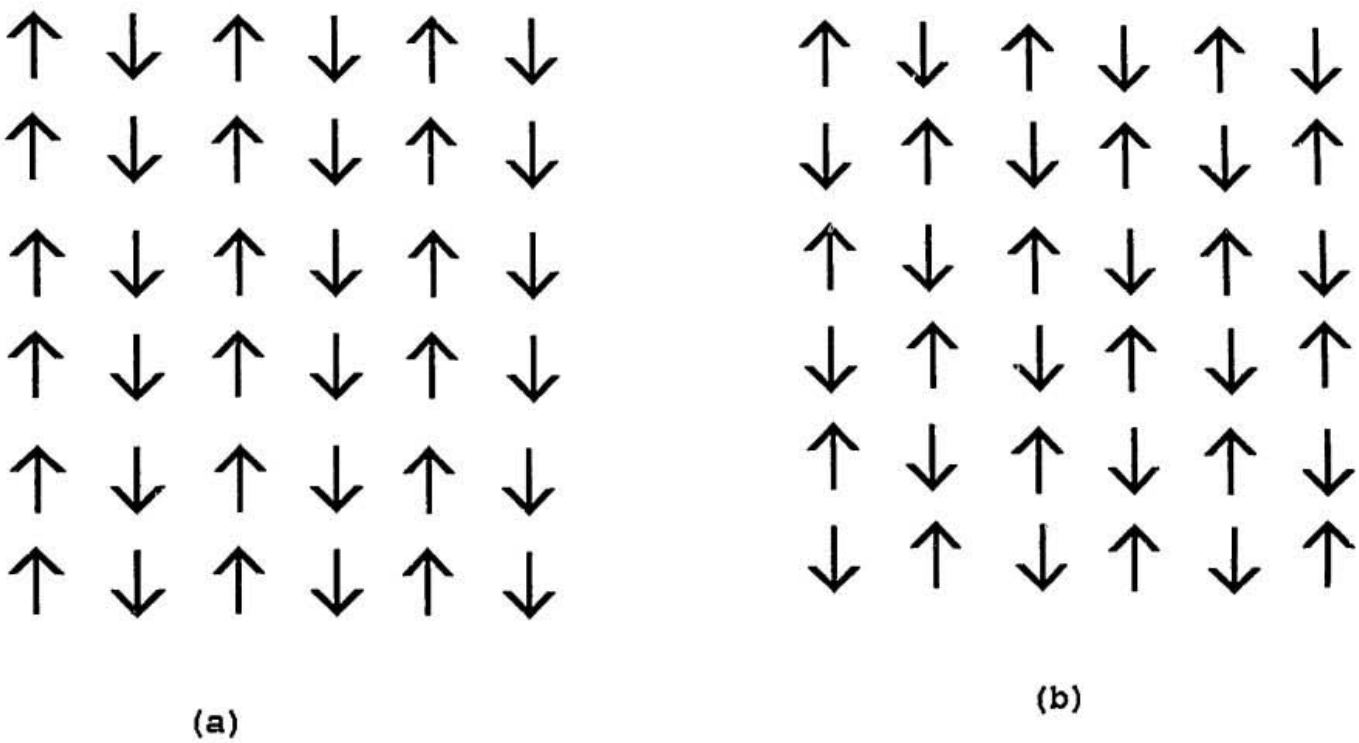

Figure 1.3: The spin arrangement for (a) AF and (b) AA phases

Later work was done by McK. Paul *et al.* [9] on a composite crystal composed of five smaller crystals. Each crystal had dimensions of about $3 \times 3 \times 0.2mm^3$. McK. Paul *et al.* found the same transition temperature and a-b plane ordering as Lynn *et al.* and Shelton *et al.* McK. Paul *et al.* reported that they did not find two-dimensional

ordering, but found that the ordering was three dimensional in nature, starting from the transition temperature and for all lower temperatures. McK. Paul *et al.* suggested that perhaps the powder samples used by Lynn *et al.* and Shelton *et al.* had caused their data to show two-dimensional character. In another study Chattopadhyay *et al.* [10] used a composite crystal, formed of two single crystals. Chattopadhyay *et al.* stated that they had clearly established the transition as three dimensional from 500 mK down. They then state that the temperature variation of the sublattice magnetisation shows "typical two-dimensional behaviour." Both McK. Paul and Chattopadhyay *et al.* had difficulty establishing the exact nature of the ordering in the c direction, and reasoned that the ordering was dependent upon the oxygen content of a crystal. Thus with their composite crystal, it was possible that they had two different types of order due to two crystals with different oxygen contents. Further work by Lynn *et al.* [11] found that at a temperature of 140 mK one could detect complicated three dimensional ordering, implying a crossover from two- to three-dimensional order somewhere below 500 mK.

In 1989 Lynn *et al.* [12] published further experiments on a single, high quality crystal of $ErBa_2Cu_3O_{7-\delta}$ weighting 31mg. Lynn *et al.* reported that, again, they found that at $T_n = 618mK$ there was ordering, which they described as having two-dimensional characteristics above T_n, with a change to three dimensional character at lower temperatures. They were unable to determine whether the ordering in the c direction was ferromagnetic or anti-ferromagnetic. By two-dimensional Lynn *et al.* are referring to a lack of dependence on K_z in the neutron scattering intensity just above T_n. The order parameter was fit well by to the solution of the two-dimensional, S=1/2 Ising model. This result is supported by numerous reports on the specific heat of $ErBa_2Cu_3O_{7-\delta}$ at low temperatures, [13][14][15] [16] but one must be careful because there is still disagreement between experiments.

In all of the above papers concerning the specific heat of $ErBa_2Cu_3O_{7-\delta}$, it is confirmed

that there is a transition at approximately 600 mK which is fitted very well by the two-dimensional Ising Model. Further, the molar entropy at 6K is Rln(2), characteristic of a doublet ground state, instead of a 16-fold degeneracy as given by Hund's rule.[17] Most likely the reduction in degeneracy is the result of crystalline electric fields (C.E.F).[16] Thus the specific heat measurements agree with Lynn's neutron scattering results, that $ErBa_2Cu_3O_{7-\delta}$ appears to order in a manner characteristic of a two-dimensional, S=1/2 system, similar to the Ising Model, with a transition temperature of 618 mK. [13][14][15] [16]

Neutron scattering experiments on $DyBa_2Cu_3O_{7-\delta}$ by Goldman *et al.* [18] found a transition from the disordered to ordered state at 1.0 K ± 0.05 K. Goldman *et al.* reported three dimensional ordering which was anti-ferromagnetic in all three lattice directions. Further, Goldman *et al.* were able to determine that the moment on the Dy ions was oriented to point along the c crystal axis. This spin arrangement is shown in figure 1.3b and is referred to as (AA) ordering. Goldman *et al.* did not speculate on whether the temperature dependence of the magnetic order parameter was characteristic of either two- or three-dimensional behaviour. The results of Goldman *et al.* were confirmed by Fischer *et al.* [19], with a correction to the Néel temperature. Fischer found that $DyBa_2Cu_3O_{7-\delta}$ ordered at 900 mK rather than 1000 mK. Again, while the neutron scattering data clearly showed three dimensional ordering, Fischer *et al.* did not speculate on whether temperature dependence of the order parameter was characteristic of two- or three-dimensional ordering. Specific heat data showed the transitions from disordered to ordered at 900 mK, but the data fit the two-dimensional S=1/2 Ising result very well. The molar entropy at 6 K is Rln(2) implying that the 16-fold degeneracy of the Dy ion has been reduced to a doublet. This reduction in the degeneracy of the ground state is most likely due to C.E.F.[13][15] Again, work done using a single crystal by Clinton and Lynn [20] showed that there is scattering which appears to be two-dimensional in

nature in $DyBa_2Cu_3O_{7-\delta}$ as was found for $ErBa_2Cu_3O_{7-\delta}$. They found that the ordering in the a-b plane was (AA), consistent with a dipolar interaction if the spins are forced, by virtue of C.E.F., to align perpendicular to the plane.

Considerable experimental work, both neutron scattering and specific heat measurements are available for $GdBa_2Cu_3O_{7-\delta}$. The Gd compounds are different, because according to Hund's rule $L = 0$, and therefore $J = S = \frac{7}{2}$. This means that to lowest order the energy levels and degeneracy of Gd are not affected by C.E.F. and the ground state will retain the full $2J + 1 = 8$ fold degeneracy.[17] This is confirmed by the $R\ln(8)$ value for the molar entropy at 6 K. [16][21][22] $GdBa_2Cu_3O_{7-\delta}$ has a transition temperature of 2.23 K, more than twice that of $ErBa_2Cu_3O_{7-\delta}$ and $DyBa_2Cu_3O_{7-\delta}$. Neutron scattering showed the ordering to be three dimensional with no initial scattering of two-dimensional character. This ordering was antiferromagnetic in all three lattice directions, with the moments aligned along the c axis.[23] This is not the ground state of a pure dipolar system [24] [25] and the lack of significant crystal fields does not allow one to attribute the existence of an easy axis along the c axis to the effect of C.E.F.. We will discuss this later.

Measurements of the critical exponent β, for $GdBa_2Cu_3O_{7-\delta}$ give $\beta = 0.16 \pm 0.01$[26] and $\beta = 0.15$[23] for $\delta \approx 0$ and $\beta = 0.11$[26] for $\delta > 0.5$. The critical exponent β is defined in terms of the temperature dependence of the sublattice magnetisation, M, as T approaches T_c from below: [27]

$$M \sim \left(\frac{T_c - T}{T_c}\right)^{\beta} \text{ in the limit } (T - T_c) \to 0^- \tag{1.1}$$

For the two-dimensional Ising model $\beta = 0.125$, while in three dimensions $\beta \approx \frac{1}{3}$ for both the Ising and Heisenberg models, although it is well known that β is not a rational number and has a different value in the two models. Thus the temperature dependence of the sublattice magnetisation is characteristic of a two-dimensional Ising system rather than

a three dimensional system. As well, although the Gd ion retains its 8 fold degenerate ground state, a naive comparison of the experimental specific heat to the two-dimensional, S=1/2 Ising model also shows very good agreement. [28]

Studies on the other Kramers ions are not comprehensive or in some cases not available. Specific heat studies yield a transition temperature of 0.52K for $NdBa_2Cu_3O_{7-\delta}$, and 0.61K for $SmBa_2Cu_3O_{7-\delta}$. [29] In both compounds the specific heat may be fit to a two-dimensional Ising model if a strongly anisotropic exchange is assumed. Neutron scattering results are not yet available.

If we limit ourselves to a discussion of only the Er and Dy compounds, we can gain more insight concerning the interactions involved by looking at the related compounds, $ErBa_2Cu_4O_8$ and $DyBa_2Cu_4O_8$. These compounds have the same basic building blocks as the $REBa_2Cu_3O_{7-\delta}$ compounds but with an extra copper-oxygen layer and each successive layer displaced a half lattice length along the b axis. Thus in these compounds the rare earth ions are separated by a larger c lattice vector than in the 123 compounds. There will be other differences between these compounds but we naively disregard these differences for now. Both compounds show neutron scattering results which, near the ordering transition, have two-dimensional characteristics. The Néel temperatures are 0.49 K and 0.9 K for Er and Dy respectively.[30] In $ErBa_2Cu_4O_8$ one finds that as one passes through the transition three dimensional ordering begins to develop. In $DyBa_2Cu_4O_8$ the neutron scattering showed no three dimensional behaviour at any temperature. Of further significance is that the Néel temperature for Er is lower in the 248 compound than it is in the 123 compound, implying the reduction of some interplanar interaction due to the increased c lattice vector. The Néel temperatures for the Dy compounds are identical. This has been accounted for in terms of a geometric cancellation of the interplanar interactions due to the symmetry introduced by the displacement of successive layers along the b axis. [30] In fact $DyBa_2Cu_4O_8$ is referred to by one group of experimentalists

as the best example of a two-dimensional magnetic system found in nature.[30]

All samples which have been referred to in the studies above are, of course, three dimensional, having a length, width, and height. Regardless of how weak the interplaner interaction is, as long as there is some interplaner interaction, the system will order in all three dimensions. To refer to a system as having two-dimensional characteristics implies that, just above the critical temperature, there is critical scattering which reaches its maximum value along reciprocal lattice rods, instead of at reciprocal lattice points. In a real two-dimensional system the thermally averaged pair correlation function $< S_0^{\alpha}(0) S_{\mathbf{r}}^{\beta}(t) >$, t being time, and $\mathbf{r}$ being the displacement from some arbitrary origin, vanishes if the z component of $\mathbf{r}$ differs from zero, both above and below the transition temperature. In neutron scattering the differential cross section is related to the Fourier transform of the the pair correlation function by

$$\frac{d^2\sigma}{d\Omega' dE'} \propto \sum_{\alpha\beta} \left\{ (\delta_{\alpha\beta} - \frac{K_\alpha K_\beta}{K^2}) \frac{1}{2\pi} \int_{-\infty}^{\infty} dt \exp(-i\omega t) \sum_{\mathbf{r}} < S_0^{\alpha}(0) S_{\mathbf{r}}^{\beta}(t) > \exp(i\mathbf{K}\cdot\mathbf{r}) \right\}, \tag{1.2}$$

where α and β denote components of $\mathbf{K}$, which is the difference in the incoming neutrons wave vector $\mathbf{k}$ and the scattered wave vector $\mathbf{k}'$ ($\mathbf{K} = \mathbf{k} - \mathbf{k}'$). In a two-dimensional system the scattering cross section will be independant of the z component of $\mathbf{K}$ and in a scattering experiment one will get maximum scattering along rods instead of at points as one would for three dimensional ordering. If one were to scan the scattering intensity along the $(1, 0, \ell)$ line in the reciprocal lattice just above T_n one would find non-zero intensity at all ℓ. Below T_n one may find the three dimensional Bragg peaks at (1,0,0), (1,0,1) etc. superimposed on the two-dimensional critical scattering. It is the two-dimensional critical scattering which is used to define a two-dimensional system. For a more detailed discussion one is referred to an excellent discussion of critical neutron scattering by Jens Als-Nielsen in the fifth volume of the series *Phase Transitions and*

Critical Phenomenon edited by Domb and Green [31] and a short discussion specific to these superconducting compounds by Zhang *et al.* [30]

We have been attributing the S=1/2 nature of all the Kramers ions, with the exception of Gd, to the C.E.F. A detailed calculation of the crystalline electric fields in these compounds is necessary to establish the existence and the magnetic character of the doublet ground state.

1.2 Exchange interactions

An important goal of this thesis is to estimate the relative strengths of the various interactions which might be responsible for the observed ordering at low temperature. While a major conjecture of this paper is that the dipole-dipole interaction is a significant interaction, we also study the inclusion of an exchange interaction. There are many different types of exchange interaction, all of which are the result of electronic charge density overlap. The distinction between the different types of exchange interaction is the manner in which this overlap occurs or how the interaction is mediated. In direct exchange two magnetic ions interact because their charge distributions overlap. In superexchange the charge distributions of two magnetic ions both overlap with some intermediate non magnetic ion. Thus a superexchange interaction is mediated by a non-magnetic ion. In indirect exchange there is no direct overlap of the charge distributions of ions, but instead there is an exchange interaction mediated by the conduction electrons.

1.3 Synopsis

The important experimental results may be summarised as follows. The degeneracy of the ground state in erbium and dysprosium compounds has been reduced to a doublet, most likely due to C.E.F. A S=1/2 model should be appropriate, since it provides the

proper degeneracy of the ground state. For gadolinium a S=7/2 model would be more appropriate. In the critical region the neutron scattering has spin fluctuations which characterise the systems as two-dimensional. The specific heat in all systems may be fit reasonably by the S=1/2, two-dimensional Ising model. The transition temperatures for $REBa_2Cu_3O_{7-\delta}$ with RE = Gd, Er, and Dy are of the order of 1 K. In this temperature range the dipolar interaction will be significant. The observed ordered states are consistent with the orientation of the rare ion's spin and a dipolar interaction, with the exception of Gd. The dipolar coupling between layers has been shown to be very weak, compared to the intraplaner interaction in this class of compounds.[24] The superconducting state is not affected by the substitution of the magnetic rare earths for the non-magnetic yttrium. As well, experiments on both the superconducting, orthorombic and the semi-conducting, tetragonal phases of $REBa_2Cu_3O_{7-\delta}$ with RE = Gd, Er, and Dy, show no change in the Néel temperature, which implies that the conduction electrons are not involved in the interaction.[15][26] [28] [32] [33] [34] This suggests that any indirect exchange interaction will be weak. The localised nature of the 4f shell in the rare earth ion makes a direct exchange unlikely. Therefore if there is an interaction besides the dipolar it will be most likely be a superexchange interaction.

By using the available experimental information, we have been able to determine that a spin 1/2 Ising model with a dipole-dipole and a possible superexchange interaction would be a good choice as an initial model for $REBa_2Cu_3O_{7-\delta}$, where the RE is one of the Kramers ions. While we do not expect that a simple model, such as we are proposing, will be sufficient to explain all the magnetic phenomena exhibited by these compounds, it is important to have a starting point from which to develop a basic understanding of the phenomena. Indeed, if there are features of the experiments which are not well explained in terms of this proposed model, then the comparison provides guidance in determining a more realistic model. In chapter 3 we will discuss the implementation of our model;

readers who are familiar with Monte Carlo simulation may wish to skip chapter 2 and proceed directly to this discussion.

Chapter 2

Monte Carlo Simulations

2.1 Introduction

Since much of the data presented in the thesis is derived from Monte Carlo simulations, it is important to offer the reader a basic understanding of the theory behind such simulations. It is also important to discuss the actual implementation of such a simulation. In doing so we are able to show the power, versatility, and fundamental simplicity of the technique.

2.2 Theory of Monte Carlo Simulations

The Monte Carlo method involves the use of a computer simulation to generate a collection of states for a model system. In equilibrium studies these states may be generated with a probability proportional to their thermodynamic probability, and from this collection thermodynamic quantities may be calculated. As well, because each state is generated sequentially according to some model Hamiltonian, it is also possible to to use the Monte Carlo method to study relaxation or transport phenomena. [35] The uses of the Monte Carlo method are too numerous to mention all of them here, but the interested reader may refer to book *Monte Carlo method in statistical physics* by K. Binder [35] for more information. We will use the Monte Carlo method to evaluate equilibrium properties for a model magnetic system.

In general, the partition function of a system in the canonical ensemble is

$$\mathbf{Z} = \int d\{x\} \exp\left[\frac{-\mathcal{H}(\{x\})}{k_B T}\right], \tag{2.1}$$

and the thermodynamic average of a macroscopic observable $A(\{x\})$ is

$$\langle \mathbf{A}(\{x\}) \rangle = \frac{\int d\{x\} \mathbf{A}(\{x\}) \exp\left[\frac{-\mathcal{H}(\{x\})}{k_B T}\right]}{\int d\{x\} \exp\left[\frac{-\mathcal{H}(\{x\})}{k_B T}\right]}. \tag{2.2}$$

The set $\{x\}$ is a set of variables describing a configuration of a system or its position in phase space and $\mathcal{H}$ is the Hamiltonian of the system. An example of a simple $\{x\}$ might be the positions and momenta of a number of electrons interacting via Coulomb forces. These integrals are typically over a volume in a very large dimensional phase space. It is possible that $\{x\}$ may consist of discrete variables, in which case the integrals of equations 2.1 and 2.2 are converted to summations over the discrete phase space.

As an example let us look at the ideal gas of N particles without using any simplifications due to symmetry. In this model $d(\{x\})$ is a 6N-component vector; three components for each momentum and three components for each position of the N particles. Therefore we have an integration over a 6N dimensional phase space. Since statistical mechanics is applicable to systems with a large number of particles, we would have an integration in a phase space of large dimensionality. In the case of the perfect gas it is possible to do these integrations analytically. In most realistic cases, where there is some interaction between particles, it is not possible to do these integrations analytically. We must somehow approximate the integrations, even numerically, if necessary.

To integrate numerically over such a large dimensional space would be very time consuming if we were to attempt such an evaluation in the normal manner. By normal manner, I am referring to a process where we would divide the phase space into small multi-dimensional cubes (hypercubes) of volume $(\Delta x)^N$, N being the number of degrees of freedom, and then to approximate the integration by the sum over the value of the

integrand in the center of these small cubes multiplied by the volume of a hypercube. The large dimensionality of the phase space makes this an impractical method, since the number of small multi-dimensional cubes would be extremely large. A widely used method to improve the efficiency of the numerical integration is to randomly choose a set of points, $[\{x\}_\nu]$, where ν labels each chosen set of variables. We still divide phase space into small hypercubes, but we do not include all hypercubes in the sum approximating the integral. Instead, we include only some small percentage of the hypercubes or points in phase space in our evaluation of the integral. The points in phase space that we include are chosen randomly. This random choice of points is in fact a form of the Monte Carlo method, but not a very efficient one. The main problem with choosing random points in phase space, in our attempt to numerically evaluate integrals of the form 2.1 and 2.2, is that the integrand of these integrals will have variations of many orders of magnitude in the regions of greatest interest, at temperatures near $\langle \mathcal{H} \rangle \approx N k_B T$, so we would spend a great deal of our time adding insignificant contributions to the integration. Therefore we want to choose the points from our multi-dimensional phase space in some appropriate fashion, such that the "important" regions are represented more often in our choice of points to include in the numerical integration. By important we mean those regions of phase space that will contribute significantly to the integration. To give a trivial example, if we wish to calculate

$$A = \int_{-100}^{+100} \theta(x - 10)\theta(x + 10)dx \tag{2.3}$$

which is the integral of a square pulse as shown in figure 2.1. If we were to select x (here the phase space is one dimensional) randomly from -100 to $+100$ then the majority of the time we would be adding zero to our value of A. If instead we somehow knew that the important points are those where x is between -10 and $+10$ and chose random points only between -10 and $+10$, our evaluation of the integral would be much more efficient.

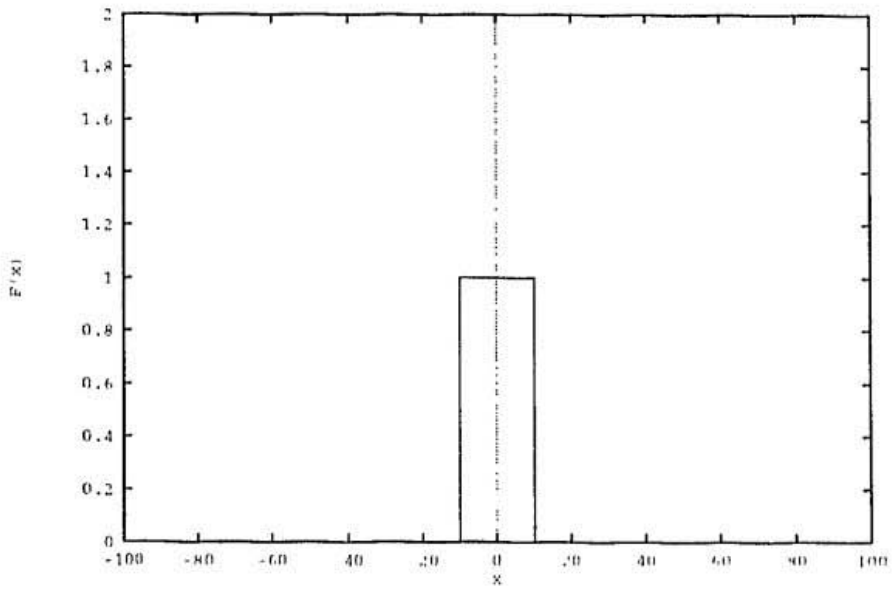

Figure 2.1: Square pulse

What we have described above is a simple case of the concept of "importance sampling", which was developed by Metropolis [36]. If we choose $\{x\}_\nu$ according to a probability $P(\{x\}_\nu)$, then we may rewrite equation 2.2 as

$$\langle \mathbf{A} \rangle \approx \overline{\mathbf{A}} = \frac{\sum_{\nu=1}^{M} \mathbf{A}(\{x\}_\nu) P^{-1}(\{x\}_\nu) e^{\frac{-\mathcal{H}(\{x\}_\nu)}{k_B T}}}{\sum_{\nu=1}^{M} P^{-1}(\{x\}_\nu) e^{\frac{-\mathcal{H}(\{x\}_\nu)}{k_B T}}}, \tag{2.4}$$

M being the number of points we have sampled in phase space. By $P(\{x\}_\nu)$ we mean the probability of chosing $\{x\}_\nu$ as a configuration to include in our evaluation of the partition function. If we are able to chose $P(\{x\}_\nu)$ in an enlightened manner, we should sample the "important" regions more frequently and hence should have a much more efficient evaluation of $\langle \mathbf{A} \rangle$. A natural and straightforward choice of $P(\{x\}_\nu)$ would be the Boltzman probabilities for a classical system in equilibrium, that is, let

$$P(\{x\}_\nu) = P_{eq}(\{x\}_\nu) \propto e^{\frac{-\mathcal{H}(\{x\}_\nu)}{k_B T}}. \tag{2.5}$$

We then have for the average value of a thermodynamic observable **A**,

$$\overline{\mathbf{A}} = \frac{1}{M} \sum_{\nu=1}^{M} \mathbf{A}(\{x\}_\nu). \tag{2.6}$$

In most cases we do not know $P_{eq}(\{x\}_\nu)$ exactly, since we lack the constant of proportionality in equation 2.5. Calculating this constant is equivalent to evaluating the partition function, and hence is not practical. We can, however, construct a random walk through our phase space, such that

$$P(\{x\}_i, \{x\}_f, t) \rightarrow P_{eq}(\{x\}_f) \ as \ t \rightarrow \infty. \tag{2.7}$$

The probability $P(\{x\}_i, \{x\}_f, t)$ in equation 2.7 is the probability of finding the system in state $\{x\}_f$ after t steps in the random walk, starting in initial state $\{x\}_i$. If t is large enough that equation 2.7 is valid then we may use the final states of a large number of random walks as our ensemble to evaluate equation 2.6. In this case we would associate the M in equation 2.6 with the number of walks in our ensemble. We note at this point that instead of the final state of a large number of random walks, one may equivalently use an ensemble composed of a suitably chosen subset of the final states of a single random walk, if the collection of states in the random walks is ergodic. Therefore we will require that our method of generating the random walks yield an ergodic collection of walks. What is meant by "suitably chosen" will be discussed below.

The random walks are defined in terms of a Markov process, which in turn is defined in terms of a transition probability from one state to another or from one point in phase space to another. We name this transition probability as $W(\{x\}_\nu \rightarrow \{x\}_{\nu'})$, which is the probability of moving, in phase space, from the point $\{x\}_\nu$ to the point $\{x\}_{\nu'}$. In other words, it is the probability of changing from a configuration specified by the variables $\{x\}_\nu$ to a configuration specified by the variables $\{x\}_{\nu'}$. To insure equation 2.7 is satisfied, it is sufficient to demand that W satisfy the condition of detailed balance,

which in mathematical terms is expressed in equation 2.8:

$$P_{eq}(\{x\}_\nu)W(\{x\}_\nu \rightarrow \{x\}_{\nu'}) = P_{eq}(\{x\}_{\nu'})W(\{x\}_{\nu'} \rightarrow \{x\}_\nu). \tag{2.8}$$

The condition of detailed balance states that the probability of the system being in state $\{x\}_\nu$ and then moving to state $\{x\}_{\nu'}$ is the same as being in state $\{x\}_{\nu'}$ and making a transition to state $\{x\}_\nu$. To show that detailed balance, equation 2.8, is sufficient to ensure that equation 2.7 is satisfied, we will replicate a simple and physically intuitive argument of Binder.[35] We first imagine that we have a large collection of Markov processes, so we are looking at many systems each at some point in phase space. Suppose that we have N_r systems at point $\{x\}_r$ and N_s systems at point $\{x\}_s$ at some particular time, and we know that $\mathcal{H}(\{x\}_r) < \mathcal{H}(\{x\}_s)$. The probability of moving from state $\{x\}_r$ to state $\{x\}_s$ if we are moving in a completely random fashion is simply 1 over the volume of phase space. Denoting this probability by W_{rs}, we know that since everything is random $W_{rs} = W_{sr}$. Of course these probabilities do not satisfy equation 2.8. But having defined W_{rs} and W_{sr}, we can easily find a set of $W(\{x\}_r \rightarrow \{x\}_s)$ and $W(\{x\}_s \rightarrow \{x\}_r)$ which does satisfy equation 2.8. In particular we have

$$\begin{aligned} W(\{x\}_r \rightarrow \{x\}_s) &= W_{rs}\exp^{\frac{-\Delta H}{k_B T}}, \\ &= W_{rs}\exp^{\frac{-[H(\{x\}_s)-H(\{x\}_r)]}{k_B T}}, \end{aligned} \tag{2.9}$$

and

$$W(\{x\}_s \rightarrow \{x\}_r) = W_{sr} = W_{rs}. \tag{2.10}$$

This set of transition probabilities does satisfy equation 2.8 and it is this set we would use in a simulation.

We can now find $N_{r\rightarrow s}$, the total number of transitions from state $\{x\}_r$ to state $\{x\}_s$, as well as $N_{s\rightarrow r}$. The former is given by

$$N_{r\rightarrow s} = N_r W(\{x\}_r \rightarrow \{x\}_s)$$

$$= N_r W_{rs} \exp^{\frac{-[\mathcal{H}(\{x\}_s)-\mathcal{H}(\{x\}_r)]}{k_B T}}. \tag{2.11}$$

and the latter by

$$\begin{aligned} N_{s\to r} &= N_s W(\{x\}_s \to \{x\}_r) \\ &= N_s W_{rs}. \end{aligned} \tag{2.12}$$

The net number of transitions, $\delta N_{r\to s}$, is

$$\begin{aligned} \delta N_{r\to s} &= N_{r\to s} - N_{s\to r}, \\ &= N_r W_{rs} \left[\frac{\exp(\frac{-\mathcal{H}(\{x\}_s)}{k_B T})}{\exp(\frac{-\mathcal{H}(\{x\}_r)}{k_B T})} - \frac{N_s}{N_r} \right], \qquad (2.13) \\ &= N_r W_{rs} \left[\frac{P_{eq}(\{x\}_s)}{P_{eq}(\{x\}_r)} - \frac{P(\{x\}_s)}{P(\{x\}_r)} \right]. \qquad (2.14) \end{aligned}$$

We see from equation 2.13 that if N_s/N_r is less than $\exp^{\frac{-\delta\mathcal{H}}{k_B T}}$ then $\delta N_{r\to s} > 0$ and N_s/N_r increases, on the other hand, if N_s/N_r is larger than $\exp^{\frac{-\delta\mathcal{H}}{k_B T}}$ then $\delta N_{r\to s} < 0$ and N_s/N_r decreases. As we move further along our Markov processes a steady state is reached where $N_s/N_r = \exp^{\frac{-\delta\mathcal{H}}{k_B T}}$, which is precisely equation 2.7. Finally instead of looking at many Markov chains, we may equally consider the parts of a single long chain, and our argument and result will be the same. It is important to note that detailed balance does not restrict our choice of $W(\{x\}_\nu \to \{x\}_{\nu'})$ to a single function, but rather it limits acceptable functions. Two very widely used choices for $W(\{x\}_{\nu'} \to \{x\}_\nu)$ are

$$W(\{x\}_{\nu'} \to \{x\}_\nu) = \frac{\exp^{\frac{-\delta\mathcal{H}}{k_B T}}}{1 + \exp^{\frac{-\delta\mathcal{H}}{k_B T}}}, \tag{2.15}$$

and

$$\begin{aligned} W(\{x\}_{\nu'} \to \{x\}_\nu) &= \exp^{\frac{-\delta\mathcal{H}}{k_B T}} \quad \text{if } \delta\mathcal{H} > 0 \\ &= 1 \qquad\quad \text{if } \delta\mathcal{H} < 0\,. \end{aligned} \tag{2.16}$$

In all simulations in this thesis we have made use of equation 2.16, as it equilibrates a system very efficiently.[35] [36]

2.3 A Simulation

Let us begin to develop our understanding of a Monte Carlo simulation by looking at how a simulation might proceed for a general example. Let us assume, for this discussion, that we have a spin model, where we have N spins which may assume either of two states, $S = 1$ or $S = -1$. The Hamiltonian for the system will be a function of the state of each of the spins, $\mathcal{H}(\{S\})$. The degrees of freedom are the states of each of the spins. We now describe how we would form our Markov chains of configurations. This description is augmented by the flow chart in figure 2.2.

To begin a simulation specify a temperature, any parameters in the Hamiltonian, and an initial state $\{S\}_0$. We then begin a Markov process to move through phase space. To do this we choose a random spin, which we label k. We next calculate the change in energy $\delta\mathcal{H}$, if we change S_k to $-S_k$. From this change in energy we calculate $W(S_k \rightarrow -S_k)$, using equation 2.16. We then generate a random number Z, $0 < Z < 1$. This use of random numbers is the reason for the name, Monte Carlo simulation. We then compare Z to $W(S_k \rightarrow -S_k)$, and if $Z < W(S_k \rightarrow -S_k)$ we change S_k to $-S_k$. If $Z > W(S_k \rightarrow -S_k)$ we do not change S_k. In both cases we have a new configuration (it may be the same as the previous configuration, but we must consider it a new configuration). This process constitutes one Monte Carlo step and we define time in terms of Monte Carlo steps per degree of freedom. For example, in a spin system with N spins, one Monte Carlo time unit is equivalent to N Monte Carlo steps. For most purposes there is no relation between Monte Carlo time and real time. The introduction of a Monte Carlo time is generally for conceptual purposes and it defines position along a Markov chain.

Note that we have only changed one degree of freedom -the variable S_k- and therefore this configuration and the initial configuration are highly correlated. The system may not be in equilibrium if this initial configuration is far from equilibrium. Before we begin

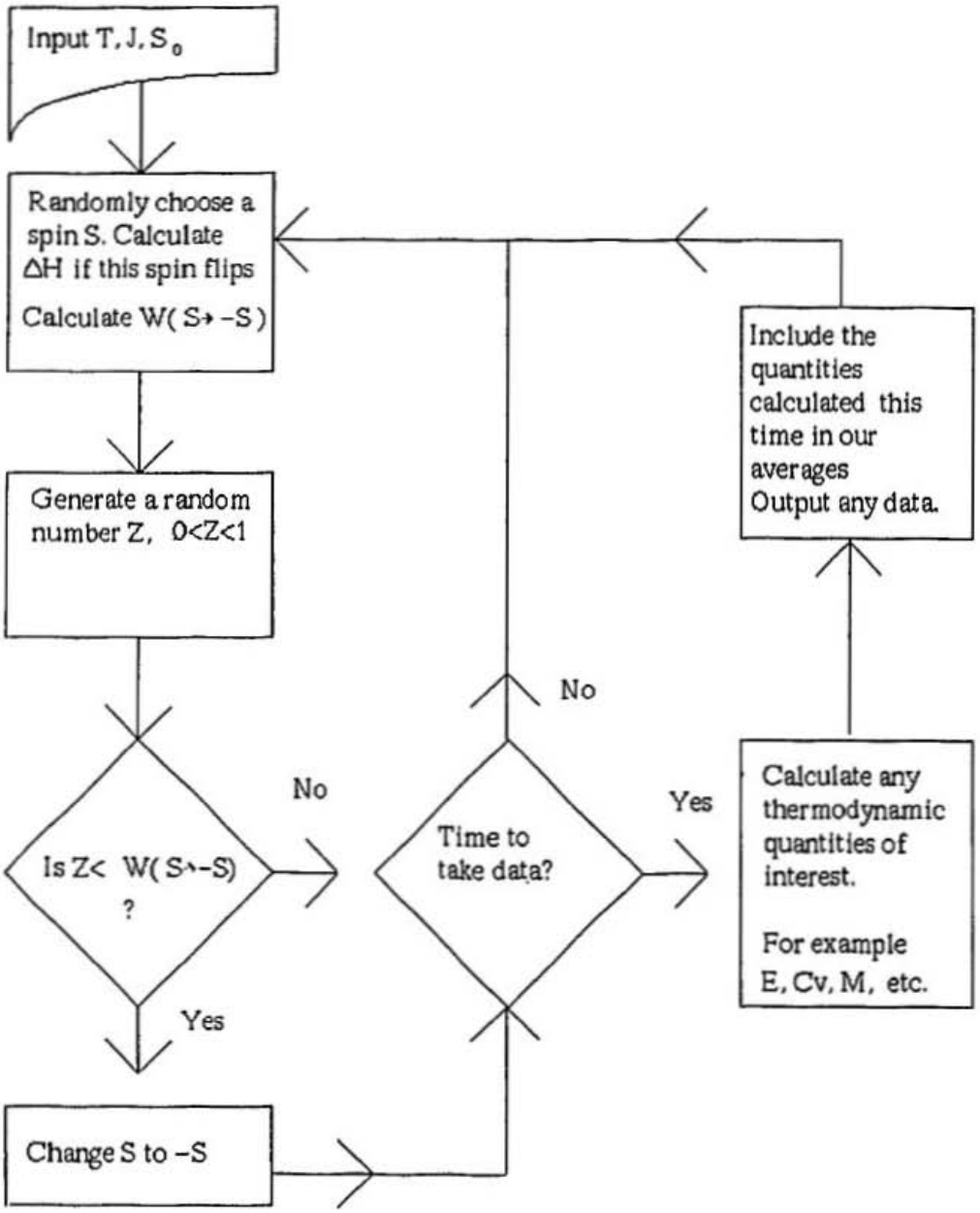
Input T, J, S_0
Randomly choose a spin S. Calculate ΔH if this spin flips
Calculate W(S→ -S)
Generate a random number Z, 0<Z<1
Is Z< W(S→-S) ?
No
Yes
Change S to -S
Time to take data?
No
Yes
Include the quantities calculated this time in our averages
Output any data.
Calculate any thermodynamic quantities of interest.
For example E, Cv, M, etc.

collecting data we must make sure that we have allowed the system to reach thermodynamic equilibrium and that our choice of an initial configuration is not influencing our Monte Carlo averages: this is assured if equation 2.7 is valid. To do this we must ignore, in our data analysis, some initial number of configurations corresponding to, $n_0 \times N$ Monte Carlo steps or n_0 time steps. The exact number of configurations we must ignore is generally not known before a simulation, and only by analysis of data after a simulation can we determine if have eliminated a sufficient number of configurations. To determine if we have chosen n_0 sufficiently large we may compare n_0 to the largest relaxation time characteristic of the approach to equilibrium. If we assume that the largest relaxation time is the order parameter relaxation time, $\tau_\mu^{\Delta T}$, then the condition for n_0 becomes $n_0 \gg \tau_\mu^{\Delta T}$. The temperature difference, $\Delta T = T - T'$, is the difference between the the temperature of the simulation, T, and the temperature defined by the initial configuration T'. By the temperature of the initial configuration we mean that temperature for which the configuration is an equilibrium configuration. For example, if the initial system is the ground state then its temperature would be $T' = 0$. A non-equilibrium relaxation time for a thermodynamic variable A is defined in terms of the integral of the non-equilibrium relaxation function $\phi_A^{\Delta T}(t)$. We define

$$\phi_A^{\Delta T}(t) = \frac{< A(t) >_{T'} - < A(\infty) >_{T'}}{< A(0) >_{T'} - < A(\infty) >_{T'}}, \tag{2.17}$$

and the relaxation time

$$\tau_A^{\Delta T} = \int_0^\infty \phi_A^{\Delta T}(t) dt. \tag{2.18}$$

The t in equations 2.17 and 2.18 is measured in terms of Monte Carlo time units. We have introduced the time dependent ensemble average $< A(t) >_T$, given by

$$< A(t) >_T = \sum_{\{x\}_i, \{x\}_f} P(\{x\}_i, \{x\}_f, t) A(\{x\}_f), \tag{2.19}$$

where the sum over $\{x\}_i$ is over those states which are equilibrium configurations at temperature T, and the sum over $\{x\}_f$ is over all states.

For a visual explanation the reader is referred to figure 2.3. In this graph we show the time variation of a fictitious observable $< AB(t) >$. Each point represents a change in only one degree of freedom from the previous point. The region we wish to exclude from our Monte Carlo averages is the region between t = 0 and the point labeled $\tau_{AB}^{\Delta T}$, since for $t < \tau_{AB}^{\Delta T}$ the system is still very much dependent on our initial choice of configuration and has not reached equilibrium. To insure we have excluded this region we skip all configurations from t=0 up until $t = n_0$.

Once we have reached equilibrium we may calculate the properties of this equilibrium configuration. Having done this we must generate other equilibrium configurations. We could discard are previous Markov process, and from some new initial configuration begin again to equilibrate this new system. This is very inefficient! A more efficient method takes advantage of the ergodic property of the random walk. Instead of choosing a new initial configuration randomly, we will use the final configuration of our first random walk as the initial configuration of our next random walk. Then we do not have to worry about the system being near equilibrium. We must however still be careful because we will have successive configurations which are highly correlated. We must allow the correlations to the initial system to effectively go to zero. To accomplish this, we will include every $(n \times N)th$ system in our summations, where n is an integer which is large enough that the correlation between the $\{S\}_\nu$ configuration and $\{S\}_{\nu+n\times N}$ configuration is small enough that the fluctuation of any thermodynamic observable of interest, from its average, is purely statistical.

The choice of an appropriate n is generally not *a priori* knowledge, but again after a simulation is completed it is possible to tell if we have chosen n sufficiently large. The condition for a sufficiently large n is related to the linear relaxation time, τ_{AA}, where A

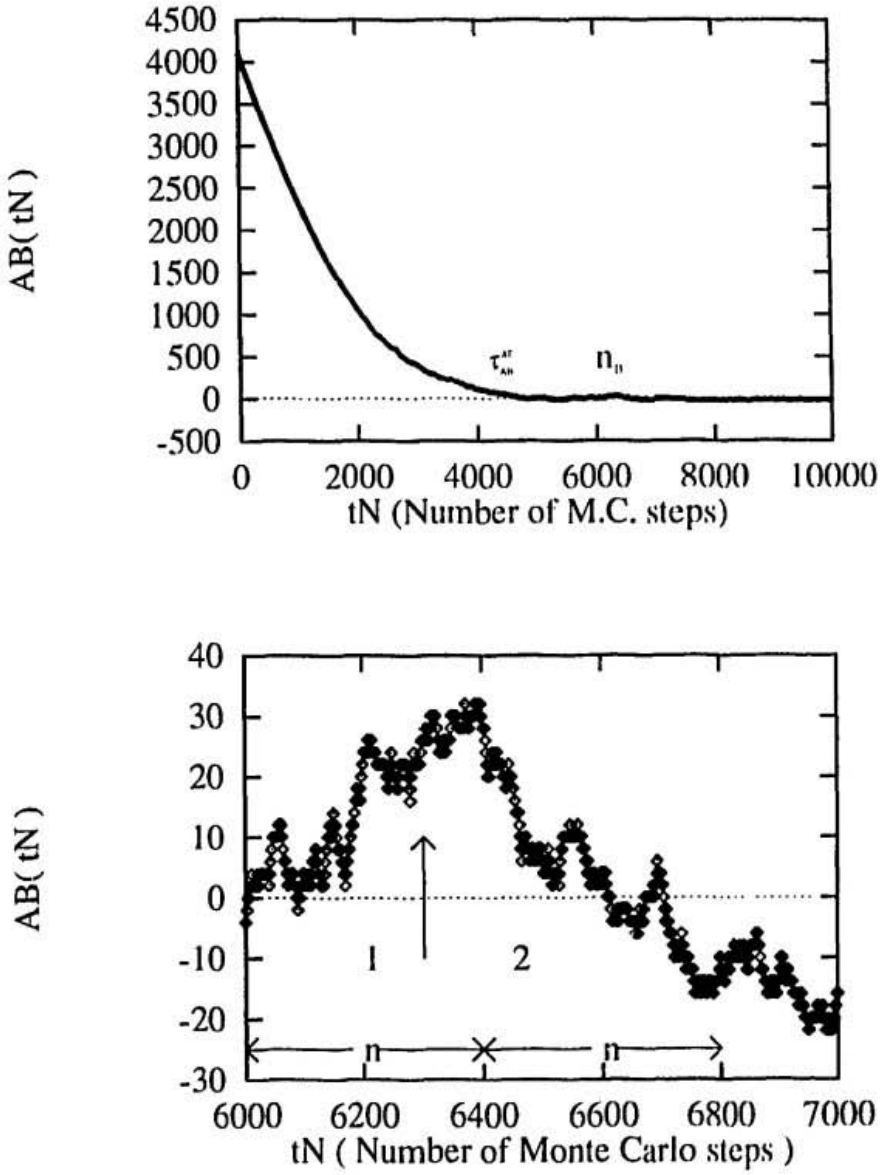

Figure 2.3: The time variation of a fictitious observable. The second graph is an expanded view of the upper graph.

is a thermodynamic observable whose value we wish to calculate. The linear relaxation time is defined in terms of the linear relaxation function $\phi_{\Delta A \Delta A}(t)$ which is defined as

$$\phi_{\Delta A \Delta A}(t) = \frac{< A(0)A(t) > - < A(0) >< A(t) >}{< A^2 > - < A >^2}, \tag{2.20}$$

and then we may define τ_{AA} as

$$\tau_{AA} = \int_0^\infty \phi_{\Delta A \Delta A}(t) dt. \tag{2.21}$$

One will note that the that averages in equations 2.20 and 2.21 do not have a subscript, as in equations 2.17 and 2.18. This is because the ensemble averages in equations 2.20 and 2.21 are given by

$$< A(t) >= \sum_{\{x\}_i,\{x\}_f} P(\{x\}_i, \{x\}_f, t) A(\{x\}_f), \tag{2.22}$$

and

$$< A(0)A(t) >= \sum_{\{x\}_i,\{x\}_f} P(\{x\}_i, \{x\}_f, t) A(\{x\}_i) A(\{x\}_f), \tag{2.23}$$

where the sums over $\{x\}_i$ and $\{x\}_f$ are over all states. Now to insure that we are getting an unbiased estimate for $< A >$ and its fluctuations it must be the case that $n >> \tau_{AA}$ otherwise we will have a situation where $< A >$ may be dominated by a few large fluctuations, which are the result of the correlation between successive configurations, To see graphically what is meant by the above discussion the reader is again referred to figure 2.3. In this graph we show the time variation of a fictitious observable $< AB(t) >$. Each point represents a change in only one degree of freedom from the previous point. The region of the graph marked by 1 and 2 and pointed to by an arrow shows that there is a very large fluctuation from the actual average shown by the horizontal line. This fluctuation is not purely statistical, but is due to the high correlation between the successive configurations. If we include all configurations in our evaluation of $<$

$AB >$ then this large fluctuation, will skew our measurement, since we will include many measurements in this region. An appropriate choice of n is shown in figure 2.3.

In both situations described above, it seems that we must know a lot about the system we are simulating before we can actually start a simulation. It all appears very *ad hoc*, and in reality this is the case. Generally we have a reasonable understanding of the magnitude of n and n_0 and then we try to err on the side of of safety and overestimate both values. It is normally quite easy to see if we have failed to chose either value properly, since we may compare data using different values of either n or n_0. When both are large enough we will see no change in thermodynamic averages.

2.4 Finite Size Effects

In our Monte Carlo simulations, we are dealing with finite systems, but we are interested in properties of infinite systems, since we wish to compare our results to the bulk properties of experimental systems. Therefore, we must be able to obtain reasonable estimates of the values of thermodynamic observables in the thermodynamic limit for our simulations to be useful. This type of analysis is known as finite size analysis. If we have a system with a defined system size characterised by some variable L, the variation of properties with L can be studied and we can extrapolate to the limit of $L \to \infty$. In order to do such an analysis we must known the basic dependence of the observable on L, and we must also know the range of values for L where this basic dependence on L is valid. [35] For example in the S = 1/2, two-dimensional Ising model with periodic boundary conditions, the critical temperature in a finite system is related to the lattice size L^2, and the critical temperature of the infinite system by the equation,

$$\theta_c(L) - \theta_c(\infty) = AL^{\frac{-1}{\nu}} \tag{2.24}$$

where $\nu = 1$ in this model, and L is large. If we evaluate $\theta_c(L)$ for various L, then a graph of $\theta_c(L)$ vs L^{-1} will have an y-intercept of $\theta_c(\infty)$. In this manner, from simulations on finite systems we can obtain θ_c in the thermodynamic limit. Similar relations may be found for other thermodynamic observables, and similar analysis may be done.[27]

Chapter 3

The Model

3.1 Description of Model

Our goal is to study a two-dimensional Ising model with dipolar and superexchange interactions using Monte Carlo simulation. With each point on an infinite two-dimensional square lattice we will associate an ion with magnetic moment $\vec{\mu}$ and spin $\vec{S}$. These ions will interact via a dipole-dipole as well as a superexchange interaction. Thus in simple terms the Hamiltonian can be written as

$$\mathcal{H} = \mathcal{H}_d + \mathcal{H}_{ex}, \tag{3.1}$$

with $\mathcal{H}_d$ containing terms involving the dipolar interaction and $\mathcal{H}_{ex}$ having all terms concerning the superexchange.

We will restrict the exchange interaction to involve nearest neighbours only and thus

$$\mathcal{H}_{ex} = \frac{1}{2}\mathcal{J} \sum_{<nn>} \vec{S}(\vec{R}_n) \cdot \vec{S}(\vec{R}_m), \tag{3.2}$$

where $< nn >$ signifies a summation over all nearest neighbours, and $\vec{S}(\vec{R}_n)$ is the spin at $\vec{R}_n$. For our model $\vec{S}(\vec{R}_n)$ will be uniaxial and

$$\vec{S}(\vec{R}_n) = S_{\text{eff}} \sigma_n \hat{e}_\alpha, \tag{3.3}$$

where $\alpha = 1, 2, 3$ specifies the easy axis, $\sigma_n = \pm 1$ defines the orientation of the spin at $\vec{R}_n$, and S_{eff} is the magnitude of the spins. We rewrite equation 3.2 as,

$$\mathcal{H}_{ex} = \left(\frac{\mu_{\text{eff}}^2}{a^3}\right) \frac{1}{2} J \sum_{<nn>} \sigma_n \sigma_m, \tag{3.4}$$

with J given by

$$J = \mathcal{J}a^3\left(\frac{S_{\text{eff}}}{\mu_{\text{eff}}}\right)^2 \tag{3.5}$$

$$= \mathcal{J}a^3\left(\frac{g_J - 1}{g_J}\right)^2. \tag{3.6}$$

Here g_J is the Landé g factor. [5] [17] [37] [38] The parameter J is known as the coupling constant or exchange parameter and may assume any positive or negative value. A positive value for J would favour spins which are orientated anti-ferromagnetically, while a negative J would favour spins orientated ferromagnetically. One may note that we have not followed the usual convention in equation 3.4, which would have $-J$ where we have positive J. Our reason for not following convention is because we are more interested in the anti-ferromagnetic regime and it was more natural to have this along the positive J axis of our phase diagram.

The isotropic exchange Hamiltonian in equation 3.2 been studied extensively (See for example [27], [39], and [40] and references therein) and the application of periodic boundary conditions is standard. By applying periodic boundary conditions it is possible to mimic an infinite system with a finite number of lattice points. This will allow us to use standard finite-size scaling techniques.

The dipolar interaction is a long-range interaction, which makes the application of periodic boundary conditions less straightforward than with the short-range exchange interaction. It might at first seem as if a long range interaction might be inappropriate for a Monte Carlo simulation, which by necessity is restricted to a finite-sized system. This problem was examined by Kretschmer and Binder [41] in work concerning three-dimensional dipolar systems. As well, in a general discussion of long range interactions in Monte Carlo simulations of hard particles interacting via coulombic forces, J. P. Valleau examined similar problems and reached similar conclusions to Kretschmer and Binder.

[42] Kretschmer and Binder examined the apparent incompatibility caused by finite system size and long range interaction. The easiest manner of dealing with the long range nature of the dipole interaction on a finite system would be to truncate the interaction at at some finite distance r. But this is equivalent to creating a surface current at radius r, which acts counter to the magnetisation of the bulk system. In an effort to counteract the effects of the truncation, many attempts to include some compensating field have been made. Some examples cited by Kretschmer and Binder include a demagnetising field given by $H = (\hat{L} - \hat{D})M$, or $H' = (\hat{L}M - \hat{D}M_r)$, where $\hat{L}$ is the demagnetising factor of the total cell, $\hat{D}$ is the demagnetising factor of the truncation volume, M is the magnetisation of the total cell, and M_r is the magnetisation of the finite cell. Both these examples overestimated the ordering in three dimensional simulations. Kretschmer and Binder also discussed the use of an Onsager reaction field

$$H_r = \frac{8\pi\chi M_r}{[(3 + 8\pi\chi)r^3]}, \tag{3.7}$$

χ being the ferromagnetic susceptibility. They determined that even this more sophisticated method does not yield results comparable to the Ewald summation method (E.S.M.). Based upon the findings of Kretschmer and Binder we decided to use the E.S.M., which we will discuss below. As a comparison to the E.S.M. we also do some simulations using the minimum image technique (M.I.T.). The M.I.T. was compared to the E.S.M. by Kretschmer and Binder for three dimensional dipolar systems and a similar comparison for two dimensional systems will be discussed in this work. The M.I.T. is a truncation of the long range interaction at the boundaries of the system under study, with no compensating fields. In this technique the "neighbourhood" of spins with which a given spin interacts is a volume in three dimensions or an area in two dimensions equal to the volume or area of the system understudy and centered on the given spin.

In order to implement the E.S.M. on a theoretically infinite two dimensional system we

must restrict the allowed configurations to those which satisfy a strict periodic boundary condition. That is, we will require that any moment $\vec{\mu}_n$ satisfy

$$\vec{\mu_n} = \vec{\mu_{n'}} \quad \text{when} \quad \vec{r}_{n'} = \vec{r}_n + \vec{G}\,, \tag{3.8}$$

where $\vec{r}_n$ refers to the position of the n^{th} lattice site and $\vec{G}$ is any lattice vector. The lattice vector, $\vec{G}$, is defined as

$$\vec{G} = aL \times (n_1\hat{c}_1 + n_2\hat{c}_2) \text{ where } n_1, n_2 = \{0, \pm 1, \pm 2, ...\}\,. \tag{3.9}$$

We have defined the lattice spacing to be a, and the size of the system to be $(a \times L)^2$, so we have a system of L^2 spins. The periodicity of the allowed configurations will be determined by L. We have associated the plane of the system with the unit vectors $\hat{c}_1$ and $\hat{c}_2$. All spins which are not in our finite system are referred to as images of the spin to which they are related by equation 3.8. The restriction on the allowed configurations will allow us to specify the state of an infinite system in terms of the finite L^2 spins of our basic unit cell. As well it will allow the use of Ewald sums to rewrite the dipolar Hamiltonian in terms of this finite number of spins and thus will allow us to obtain results for an infinite system using standard finite size scaling techniques. An example of an allowed configuration is given in figure 3.1.

The Hamiltonian of a system of ions interacting via the magnetic dipolar interaction may be written

$$\mathcal{H}_d = \frac{1}{2}\sum_{n,m,\alpha,\beta} \mu_n^\alpha \mu_m^\beta \lim_{\vec{r}\to 0} \frac{\partial}{\partial r_\alpha}\frac{\partial}{\partial r_\beta}\frac{1}{|\vec{R}_{nm} - \vec{r}|}, \tag{3.10}$$

where α and β label the components of the magnetic moment, $\vec{\mu}$ and $\vec{R}_{nm}$ is the displacement of moment n relative to moment m.

If we assume a uniaxial magnetic moment we may may write the magnetic moment at $\vec{R}_n$ as

$$\vec{\mu}_n = \mu_{\text{eff}}\sigma_n\hat{c}_\alpha, \tag{3.11}$$

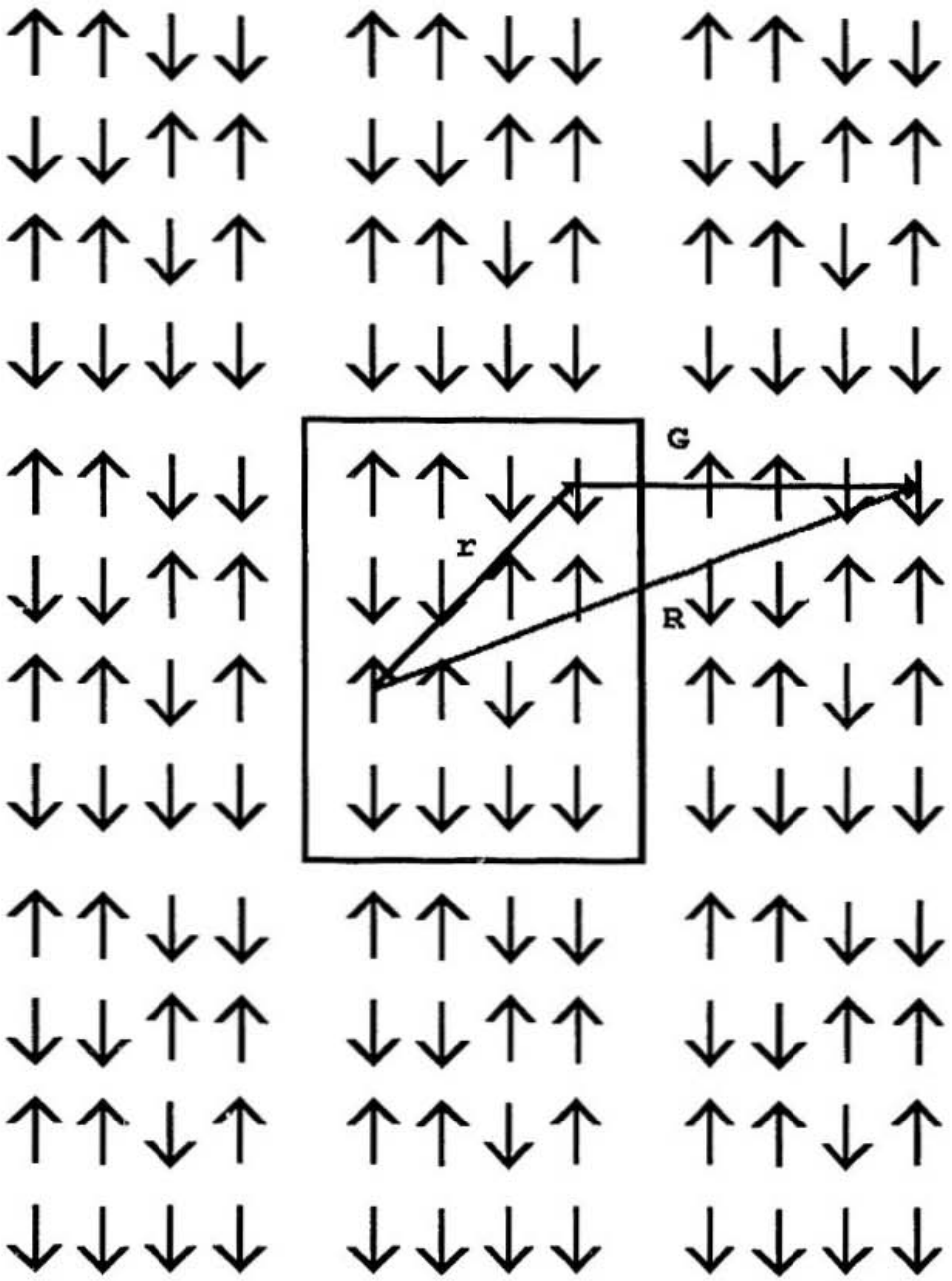

Figure 3.1: An example of an allowed configuration, with a basic unit cell which is 4×4.

where $\alpha = 1,2,3$ defines the easy axis, $\sigma_n = \pm 1$ specifies the orientation of the spin at $\vec{R}_n$, and μ_{eff} is the magnitude of the moment. The vector $\vec{R}_{nm}$ may be written in terms of the reduced vector $\vec{r}_{nm}$ where

$$\vec{R}_{nm} = \vec{r}_{nm} + \vec{G}, \tag{3.12}$$

and we chose $\vec{G}$ such that $\vec{r}_{nm}$ lies within our finite system. For a visual example one may refer to figure 3.1. Equations 3.12 and 3.8 allow us to rewrite the Hamiltonian as a sum over the spins in our finite system and over all lattice vectors $\vec{G}$, so the Hamiltonian becomes

$$\mathcal{H}_d = \frac{1}{2}\frac{N\mu_{\text{eff}}^2}{L^2}\left[C + \sum_{\vec{G}}{\sum_{n,m}}' \sigma_n\sigma_m \lim_{\vec{r}\to 0}\frac{\partial}{\partial r_\alpha}\frac{\partial}{\partial r_\alpha}\frac{1}{|\vec{r}_{nm}+\vec{G}-\vec{r}|}\right], \tag{3.13}$$

where C is the self energy of the spins and is given by

$$C = a^3 \sum_{n,\vec{G}} \lim_{|\vec{r}|\to 0}\left(\frac{\partial}{\partial x_\alpha}\right)^2 \frac{1}{|\vec{r}_n + \vec{G} - \vec{r}|}. \tag{3.14}$$

Making use of Ewald summation techniques we are able to rewrite the Hamiltonian as

$$\mathcal{H} = \frac{N\mu_{\text{eff}}^2}{2L^2a^3}\left[Ca^3 + \sum_{n\neq m}^{L^2} \sigma_n \mathcal{W}^{\alpha\alpha}(\frac{\vec{r}_{nm}}{a})\sigma_m\right], \tag{3.15}$$

where $\mathcal{W}^{\alpha\beta}(\frac{\vec{r}_{nm}}{a})$ is the effective interaction given by

$$\begin{aligned}\mathcal{W}^{\alpha\beta}(\frac{\vec{r}_{nm}}{a}) \;=\; & \lim_{\vec{r}\to 0} L^{-1}\frac{\partial}{\partial x_\alpha}\frac{\partial}{\partial x_\beta}\left[{\sum_{\vec{G}}}' \frac{e^{2\pi i\frac{(\vec{r}_{nm}-\vec{r})\cdot\vec{G}}{L}}}{|\vec{G}|}\text{Erfc}\left(\frac{\pi|\vec{G}|}{\eta}\right) + \right. \\ & \left. \sum_{\vec{G}} \frac{\text{Erfc}(\eta\left|\frac{(\vec{r}_{mn}-\vec{r})}{L} + |\vec{G}|\right|)}{\left|\frac{(\vec{r}_{mn}-\vec{r})}{L} + |\vec{G}|\right|}\right].\end{aligned} \tag{3.16}$$

We can therefore define an effective field at a lattice point n as

$$H_n^\alpha = \sum_{m=1}^{L^2} \mathcal{W}^{\alpha\alpha}(\frac{\vec{r}_{nm}}{a})\sigma_m, \tag{3.17}$$

and we can write the energy of a configuration in terms of these effective fields as

$$E(\{\vec{S}_n\}) = \frac{1}{2}\left[Ca^3 + \sum_n \sigma_n^\alpha H_n^\alpha\right]. \tag{3.18}$$

A more detailed derivation is presented in appendix A, where we have derived a more general form of the Hamiltonian than we use in this study. When the spins are orientated along the b axis $\vec{\mu}$ has only a y component. We call this the in-plane model, and in equation 3.17 we have $\alpha = \beta = 2$. When the spins are orientated along the c axis $\vec{\mu}$ has only a z component. This is called the out-of-plane model, and we have $\alpha = \beta = 3$.

The only difficulty left is to calculate $\mathcal{W}^{\alpha\alpha}(\frac{\vec{r}_{lmn}}{a})$ and the value of C. These quantities are dependent on both system size and the orientation (in-plane or out-of-plane) of the spins. This task is left to the the mathematical manipulation program MATHEMATICA, with which we have calculated the required values for systems ranging in size from L = 4 up to L = 64. The time required to calculate a $\mathcal{W}^{\alpha\alpha}(\frac{\vec{r}_{lmn}}{a})$ for a L=4 system is less that ten minutes, while L=64 takes the better part of three days of computer time on a DEC Station 2100. It is important to point out that it is not necessary to calculate all L^4 terms in $\mathcal{W}^{\alpha\alpha}(\frac{\vec{r}_{lmn}}{a})$, since there is considerable symmetry in the system. It is only necessary to calculate $\mathcal{W}^{\alpha\alpha}(\frac{\vec{r}_{0n}}{a})$, since there will be a mapping for all other terms.

3.2 Computer Considerations

In this section we veer away from physics for a short discussion of some programming considerations. Computer simulations involving long range interactions are very difficult to perform because of the computer time involved. It is therefore necessary to program efficiently, if we wish to simulate systems of sufficient size. To ensure a fast program we wish to avoid using anything other than one dimensional arrays since the computer deals with one dimensional arrays much more efficiently that higher dimension arrays. We also would like to keep conditional statements, in Fortran IF statements, to a minimum unless they can save large amounts of computer time. As well, as much as possible we would like to do any computations we can using bit manipulations since the computer does this

very quickly. By bit manipulations I am referring to the and, or, and bit shift intrinsic operations. Someone who is familiar with computer programming might feel these self imposed restrictions are unnecessary given the speed of modern day computers, but the time required for a simulation of dipoles increases like L^4 in two dimensions (L^6 in 3-D), so every small improvement is important. To aid in our discussion we include a copy of the program in appendix B.

The most time consuming part of the simulation is the updating of the effective field H_n^α at each lattice point following a flip of a spin. The updating procedure involves calculating the change in H_n^α as $S_m \longrightarrow -S_m$. This change is given by

$$\Delta H_n^\alpha = -2S_m \mathcal{W}(n,m). \tag{3.19}$$

The spin, S_m, refers to the state of the spin before we change its state, and we have simplified the arguments of W in the obvious manner. One problem with the form of equation 3.19 is that we do not store all of the $\mathcal{W}(n,m)$ but only store $\mathcal{W}(0,m) \equiv W(kw)$. We have to map the $\mathcal{W}(n,m)$ on to $\mathcal{W}(kw)$. This mapping is not trivial and kw is a function of both the lattice point we are considering and the position of the spin flipped. The updating of H_n^α is done in the subroutine Updatefield.f and it includes the mapping from (n,m) to kw. By restricting the system size to those where $L = 2^n$, where n is a integer, we are able to express the mapping in terms of five bit operations, and obtain an increase in computational speed.

When we include the superexchange interaction we must deal with the boundary of our system carefully, since the nearest neighbours of spins along the boundary are mapped in a different manner from those of spins not on the boundary. If a spin is not on the boundary, its four nearest neighbours are stored in our one dimensional array in locations $i-1$, $i+1$, $i+L$ and $i-L$, where i is the array location for the spin itself.

For a spin on the top boundary, for example, its upper nearest neighbour is actually

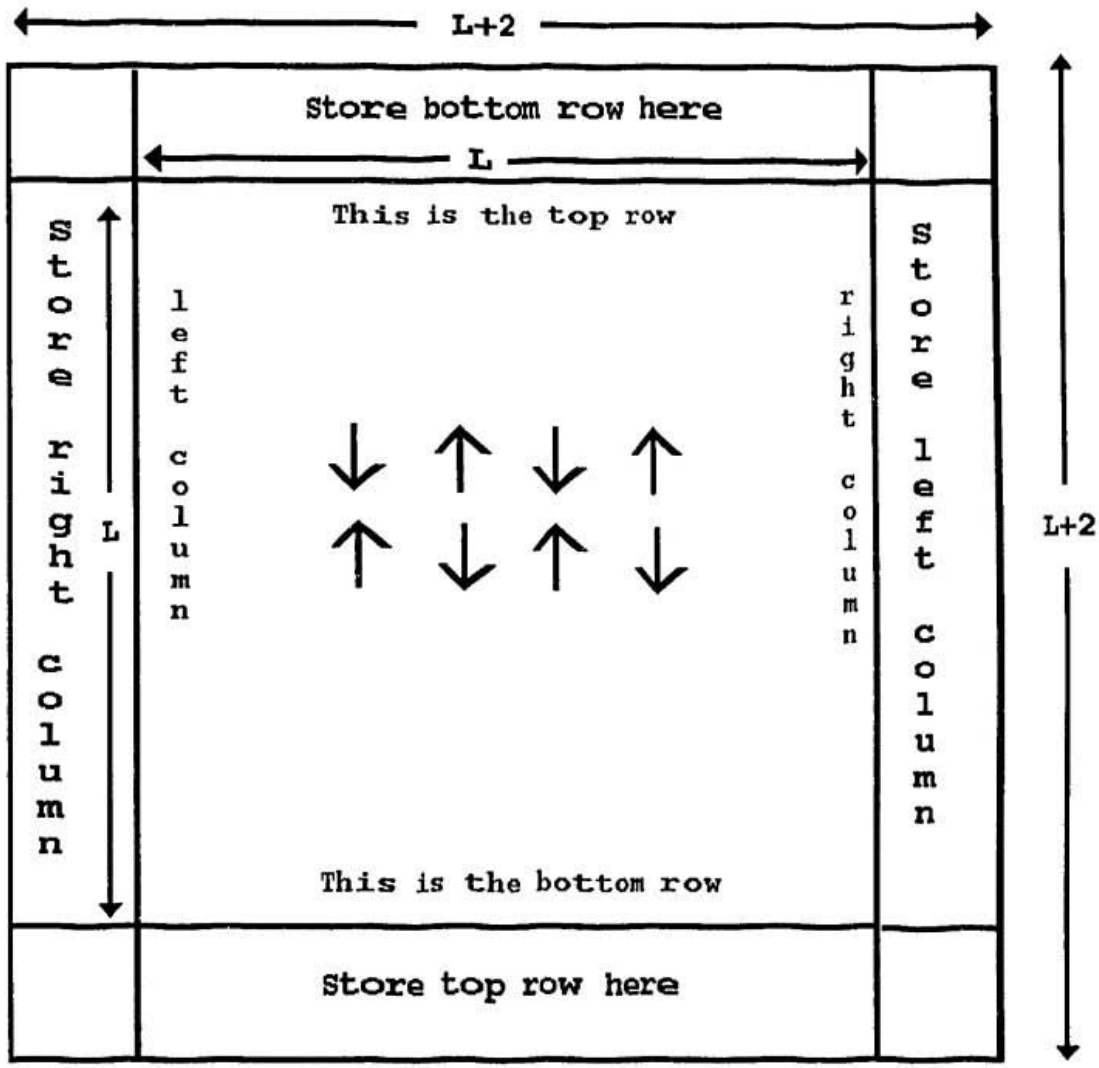

Figure 3.2: How we store the state of sites to deal with periodic boundary conditions.

stored in the bottom row, and vice versa for spins in the bottom row. Spins on the left boundary have left nearest neighbours on the right boundary. Therefore we must know if a spin is on the boundary of the system so that we may find its four nearest neighbours properly. We do not want to have to check if the spin we are updating is on the top or bottom row, or along one of the edges since this would involve a multiple number of very slow conditional statements executed every time we try to update a spin. Instead what we do is embed our $L \times L$ system in a $L+2 \times L+2$ system and store the boundary sites twice. The bottom boundary of our $L \times L$ system is stored twice, once in its normal position and once in the top row of our $L+2 \times L+2$ system. Similarly the top boundary of our $L \times L$ system is stored in its normal position as well as along the bottom of our $L+2 \times L+2$ system. We do the equivalent with the left boundary and right boundary of our $L \times L$ system: store them both in their normal position and in the right column and left column in our $L+2 \times L+2$ system. The benefit of storing the boundary in two separate locations is that now all spins in our $L \times L$ system will find their four nearest neighbours in the same manner; it doesn't matter if they are along a boundary or not. Other benefits to this method are an easier transfer to a parallel algorithm, as well as being vectorisable for use on vector processors.[43]

Chapter 4

Results and Discussion

4.1 Some basics and error checking

In this section we will present the results of our Monte Carlo simulations. We will look at some checks which were done to ensure that our computer code was working properly. This is important, as all computer code, with the exception of the random number generator, was written for this project by the author, and no similar (two-dimensional) studies could be found for comparison. As a first check, we compare the energy of the ground states for both the in-plane (AF) and the out-of-plane (AA) models, with energies calculated by De'Bell and Whitehead.[24] The agreement is excellent with differences of less then 2% even for the smallest of lattice sizes for both in the in-plane and out-of-plane models.

During a simulation with each spin flip the effective field, H_n, changes at all lattice points, due to the long range nature of the dipolar interaction. Rather than recalculate the effective field via equation 3.17 after each spin flip, we may, since only one term in each sum has changed, more efficiently record the *change* in the effective field, ΔH_n at each point. So as a function of time the effective field at a point can be calculated as

$$H_n(t) = H_n(0) + \sum_{i=1}^{N_f(t)} \Delta H_n(i). \tag{4.1}$$

We have defined $N_f(t)$ as the total number of flips up to time t. There is ample opportunity for errors to accumulate as $N_f(t)$ may become very large. To check that *significant* errors are not accumulating using equation 4.1, we have calculated H_n at some time t

where $N_f(l) > 100000$, both when we have been calculating Π_n via equation 4.1, and using equation 3.17. Despite the summation of greater than 100000 terms we find that no significant error has been introduced. Generally the use of equation 4.1, instead of equation 3.17 gives errors in the 12th or 13th decimal place.

It is possible to enumerate the states of a 4×4 system, to get exact values for thermodynamic variables, such as average energy, specific heat, order parameter, and magnetic susceptibility. We have measured these quantities by Monte Carlo simulation for various size systems including 4×4 systems. The small system size will eliminate these systems from our finite size analysis, but they do offer a further check to the accuracy of our Monte Carlo simulations. In general we find that at moderate temperatures, the Monte Carlo results are very accurate, while at low temperatures the small system size along with the problem of domain wall formations prevents an accurate Monte Carlo estimate of the order parameter and the magnetic susceptibility. In the simulations of the in-plane systems, a small shoulder in the specific heat which at first was thought to be a result of poor Monte Carlo data at low temperature, was in fact a feature of the exact solution. The formation of domain walls, particularly in the in-plane simulations, led to problems in the smaller systems, but fortunately the effects diminished at larger lattice sizes.

The solution to the problem of small system size is obviously to use larger systems. When dealing with only short range interactions one is generally able to choose systems where small size effects are not significant. This is because the time required for such a simulation grows linearly with system size, N. For long range interactions the time for a simulation grows with the system size raised to the dimension of the system. For a two-dimensional system of size $N = L \times L$, the time will increase as L^4, effectively limiting the size of the system we may simulate. The constraint of reasonable computing time, has limited this study to systems where $4 < L < 64$, where the $L = 64$ simulations

required a parallel version of the program, run on a 6 processor Silicon Graphics Iris.[44]

4.2 Typical simulation

A typical simulation will consist of approximately 10000 initialisation Monte Carlo steps (MCS) per spin, so we have set $n_0 = 10000$, where n_0 is defined in chapter 2. We then have typically 10^6 to 10^8 MCS per spin, where we include every tenth step in our data taking, meaning we have set $n = 10$, where n is defined in chapter 2. In a simulation we choose the initial configuration in one of three ways. As a first option we might choose our initial configuration randomly. Most often a final configuration from a previous simulation done at a lower temperature was used. This, of course, insured that our initial configuration was near equilibrium. We did not use configurations from previous runs at higher temperature because we found that domain wall formations which were long lived at high temperatures could "freeze in" as we lowered the temperature preventing us from seeing the true equilibrium behaviour of the system. This could be seen in the hysteresis of the order parameter as a function of temperature as we simulated a system first lowering the temperature then raising it and finally lowering the temperature again. Similar problems were encountered in simulations of three dimensional systems.[45] As a final option, particularly when simulating systems at low temperature, it was more efficient to initialise the system to the ground state and allow more initial steps to allow the system to reach equilibrium. This choice also avoided the problem of domain wall formation.

Our results are divided between those where we have a pure dipolar Hamiltonian, ($J = 0$), and results when we have both a dipolar and superexchange contribution to the Hamiltonian, ($J \neq 0$). A large percentage of our time was spent in trying to understanding the pure dipolar system as no previous simulations on two-dimensional dipolar

systems could be found.

4.3 $J = 0$

In this section we will deal with systems where the Hamiltonian is given by equation 3.15. Simulations were done for systems ranging from $L = 4$, to $L = 64$, for both systems with spins oriented along the b axis (in-plane) and for systems with spins along the c axis (out-of-plane).

4.3.1 Energy and Specific heat

In figures 4.1 and 4.2 we plot the variation of the average energy, $< E >$, with temperature for lattices of various sizes. The energy has been adjusted so that the ground state energy for each lattice size is zero. The average energy is calculated according to equation 3.18. The magnetic specific heat may be found from the differentiation of the average energy with respect to temperature at constant field, but this is not the most accurate method available in Monte Carlo simulations. It is a well known thermodynamic relation that the specific heat per spin is

$$C = \frac{1}{L^2\theta^2}\left[< E^2 > - < E >^2\right], \tag{4.2}$$

where <> denotes an ensemble average, θ is reduced temperature, and L^2 is the number of spins. It is this relationship that we used to calculate the magnetic specific heat. We plot in figures 4.3 and 4.4 the magnetic specific heat as calculated from equation 4.2 for the out-of-plane and in-plane models respectively, for various lattice sizes.

The peak of the magnetic specific heat may be used as an estimate of the Néel temperature for our dipolar systems. As discussed in 2.4, the Néel temperature should scale according to [27]

$$\theta_n(L) - \theta_n(\infty) \sim L^{\frac{-1}{\nu}}. \tag{4.3}$$

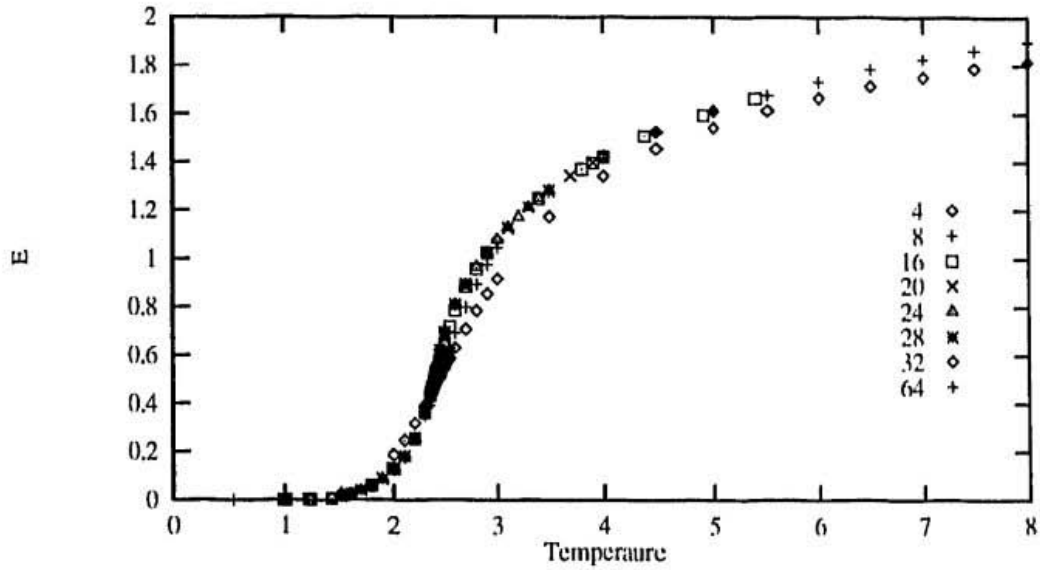

Figure 4.1: Average energy for out-of-plane system, with the ground state energy defined as zero.

A graph of $\theta_n(L)$ versus $L^{\frac{-1}{\nu}}$ should be linear with a y-intercept of $\theta_n(\infty)$. There are three unknowns in equation 4.3, ν, $\theta_n(\infty)$, and the implicit constant of proportionality. While it is possible to do a regression analysis to fit all three unknown parameters in equation 4.3, the quality of our data is not sufficient for such a fit to be meaningful. Instead we will assume that $\nu = 1$ in this model, the same as ν for the standard two-dimensional Ising model, and will check the consistency of this assumption when determining other critical exponents. In figures 4.5 and 4.6 we graph $\theta_n(L)$ versus 1/L. The estimate of $\theta_n(L)$ for $L = 4$, which is the point farthest right, is not included in our analysis. It is obvious from this analysis and further analysis below that $L = 4$ is not in the scaling region where equation 4.3 is valid. A least squares fit estimate for $\theta_n(\infty)$, gives $\theta_n(\infty) = 2.37 \pm 0.05$ for out-of-plane ordering and $\theta_n(\infty) = 3.95 \pm 0.1$ for in-plane ordering. To check for consistency we take our estimates for $\theta_n(\infty)$ for both spin orientations as exact and fit

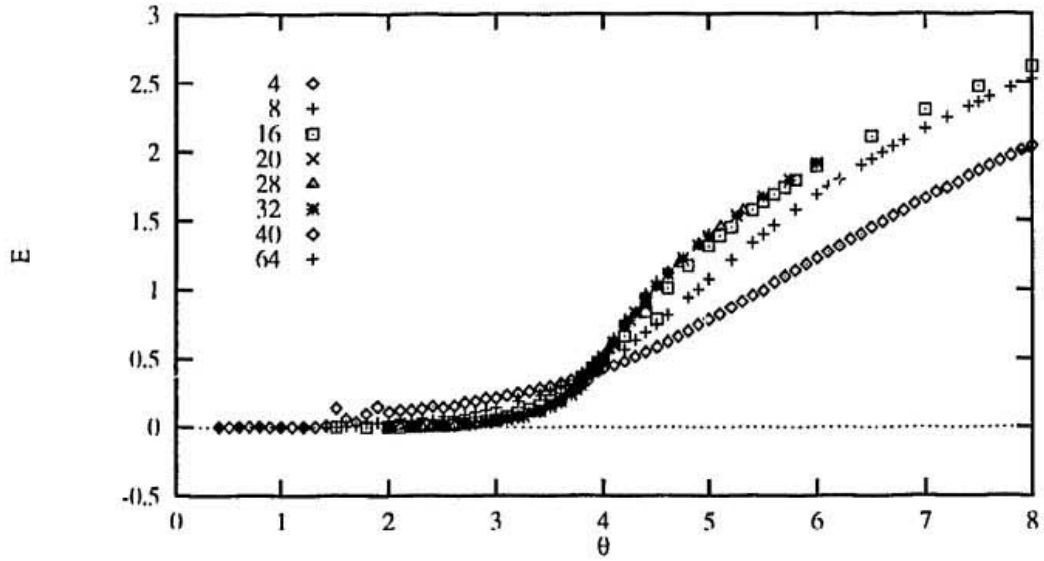

Figure 4.2: Average energy for in-plane system, with the ground state energy defined as zero.

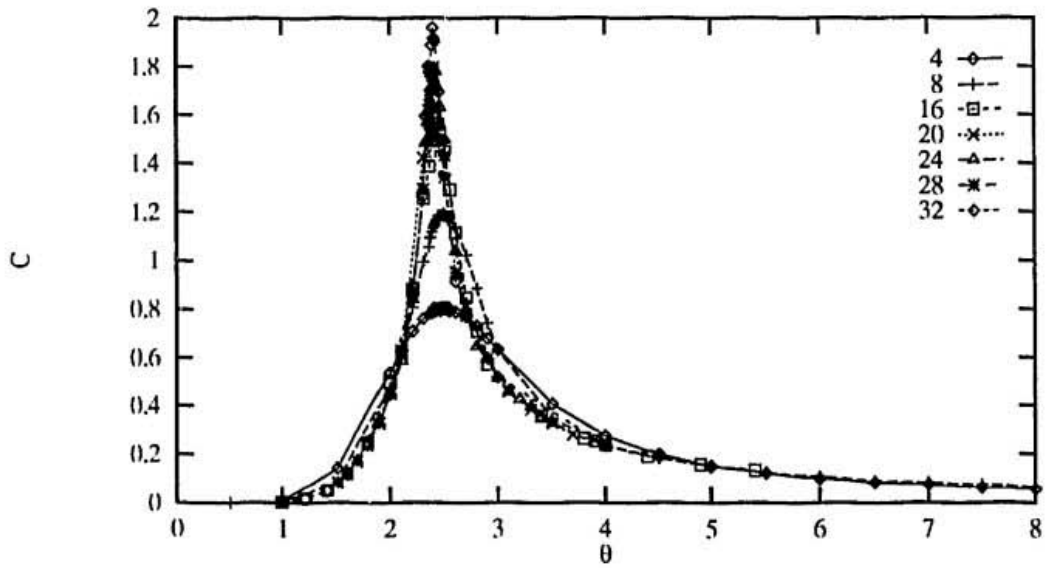

Figure 4.3: Specific heat for out-of-plane model.

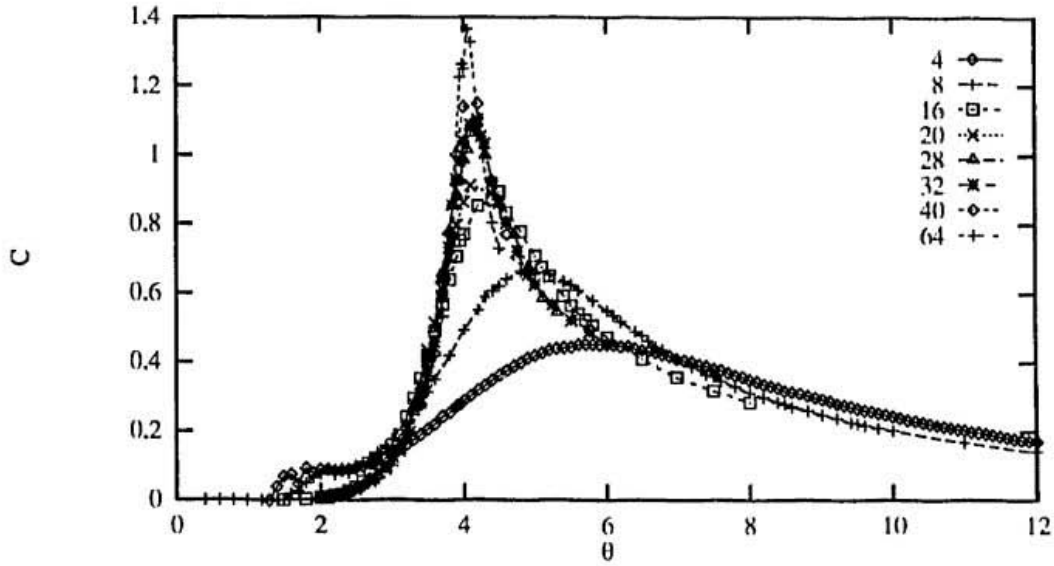

Figure 4.4: Specific heat for in-plane model.

the value of ν. For both cases a least squares fit gives $\nu = 1.0 \pm 0.1$. Before any definite determination of the universality class may be done, it will be necessary to obtain higher quality data to verify that our assumption of ν is valid. Until such time we must temper all claims with the fact that we have assumed a value for ν.

4.3.2 Order parameter and Susceptibility

In figures 4.7 and 4.8 we have graphed the order parameter for the out-of-plane and the in-plane systems respectively for various lattice sizes. The fact that the order parameter does not go to zero sharply in our Monte Carlo simulation is a result of the finite size of our systems. One can see that with increasing lattice size the tail in the order parameter becomes smaller. From these graphs it would appear that the $L = 4, 8$ systems for in plane ordering and the $L = 4$ system for out-of-plane ordering suffer due to small system size at low temperature. The lack of smoothness in the in plane data will be discussed

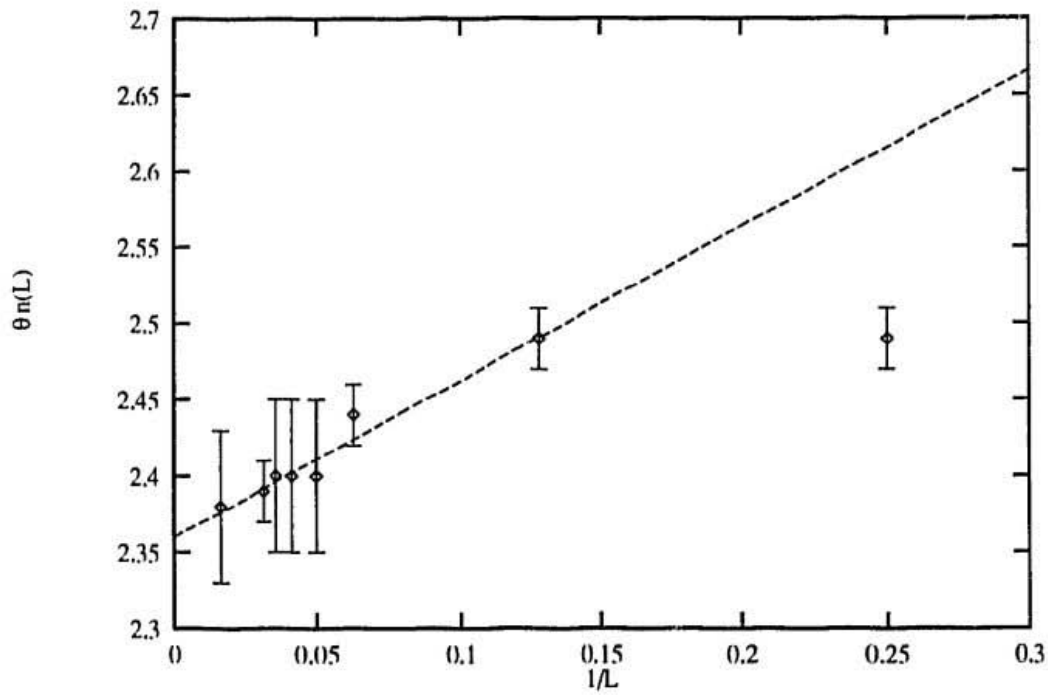

Figure 4.5: θ_n as a function of $\frac{1}{L}$ for out-of-plane model. The intercept yields $\theta_n(\infty) = 2.37 \pm 0.05$.

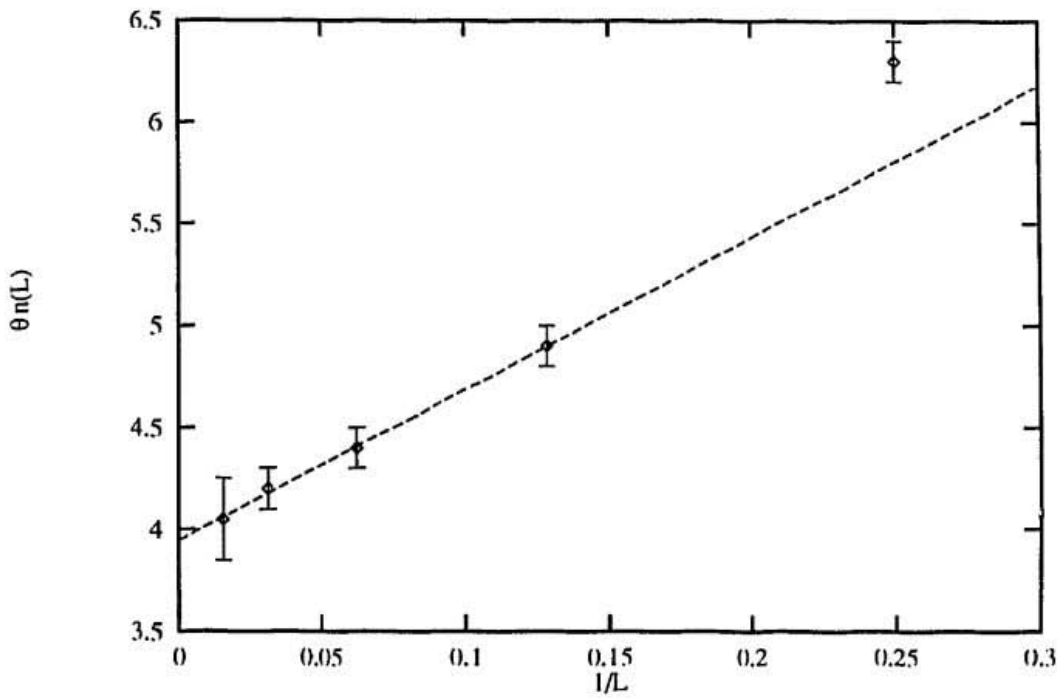

Figure 4.6: θ_n as a function of $\frac{1}{L}$ for in-plane model. The intercept yields $\theta_n(\infty) = 3.95 \pm 0.1$.

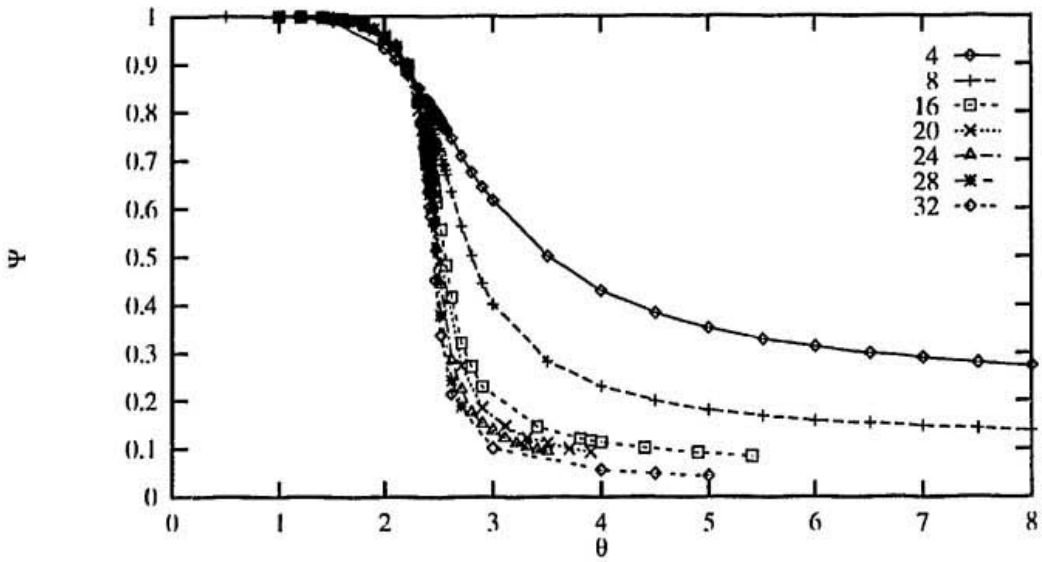

Figure 4.7: Order parameter for out-of-plane model.

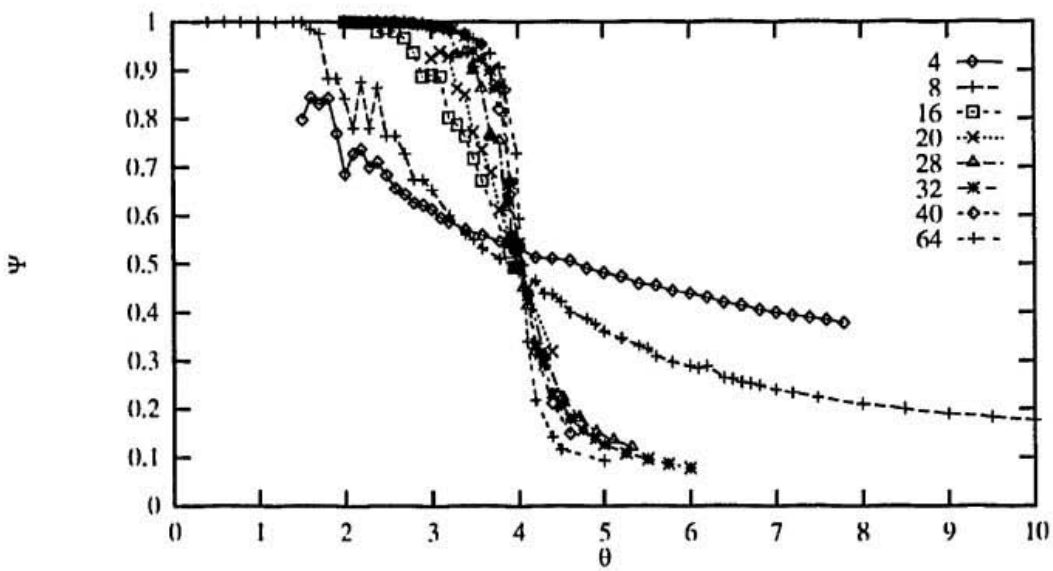

Figure 4.8: Order parameter for in-plane model.

below in section 4.5. When calculating the critical exponent β defined as

$$< M > \sim (|t|)^{\beta}(t \to 0^{-}) \tag{4.4}$$

$$\sim L^{\frac{-\beta}{\nu}}(t = 0), \tag{4.5}$$

where $t = \frac{\theta - \theta_n(\infty)}{\theta_n(\infty)}$, we have not made use of these smaller systems. We find, using equation 4.5, that $\frac{\beta}{\nu} = 0.12 \pm 0.01$ for the out-of plane systems and $\frac{\beta}{\nu} = 0.12 \pm 0.03$ for the in-plane systems by doing a least squares fit, to equation 4.5, which we have shown in figure 4.9. The exact value of $\frac{\beta}{\nu}$ for the S=1/2 two-dimensional Ising model is 0.125.

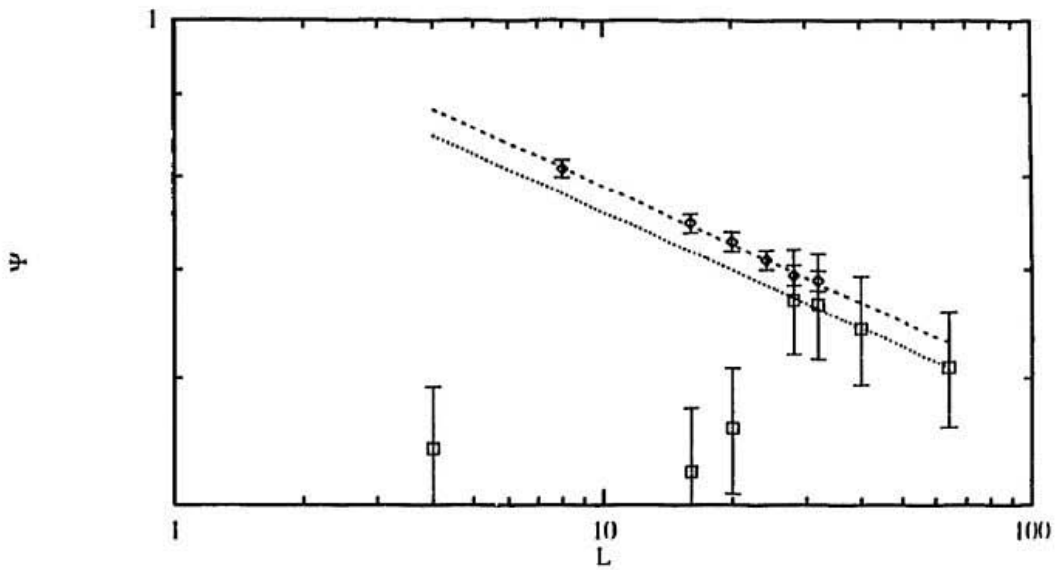

Figure 4.9: Least squares fit of the log of the order parameter at θ_n as a function of the log of L.

We may calculate the magnetic susceptibility from

$$\chi = \frac{1}{L^2\theta^2}\left[< M^2 > - < M >^2\right]. \tag{4.6}$$

In figures 4.10 and 4.11 we graph the magnetic susceptibility as a function of temperature for both spin orientations.

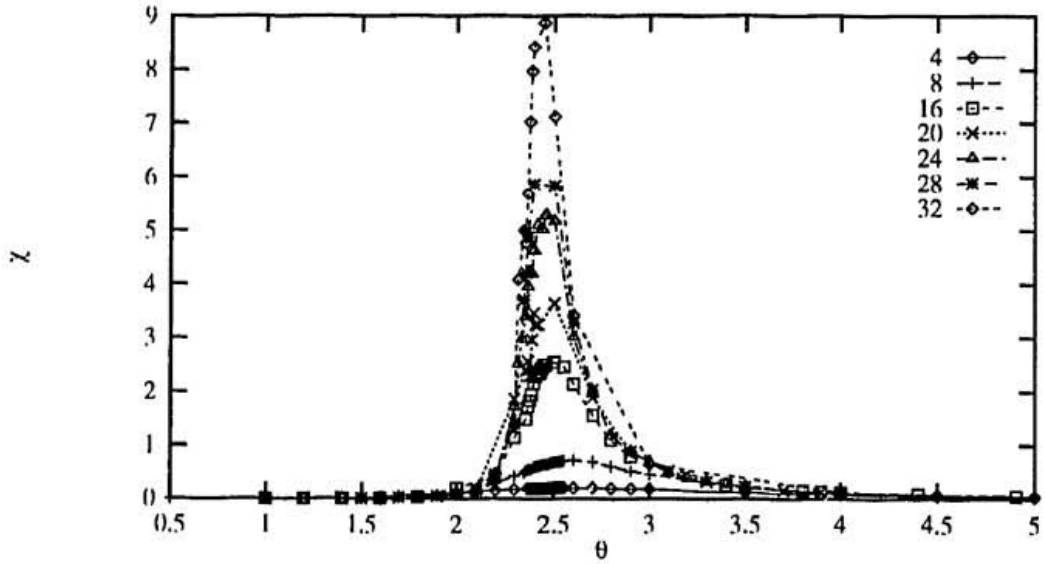

Figure 4.10: Magnetic susceptibility of the out-of-plane model.

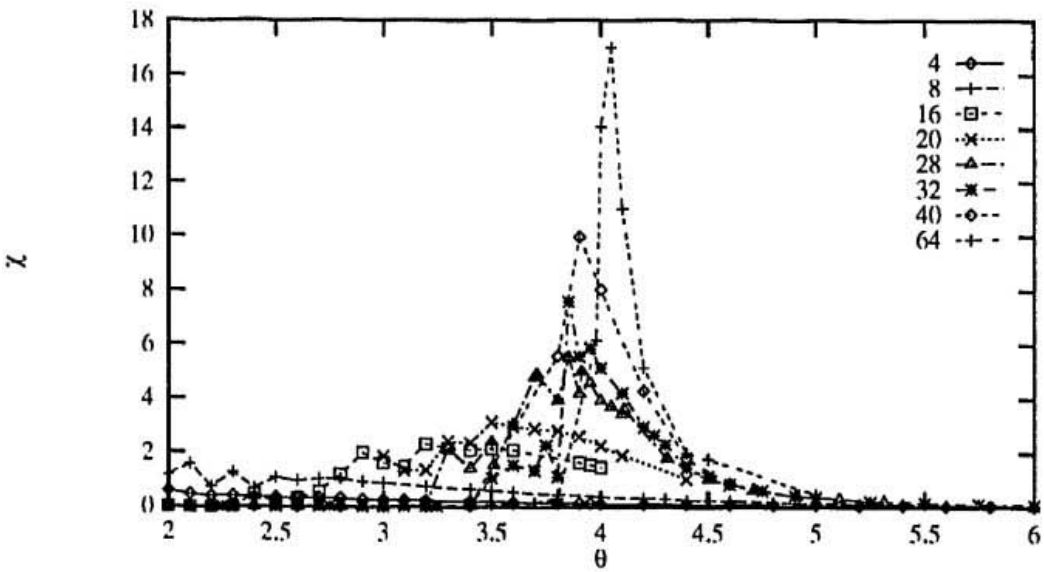

Figure 4.11: Magnetic susceptibility of the in-plane model.

We may characterise the critical behaviour of the susceptibility by measuring the critical exponent γ which is defined as

$$\chi \sim (|t|)^{-\gamma}(t \to 0^-), \tag{4.7}$$

$$\sim L^{\frac{\gamma}{\nu}}(t = 0). \tag{4.8}$$

A least squares fit to both the in-plane and out-of-plane data using equation 4.8, shown in figure 4.12, yield $\frac{\gamma}{\nu} = 1.7 \pm 0.4$ and $\frac{\gamma}{\nu} = 1.9 \pm 0.4$ for the out of and in-plane systems respectively. In the two-dimensional, spin 1/2 Ising model $\frac{\gamma}{\nu} = 1.75$

While there is some error in our estimates of the critical exponents due to the small size of our systems, our results are consistent with these systems belonging to the same universality class as the standard two-dimensional Ising model, despite the long range nature of the dipolar interaction. While it has previously been proposed that the pure dipolar system belongs to the same universality class as the two-dimensional, spin 1/21/2 Ising model, this is, to our knowledge, the first comparison of critical exponents calculated for dipolar systems, using Monte Carlo simulations, to those of the two-dimensional, S=1/2 Ising model.

4.4 Data Collapse

During prepartion of this manuscript, we learned of a similar study [46] which was still in its initial stages. The purpose of this new study was to evaluate the critical exponents of a two-dimensional S=1/2 dipolar model using a finite size scaling form for $< \Psi^2 >$, where Ψ is the order parameter. If the finite size scaling form is valid then it should allow one to graph data from simulations on lattices of various sizes in such a manner that all data falls on a single universal curve regardless of the size of the lattice. The finite size scaling form states that,[27][35][47] [48]

$$< \Psi^2 >= N^r f(tN^y), \tag{4.9}$$

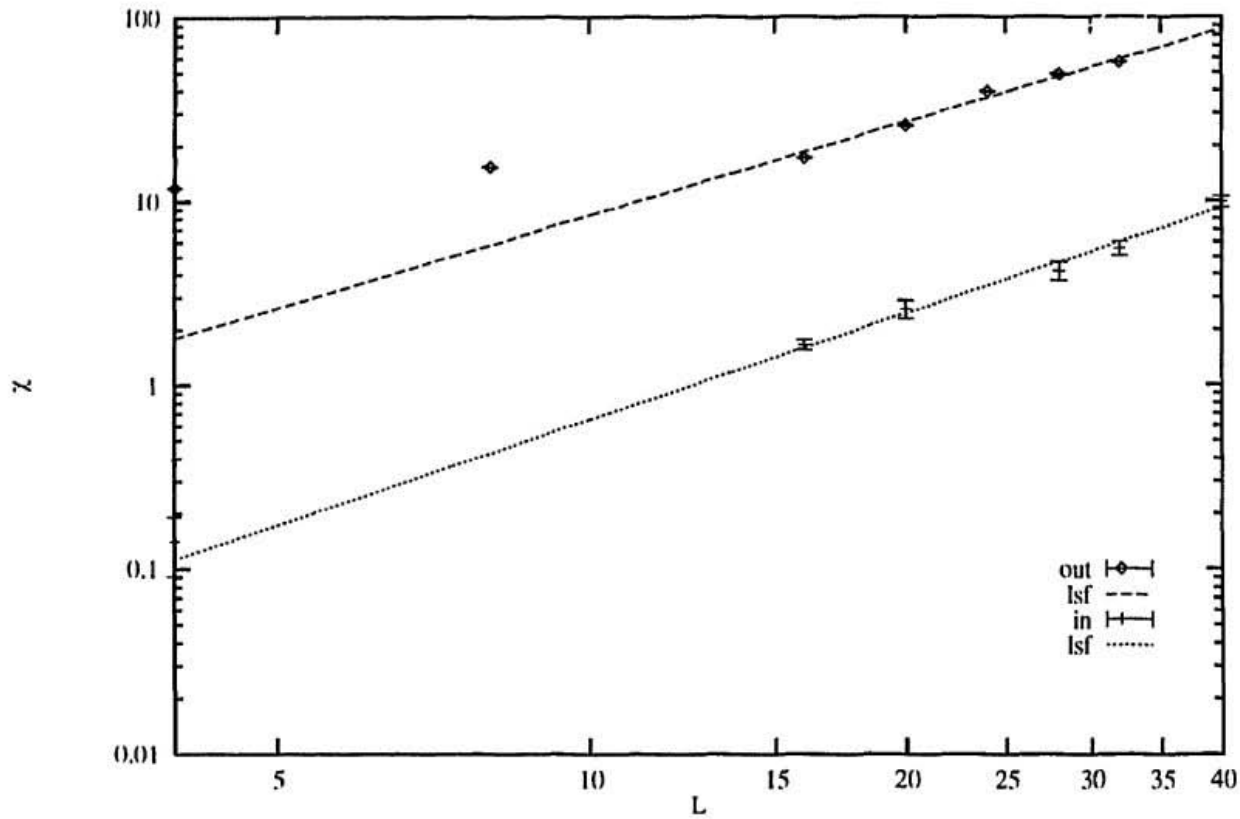

Figure 4.12: Least squares fit to $\log(\chi)$at θ_n vs $\log(L)$ for the out-of-plane and in-plane systems. The out-of-plane has been scaled by a factor of 10 to make viewing easier.

where x, y are critical exponents, N is the number of spins, t is the reduced temperature $\frac{\theta-\theta_n}{\theta_n}$ and $f(tN^y)$ is some unknown function. To fit three parameters (x, y, θ_n) is difficult when one does not know the form of the function $f(tN^y)$. We have, instead, tried to fit each of the parameters independently. We obtain a value for θ_n from our specific heat measurements. The exponent x may be fitted using equation 4.9 at $t = 0$, assuming that $f(0)$ is finite. Equation 4.9 then reduces to

$$< \Psi^2 >= N^x f(0) \tag{4.10}$$

A log-log graph of $< \Psi^2 >$ at $tN^y = 0$ versus N should have slope x. To estimate y, we look at $f(tN^y)$ near $tN^y = 0$. A Taylor expansion in the full variable tN^y, assuming that $f'(tN^y)$ near $tN^y = 0$ is well behaved, gives

$$f(tN^y) \approx f(0) + tN^y \frac{\partial f(tN^y)}{\partial tN^y}|_{tN^y=0} + \dots . \tag{4.11}$$

Substituting this result into equation 4.9, simplifying and taking the logarithm of both sides yields

$$\ln\left[\frac{< \Psi^2 >_t - < \Psi^2 >_0}{t}\right] \approx (x + y)\ln(N) + \ln(f'(0)). \tag{4.12}$$

A least squares fit of $\ln\left[\frac{<\Psi^2>_t - <\Psi^2>_0}{t}\right]$ verus $\ln(N)$ will have slope $(x + y)$. Here $< \Psi^2 >_t$ refers to $< \Psi^2 >$ evaluated at t. Our fitting gives $x = 1.9 \pm 0.2$ and $x + y = 2.4 \pm 0.2$, for the out-of-plane data and $x = 2.0 \pm 0.2$ and $x + y = 2.6 \pm 0.4$, for the in-plane data, both of which include within the error bars the two-dimensional Ising values of $x = 1.875$ and $x + y = 2.35$. The critical exponents x and y are related to the commonly used critical exponents α, β, and γ.[47][48] The relationships are,

$$\alpha = \frac{2y - 1 - 2x}{y}, \tag{4.13}$$

$$\beta = \frac{2 - x}{2y}, \tag{4.14}$$

$$\gamma = \frac{1 - x}{y}. \tag{4.15}$$

We have graphed the results of this data collapse in figures 4.13 and 4.14 in the standard manner for the out-of-plane and in-plane models respectively. We graph the logarithm of $< \psi^2 > N^{-x}$ versus $|tN^y|$. If the scaling form is correct and the exponents x and y are correct then the data should fall on a universal curve regardless of system size. The two branches in the graphs are for $t > 0$ (the lower branch) and $t < 0$ (the upper branch). The deviations from the universal curve by the smaller lattice systems are expected, since the smaller lattice systems have a smaller temperature range over which the scaling form is valid.

This supports our claim that our model is reproducing the static critical behaviour of the two-dimensional Ising model, placing our model in the same universality class as the Ising model.

4.4.1 Connections to Experiment

We may take our estimates for the critical temperatures from our specific heat data and convert these to estimates for the critical temperature for particular RE compounds. Our reduced temperature scale (Θ) is proportional to T in Kelvin. The exact relation is

$$\theta = \frac{2a^3 k_B T}{\mu_{\rm eff}^2} \tag{4.16}$$

where $\mu_{\rm eff}$ is the effective magnetic moment, and a is the lattice spacing. We again ignore the small difference between the a and b lattice vectors and assume a square system. To compare our results to experiment we graph in figures 4.15 and 4.16 the experimental Néel temperatures in units of $2a^3 k_B/\mu_b^2$ for those rare earth compounds for which $\mu_{\rm eff}$, T_n and spin orientation are known. The transition temperatures in Kelvins, effective moments, and spin orientation are also shown in table 4.1. We also graph the Monte Carlo critical temperature as a function of $\mu_{\rm eff}^2$for the two spin orientations, shown as a broken line in both figures. We find that the Monte Carlo estimate is consistently

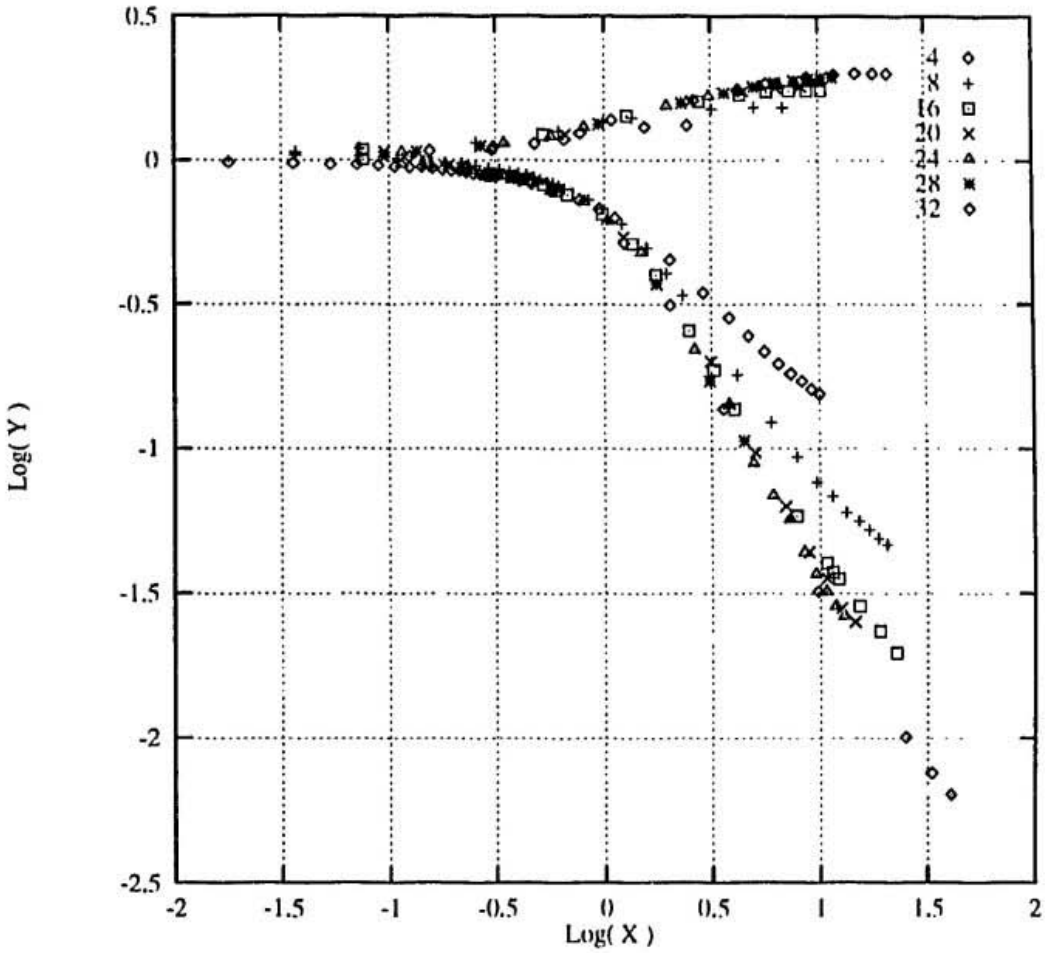

Figure 4.13: Data collapse for various sized out-of-plane systems. $X = |tN^y|$ and $Y = < \psi^2 > N^{-x}$. The critical exponent $x = 1.9 \pm 0.2$ and $x + y = 2.4 \pm 0.2$.

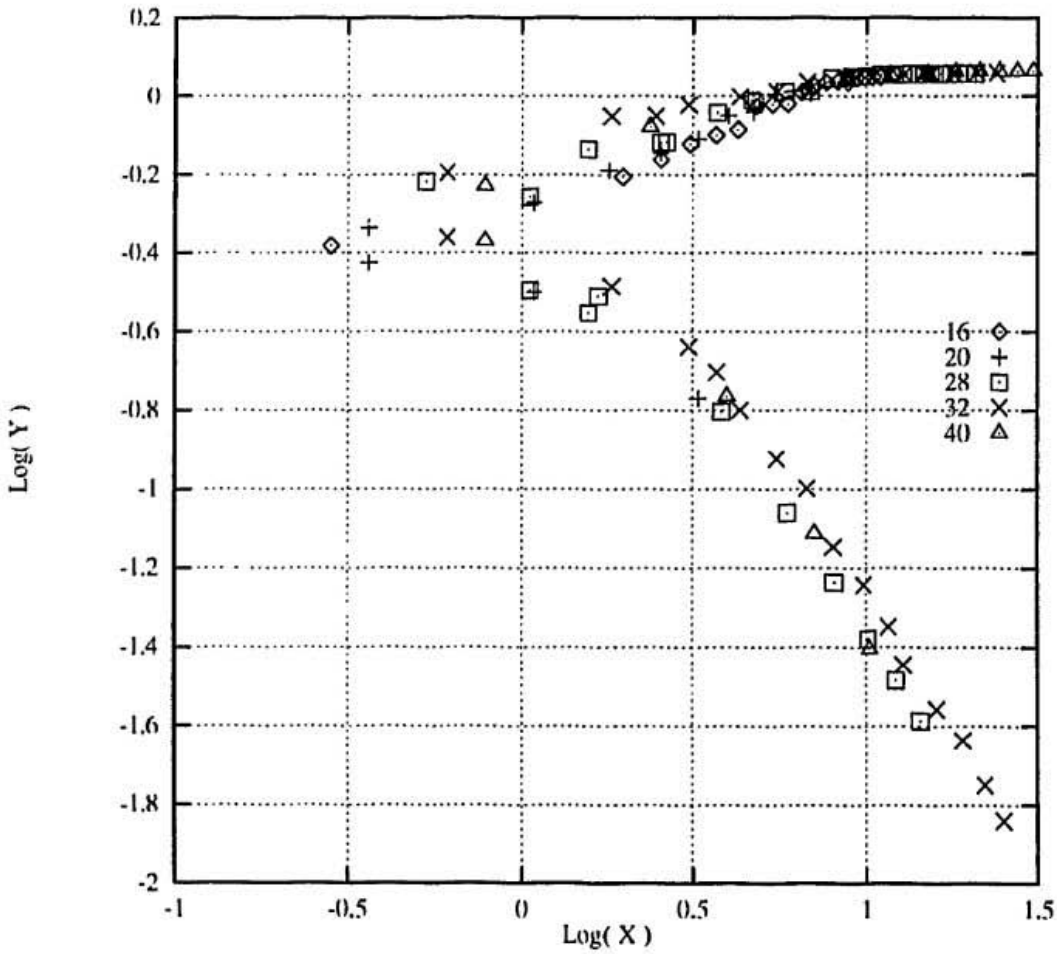

Figure 4.14: Data collapse for various sized in-plane systems. $X = |tN^y|$ and $Y = < \psi^2 > N^{-x}$. The critical exponent $x = 2.0 \pm 0.2$ and $x + y = 2.6 \pm 0.4$.

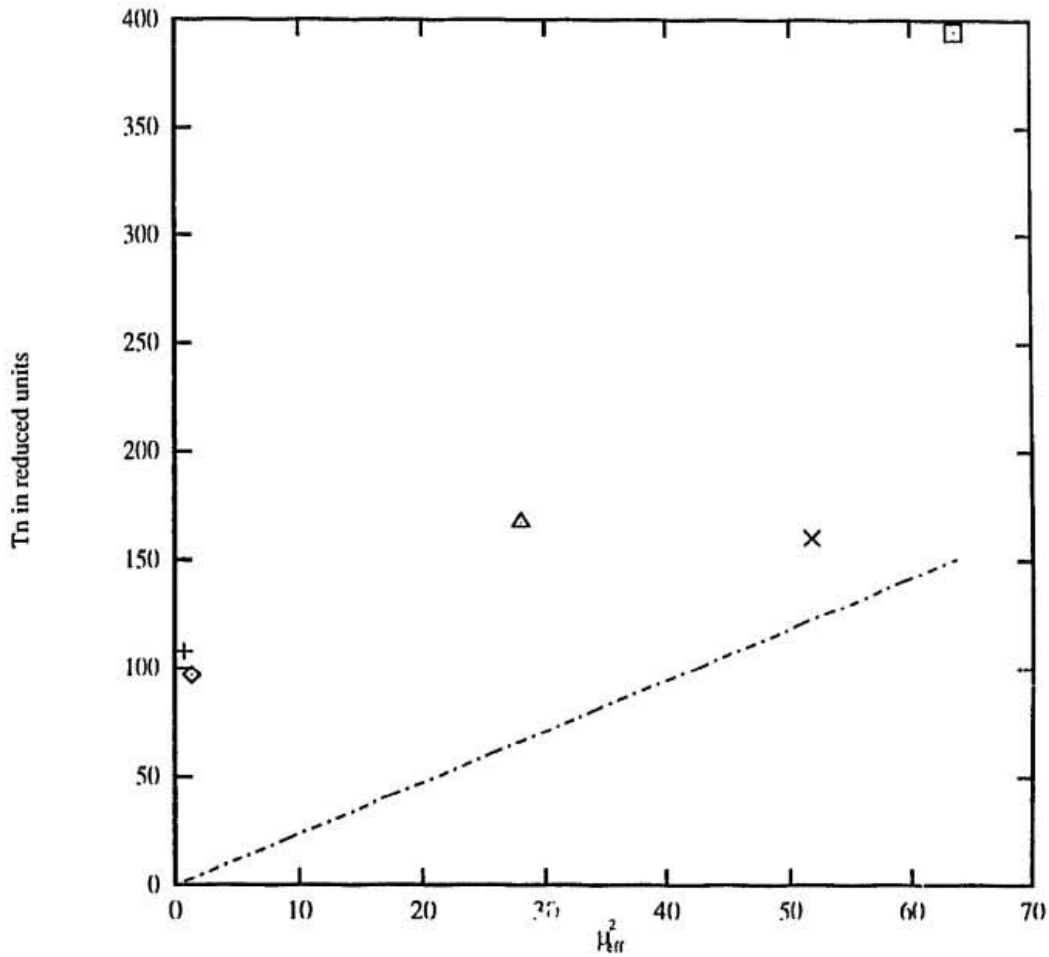

Figure 4.15: Comparison of experimental and Monte Carlo (broken line) estimates of the Néel temperature for various out-of-plane rare earths. + $NdBa_2Cu_3O_7$, ◇ $SmBa_2Cu_3O_7$ if out-of-plane, △ $DyBa_2Cu_3O_7$, × $Dy_2Ba_4Cu_8O_{16}$, □ $GdBa_2Cu_3O_7$.

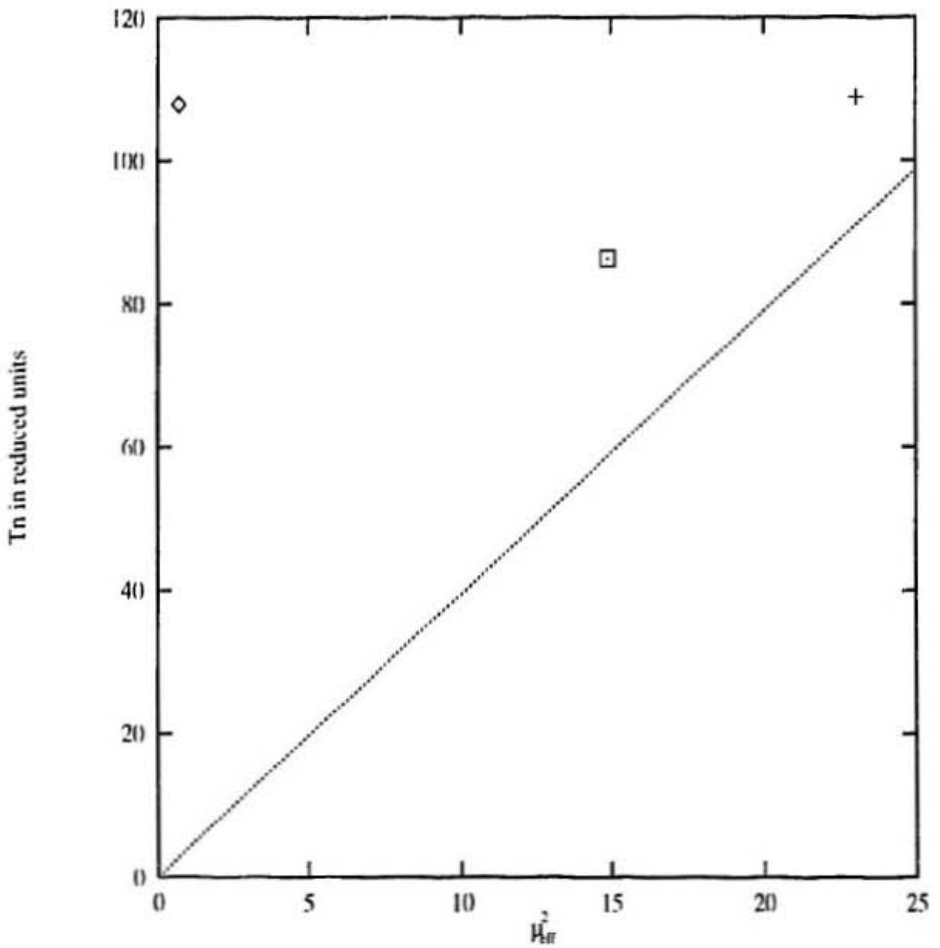

Figure 4.16: Comparison of experimental and Monte Carlo (broken line) estimates of the Néel temperature for various in-plane rare earths. ◇ $SmBa_2Cu_3O_7$ if in-plane, □ $Er_2Ba_4Cu_8O_{16}$ + $ErBa_2Cu_3O_7$.

Compound	μ_{eff}	T_n(exp)	T_n(MC)
$NdBa_2Cu_3O_7$	$1.14\mu_b$	0.551±0.05K	0.0161K
$SmBa_2Cu_3O_7$ if in-plane	$0.8452\mu_b$	0.612±0.05K	0.0148K
$SmBa_2Cu_3O_7$ if out-of-plane	$0.8452\mu_b$	0.612±0.05K	0.0089K
$GdBa_2Cu_3O_7$	$7.97\mu_b$	2.24K	0.787K
$DyBa_2Cu_3O_7$	$7.2\pm0.6\mu_b$	0.91K	0.642K
$ErBa_2Cu_3O_7$	$4.8\mu_b$	0.618K	0.478K
$DyBa_2Cu_4O_8$	$5.3\pm0.3\mu_b$	0.95K	0.348K
$ErBa_2Cu_4O_8$	$3.86\pm0.15\mu_b$	0.49K	0.309K

Table 4.1: Properties of various rare earth compounds

lower than the experimental values. This implies that the dipolar interaction alone is not sufficient to account for the observed transition temperatures. It will be necessary to include an additional interaction to account for the experimental results of chapter 1. The following sections will deal with the inclusion of a superexchange interaction in our Monte Carlo simulations.

4.5 $J \neq 0$

Since we were unable to account for the experimental Néel temperatures with a pure dipolar Hamiltonian, we will introduce a superexchange interaction as in equation 3.4. While there has been some speculation concerning a possible exchange interaction, [5][49] no mechanism of the exchange has been established. We expect that, given the layered structure and the anisotropy of these compounds, any intraplaner exchange interaction will be significantly different from any interplaner interaction.

We have limited ourselves to the case of $L = 16$, since this size of lattice has been shown to be in the scaling region of all the thermodynamic quantities we have been calculating, and yet is small enough to allow study in reasonable times.

4.5.1 Ground State Configurations

At $T = 0$ we are able to calculate using Ewald sums the energy for particular configurations as a function of the exchange parameter J. Assuming that one of our chosen configurations is the ground state, we are able to determine the change from one ground state to another. The configurations we have considered are based on the earlier findings of three dimensional studies [41] [50] as well as by direct observation of the low temperature simulations by the author and his collaborators. It is very possible that we have excluded, from our study, a configuration that for some value of J is the ground state. The long range nature of the dipole-dipole interaction, combined with the short-range exchange interaction makes it very difficult to predict the ground state for a system with both interactions. The configurations we have considered include the antiferromagnetic case (AA), the ferromagnetic case (FF), the two cases where we have antiferromagnetic ordering in one direction and ferromagnetic ordering in the second, (AF) and (FA), as well as some layered phases. These layered phases consist of a number of rows or columns of

spins pointing in one direction followed by a similar number of rows or columns of spins in the opposite direction, with this alteration of spin direction throughout the entire lattice. We will label these layered phases as (AF#) or (FA#), where # refers to the period of the antiferromagnetic ordering. For example (AF2) refers to a state which is ferromagnetic in the b direction but alternates in the a direction with two columns in the positive direction followed by two columns in the negative and so on, as shown in figure 4.17.

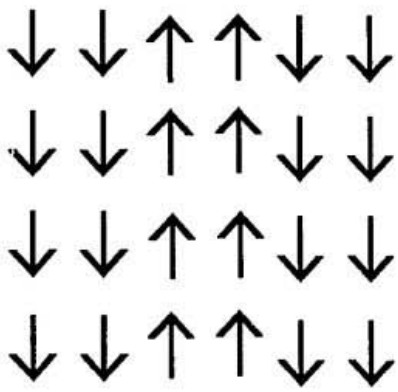

Figure 4.17: The AF2 phase.

We can see in figure 4.18 that for out-of-plane ordering at large positive J, we will have an antiferromagnetic ground state. This is reasonable as both the exchange and dipole interactions in this region favour an anti-ferromagnetic state so there is no conflict between the two interactions. As J is lowered we pass into the region of the phase diagram where J is negative, and hence the exchange interaction would separately favour the ferromagnetic state. There is now a conflict between the two interactions. There is a transition at $J = -0.855$, where the lowest energy state is the (AF) or (FA) state , since this state minimises the frustration of the two interactions. Note that since the a

and b lattice directions are equivalent for out of plane systems, when discussing the AF and AF# we will be implying both the AF and FA or the AF# and FA# states. This is only true for the out-of-plane case, as the in-plane system does not have this symmetry. The AF state continues to be the ground state until $J = -2.52$ when we move in to a region where the layered states become the ground state. The presence of a layered ground state in our phase diagram is one of the subtleties of long range interactions, that does not have to be considered when only short-range interactions are present. We have only calculated the energy of the layered states which have a period commensurate with the lattice. Since we are discussing a 16×16 lattice we only deal with a layered states with period 2,4, and 8. There is a transition from the AF to the AF2 at $J = -2.52$, from the AF2 to the AF4 at $J = -4.77$, and from the AF4 to the AF8 at $J = -7.05$. When $J = -7.896$ the ferromagnetic exchange interaction dominates over the dipolar interaction and the ground state becomes the FF state.

In our 16×16 system between the AF and the FF phase we show only four different phases. In the infinite system we might expect to see all layered phases, ie. the AF3, AF5.... In the finite system we may find regions where the lowest energy state consists of alternating layers with a period which is not commensurate with the lattice, with an extra domain wall to allow for the periodic boundary condition. This makes it very difficult at non-zero temperature to distinguish phase boundaries. To emphasise a point, one must remember that in order to determine the ground state, we must guess at possible ground states, then calculate the energy of states to determine the true ground state. It is very possible that we have excluded from consideration some states that for certain values of J are the lowest energy states.

The zero temperature portion of the phase diagram for in-plane spins, shown in figure 4.19, appears simplier than the its out-of-plane counterpart. The dipolar interaction is not symmetric for in-plane spins, hence it is no longer valid to consider the AF and

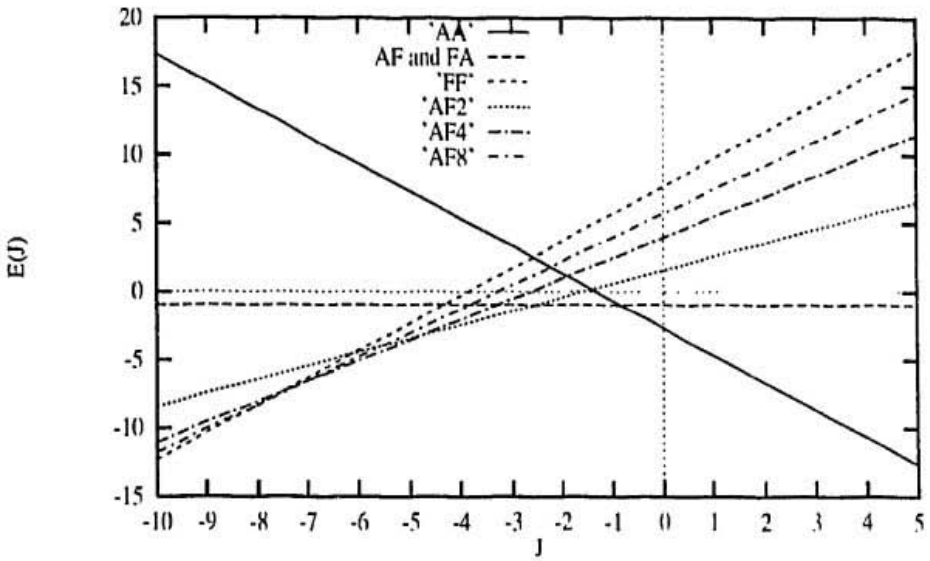

Figure 4.18: The ground state energy of various phases for the out of plane configuration, where zero is defined as the energy in the absence of all interactions.

FA phases together. At sufficiently large positive J the exchange interaction dominates, and the ground state is the pure antiferromagnetic state. When J is lowered, there is a transition at $J = 3.2$, at which point the ground state is the dipolar ground state, AF. When $J = -0.30$ it appears that the ferromagnetic exchange interaction dominates and the ground state is the (FF) state. At the boundary between the ferromagnetic phase and the AF phase, we have a very interesting set of circumstances. The layered phases, the ferromagnetic phase, and the AF phase all have the same energy. If we recall the discussion above concerning the difficulties we had with the pure dipolar system, we can understand the source of these difficulties. There will be a large number of states with energy very near the ground state. These states will allow for the formation of domain walls with only a small increase in energy. These domain walls will be very stable and as they move through the system they can cause large fluctuations in the order parameter,

making an accurate calculation of the order parameter and the susceptibility very difficult.

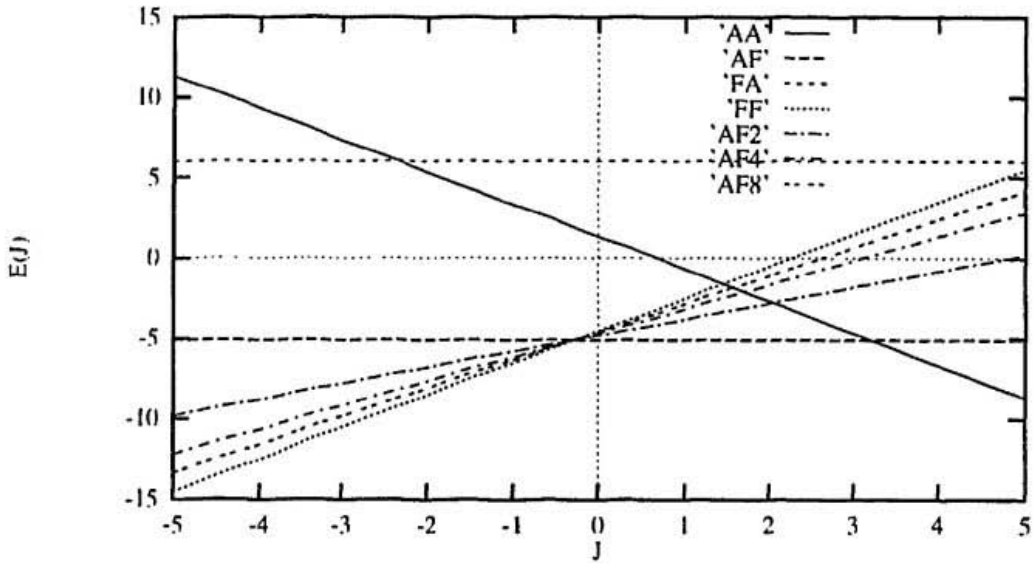

Figure 4.19: The ground state energy of various phases for the in plane configuration, where zero is defined as the energy in absence of all interactions.

4.5.2 Phase Diagram

In figure 4.20 we present the phase diagram for the out of plane model, showing the various phases in the temperature-exchange parameter plane. The upper portion of the diagram shows the disordered phase, which is separated from the ordered phases by a line of second order phase transitions. The values of θ_n for various values of J were determined from the peak of the specific heat for simulations where J was held fixed and the temperature was varied. One might note that we have transitions from the disordered state to a ferromagnetically ordered state, so, strictly speaking, we should refer to the transition temperatures as Curie temperatures instead of Néel temperatures. We will

not make a notational distinction and will refer to both types of critical temperatures as θ_n. The error in this line is approximately ± 0.2. On the far left and far right of this line one has a linear relation between θ_n and J. In these regions the short-range exchange interaction dominates the dipolar interaction and $|\frac{\Delta J}{\Delta \theta_n}|$ is constant and equal to the appropriate two-dimensional, spin 1/2 Ising value. Going from right to left we

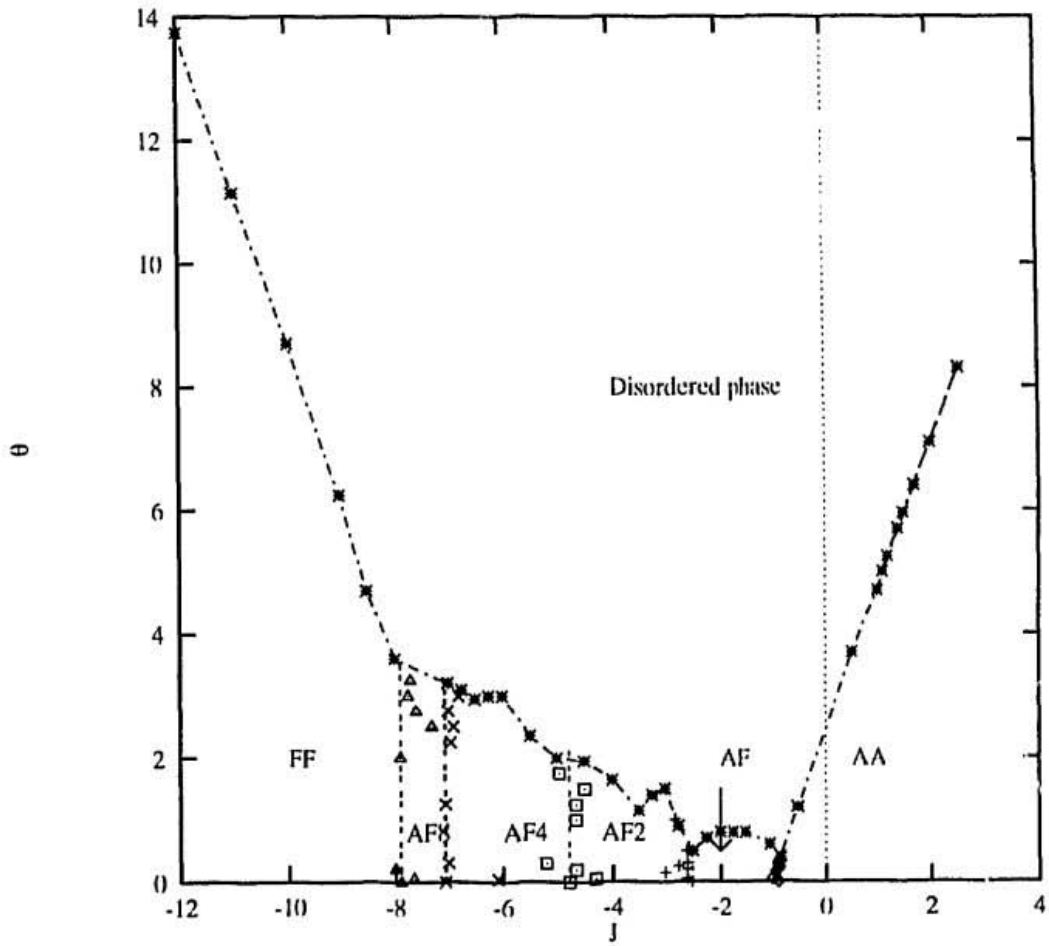

Figure 4.20: Phase diagram for out-of-plane model

see the various phases in the low temperature region. When J is sufficiently large and

positive we have a pure antiferromagnetic phase, which as J is lowered and becomes negative changes to a AF phase. As J is lowered further the ground state becomes one of the layered states. The order-disorder transition phase boundary is less than smooth in this region which is understandable since we have limited the phases we deal with to those which are commensurate with the systems dimensions. Other phases with periods not commensurate with the system will affect our results.

The vertical lines which extend from T=0 to the order-disorder transition line are drawn upward from the T=0 transition points. Simulations were done at fixed temperature with variable J, to see if one could determine the transition from one ordered phase to another. For this model it is difficult to determine the transition point exactly as the transitions are first order and there is significant hysteresis in the simulations. The results of these simulations are included in the phase diagram, and we quote no error bars on these estimates because we have no real estimate of their accuracy.

The in-plane phase diagram is simpler than the out-of-plane diagram since the layered phases are not present. In figure 4.21 we find a line of second order phase transitions separating the disordered phase from the ordered phases. This line was determined from simulations at fixed J, with the temperature varied to determine the peak of the specific heat. Beginning from the far right, at large positive values of J, the ground state is the pure antiferromagnetic state. At $J = 3.2$, the ground state switches to the AF phase, and at $J = -0.3$ the ferromagnetic state is the lowest energy state. One may note that a small ferromagnetic exchange interaction (< -0.3) is sufficient to cause a change from the dipolar ground state to the ferromagnetic ground state.

We must be careful at the transition between the AF and FF phases since the energies of all the layered phases, the ferromagnetic, and the AF phase all have the same energy. We feared that this would make the determination of the phase boundary between the AF and FF phase difficult at low temperature, but this appears not to be the case. In

simulations done with T fixed and J varying, the transition between the AF and FF phases is very evident in the energy as a function of J. A sharp change in the slope of the average energy is seen at $J = -0.3$ in the simulations done at T = 1.0, 2.0, 3.0, and 4.0. This appears as a discontinuity in the specific heat as a function of J as well. The phase boundary between the AF, and FF phases is vertical, as shown in figure 4.21. Similarly the phase boundary between the AA and AF phase is also vertical and is found at $J = 3.2$.

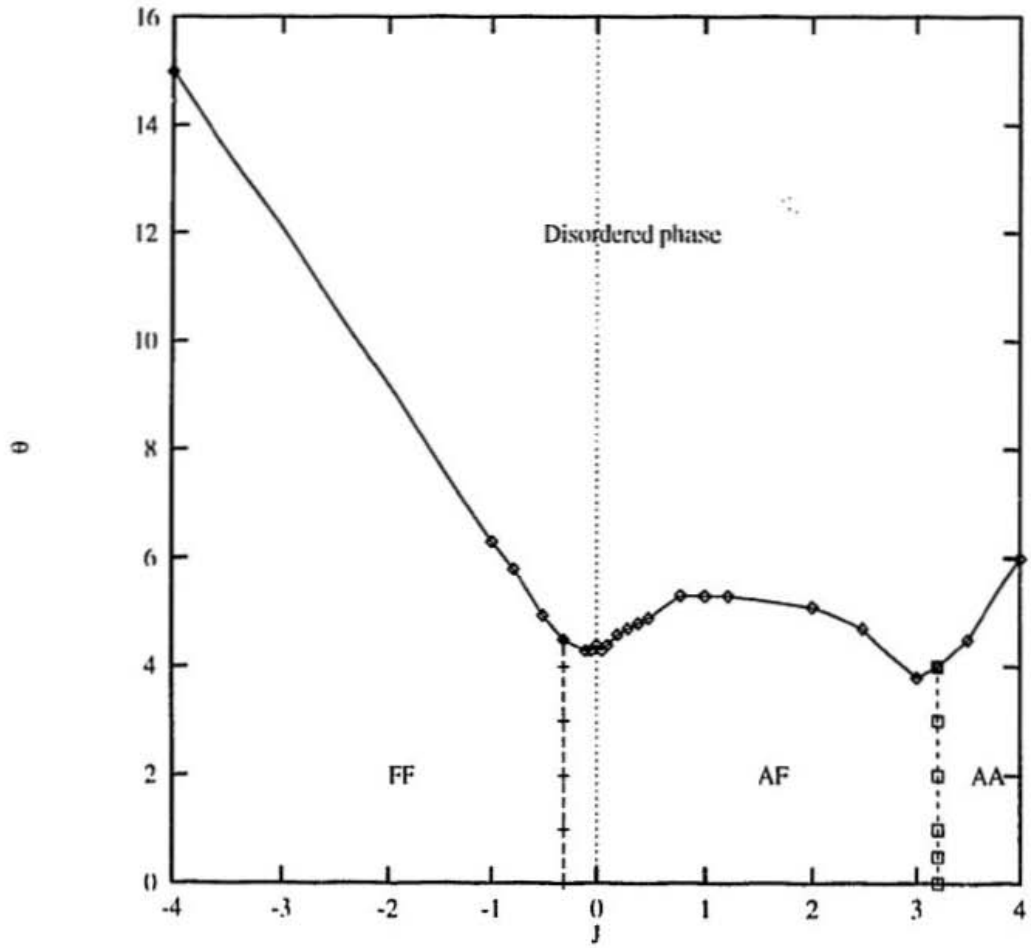

Figure 4.21: Phase diagram for the in-plane model.

4.5.3 Connections to Experiment

With the inclusion of a superexchange interaction to our Hamiltonian we have added a new parameter to our model, that being the exchange parameter J. There is some restriction to the values of θ_n which we may obtain, by adjusting the value of J. The lowest possible transition temperature is between 0.2 and 0.6 for the out-of-plane model and 3.60 and 4.00 in the in-plane model; all temperatures are in units of $\frac{\mu_{\rm eff}^2}{2a^3 k_B}$. There is a second restriction on J when comparing to experiments. As J is varied the ground state also changes, so for an estimate of the exchange parameter to be relevant it is necessary that the value of J obtained correspond to a system with the experimentally determined ground state. If we treat J as a free parameter, and adjust J to obtain the proper experimental Néel temperature for the Kramer's ions, Er, Dy, Gd, and Nd, the correct ground state is realised in each case.

Rather than simply using J as a fitting parameter it would be more constructive if we could make an independent estimate of J and then compare the resulting transition temperatures for the various compounds to those found experimentally. By assuming that $\mathcal{J}$ in equation 3.6 is a constant for all the rare earths,[3][5] we may estimate the exchange parameter J for any compound given J for one compound. If we fit J so as to get the proper T_n for $DyBa_2Cu_3O_7$, we may estimate J for $ErBa_2Cu_3O_7$: Dy and Er being the rare earths for which our model is most valid. We choose to fit to the experimental value of T_n for $DyBa_2Cu_3O_7$ because this compound, based on crystal field calculations [3], is the experimental system most similar to our model system. As well in the region of interest on the out-of-plane phase diagram, which is appropriate for Dy, we find that the critical temperature has a simple linear dependence on J.

Applying the above procedure, $J(Dy) = 0.51$, and $J(Er) = \frac{4}{9}J(Dy) = 0.23$, in units of $(\frac{\mu_{\rm eff}^2}{2a^3 k_B})$. Using this value of J to estimate the critical temperature for $ErBa_2Cu_3O_7$,

gives $T_n(Er) = 0.57K \pm 0.17K$, which agrees, within experimental error, with the experimental value $0.618K$, and differs from the experimental value by 10%, The largest error in our estimate is actually the $\approx$ 10% error in determining $\mu_{\rm eff}$ experimentally. Other uncertainties are in determining the magnitude of the lattice vector a, and the error in our estimate of θ_n from the simulations, however they do not contribute significantly to the error. Our estimate for J in $ErBa_2Cu_3O_7$ yields, in our Monte Carlo simulations, a ground state which is the same as that found experimentally.

While we do not expect our model to be valid for $GdBa_2Cu_3O_7$, mainly due to the 8-fold, degenerate ground state, it is nevertheless interesting to extend the previous arguments. With the same assumptions as above we find that $J(Gd) = 4.J(Dy) = 2.04$. If this is a reasonable estimate of the exchange interaction, then we are able to account for $GdBa_2Cu_3O_7$ having a AA ground state instead of the pure dipolar ground state, AF. For $J = 2.04$ the ground state energy of the AF phase is -5.098, while the ground state energy of the AA phase is -6.544, where both energies are in units of $\frac{\mu_{\rm eff}^2}{2a^3 k_B}$, and where we have defined the zero of our energy scale as the energy of the system in the absence of any interactions. If we naively continue our analysis, we estimate the critical temperature for $GdBa_2Cu_3O_7$ to be $T_n = 1.75K \pm 0.38$, which differs by 22% when compared to the experimental value of $2.24K \pm 0.01$. Even though our estimate of T_n does not agree, within experimental error, with the experimentally determined transition temperature, that we have even a reasonable value when we apply our model to $GdBa_2Cu_3O_7$ is quite remarkable.

4.6 E.S.M. versus M.I.T.

As a comparison to the Ewald summation method we have simulated some out-of-plane, L=16 systems using the minimum image technique. The ground state energy differs

by approximately 19% when compared to the value of De'Bell and Whitehead.[24] We graph the energy, specific heat, order parameter, and susceptibility for systems with a pure dipolar interaction using both methods in figures 4.22, 4.23, 4.24, and 4.25. We find the that the M.I.T. estimates a T_n which is smaller that the E.S.M. by 31%. The M.I.T. value being $T_n = 1.68 \pm 0.1$ and the E.S.M. transition temperature being $T_n = 2.44 \pm 0.05$ for a 16 by 16 system. In the limit of $L \rightarrow \infty$ both methods should give the same results for the critical temperature and the critical exponents. The large discrepancy, even for $L = 16$, between the results of the E.S.M. and the M.I.T. implies that the finite size effects are still very large. We expect that the finite size effects in the E.S.M. are smaller than in the M.I.T. Since system size is limited by computing time constraints, the extra complexity of the E.S.M. is a necessary complication.

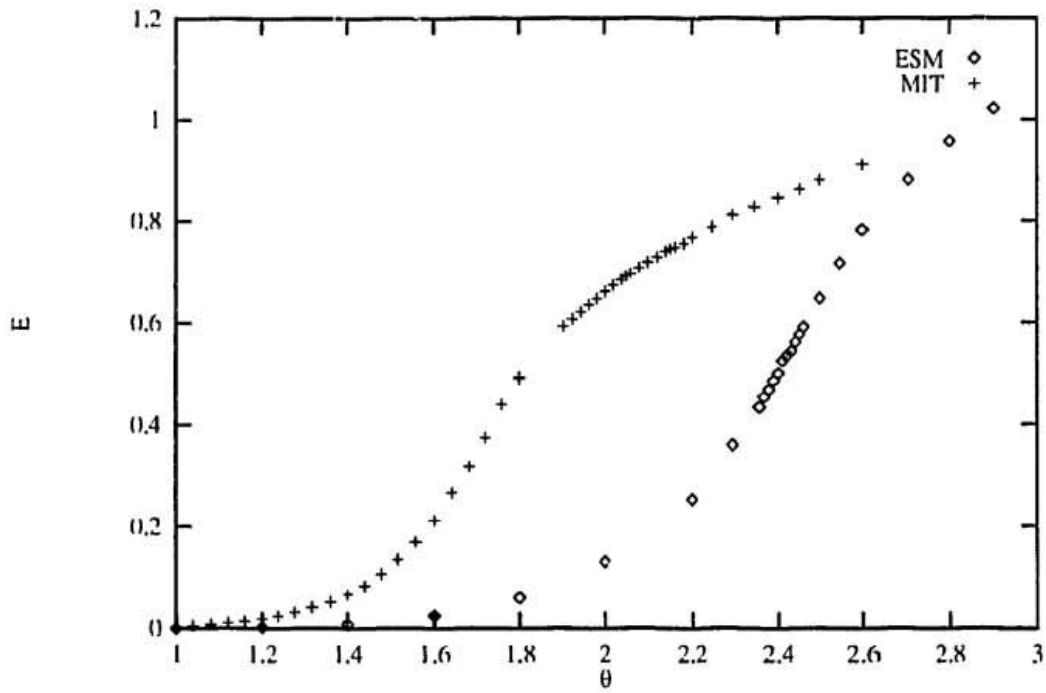

Figure 4.22: Comparison of the average energy for a 16x16 system using ESM and MIT, zero is defined as the ground state energy for each method.

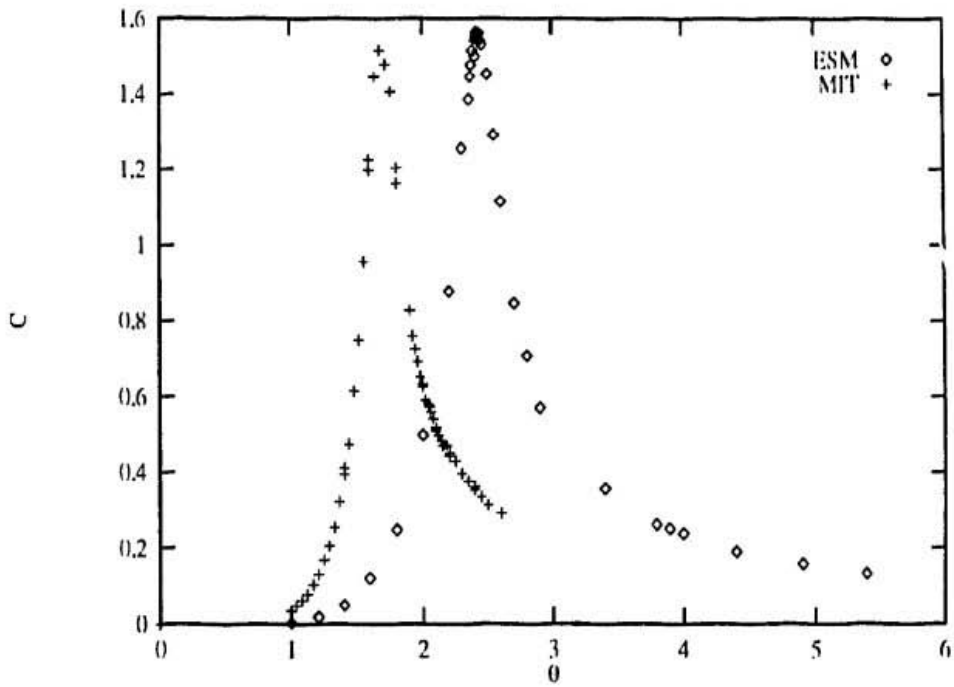

Figure 4.23: Comparison of the specific heat for a 16x16 system using ESM and MIT.

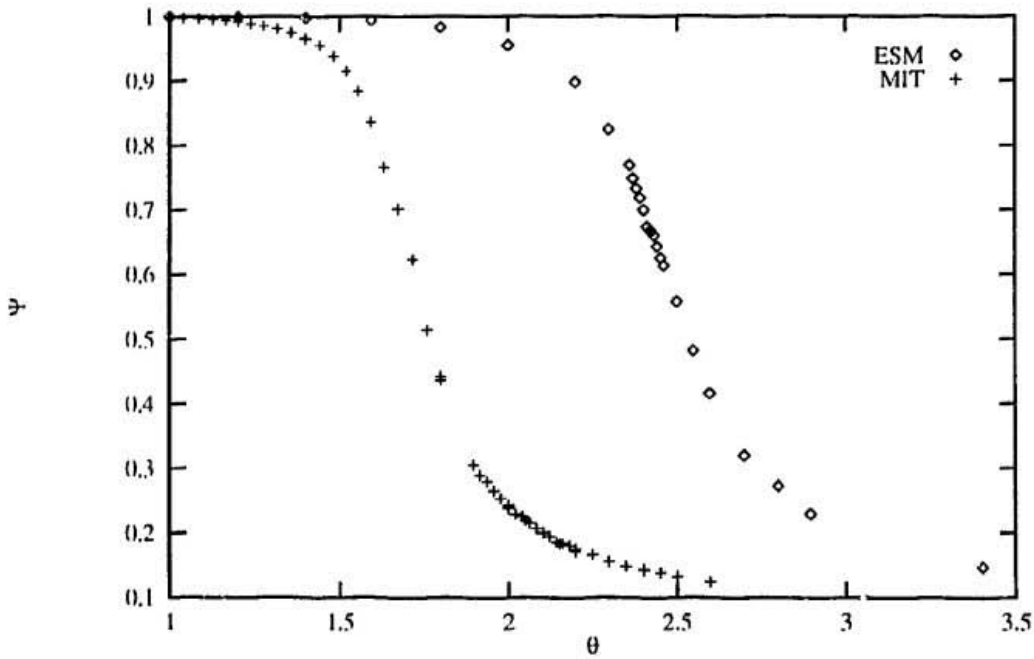

Figure 4.24: Comparison of the order parameter for a 16x16 system using ESM and MIT.

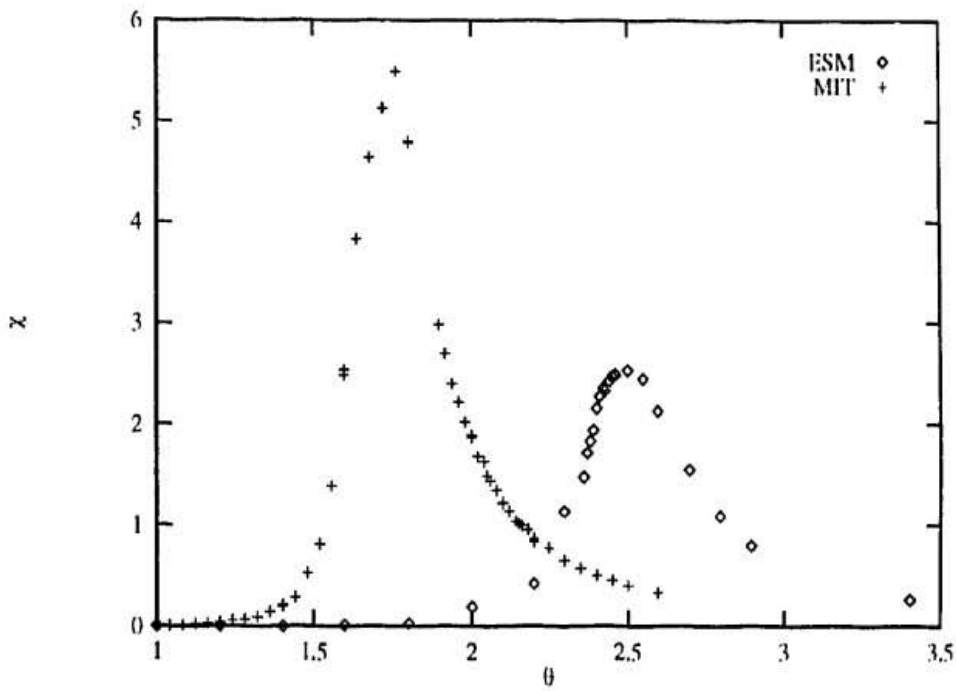

Figure 4.25: Comparison of the susceptibility for a 16x16 system using ESM and MIT.

Chapter 5

Conclusion

The results, presented in this thesis, concerning the two dimensional Ising model with a dipolar and exchange interaction are of considerable interest because of what has been learned concerning dipolar systems, and their critical properties at low temperature. As well the comparison of these results to the experimental systems $REBa_2Cu_3O_{7-\delta}$, partially answers some of the many questions concerning the magnetic ordering at low temperature, on the rare earth sublattice in these compounds.

We have been able to show, using Monte Carlo methods that a two dimensional, uniaxial spin model on a square lattice, where the spins are coupled by a pure dipolar interaction, appears to belong to the same universality class as the two-dimensional S=1/2 Ising model with a nearest neighbour exchange interaction. The critical exponents for both spins orientations are, $\frac{\beta}{\nu} = 0.12 \pm 0.01$ for the in-plane model and $\frac{\beta}{\nu} = 0.12 \pm 0.03$ and out-of-plane models, and $\frac{\gamma}{\nu} = 1.7 \pm 0.4$ for the out-of-plane, and $\frac{\gamma}{\nu} = 1.9 \pm 0.4$ for the in-plane model. The critical reduced temperature for the transition from the disordered to ordered state is $\theta_u = 2.37 \pm 0.05$ when the spins are restricted to orient perpendicular to the plane of the system, and $\theta_u = 3.95 \pm 0.1$ when the spins are confined to one of the in-plane axes. Our claims are, of course, based upon the assumption that $\nu = 1$, which is consistent with all our data, but is still an assumption.

We have also determined the phase diagram for two possible spin orientations, when there is an exchange interaction as well as the dipolar interaction. We have studied systems with the moments confined to point along the b axis and along the c axis. The

complexity of the phase diagram depends on the spin orientation, but we are able to show the regions of phase space where one finds the anti-ferromagnetic, the ferromagnetic, the dipolar ground state, as well as a number of layered states which are not found in either the pure exchange or pure dipolar models, and the disordered state. Our phase diagrams are calculated for a 16×16 system, but we expect that it qualitatively mimics the phase diagram of the infinite system.

By applying our results to the rare earth compounds, $REBa_2Cu_3O_{7-\delta}$, we have been able to better our understanding of the magnetic ordering in these compounds. We have made several assumptions in developing our model for $REBa_2Cu_3O_{7-\delta}$. We have assumed that the magnetic moments are uniaxial and the systems are quasi-two dimensional, which is most appropriate for $DyBa_2Cu_3O_{7-\delta}$ and $ErBa_2Cu_3O_{7-\delta}$. We have shown that a pure dipolar interaction is not sufficient to account for the magnetic ordering on the rare earth sublattice in these compounds. Our estimate for T_n based on a pure dipolar interaction falls consistently lower than the experimental value. With the inclusion of a superexchange interaction, which has been proposed previously by others [25], we are able to fit the experimental values of T_n, and still maintain the proper experimentally determined, in-plane, ground state. With a further assumption concerning the strength of the exchange interaction, applied to the two compounds for which the our model is most valid allows us to predict the transition temperature for $ErBa_2Cu_3O_7$ within 10% based solely on our simulations and experimental results for $DyBa_2Cu_3O_7$. If we extend this analysis to include $GdBa_2Cu_3O_7$, for which the validity of our model in very uncertain, we are able estimate the critical temperature to within 22% of the experimental value.

In this work we have, out of necessity, made some assumptions concerning the effective dimensionality of the system, and the effective dimensionality of the magnetic moment. The second phase of this work will examine the consequences of these assumptions. In particular experimental work supports the proposition that in $ErBa_2Cu_3O_7$ there

is a transition from a planar spin system to an uniaxial spin system above the Néel temperature. A dipolar XY model is much more complicated a problem than the uniaxial dipolar model, and has not been treated using Monte Carlo in any conclusive study. The next step in this study will involve a comprehensive study of the dipolar XY model. As well the two dimensional restriction in our model will have to be removed. While the dipolar interaction in the c direction has been shown to be four orders of magnitude smaller between the planes than in the planes, no such limitation can be put on an interplanar exchange interaction. As a further extension, the inclusion of an interplanar exchange interaction will be explored.

Appendix A

Derivation of Dipolar Hamiltonian

We begin with a general Hamiltonian describing the interaction between a collection of dipoles with moment $\vec{\mu} = \mu_{\text{eff}}\vec{\sigma}$, where $|\vec{\sigma}| = 1$

$$\mathcal{H} = \frac{1}{2}\mu_{\text{eff}}^2 \sum_{n,m} \sigma_n^\alpha \sigma_m^\beta \lim_{\vec{r}\to 0} \frac{\partial}{\partial r_\alpha} \frac{\partial}{\partial r_\beta} \frac{1}{|\vec{R}_{nm} - \vec{r}|} \tag{A.1}$$

The displacement of the m^{th} spin relative to the n^{th} spin is given by $\vec{R}_{nm}$.

We limit our collection of moments to those where the configuration satisfies the periodic condition.

$$\vec{\mu}_n = \vec{\mu}_{n'} \text{ when } \vec{r}_n = \vec{r}_{n'} + \vec{G} \ , \tag{A.2}$$

$\vec{G}$ being any lattice vector. Therefore any system of spins maybe reduced to a basic unit cell and replicas of this unit cell, as in figure 3.1. We will assume that our system consists of a basic unit cell with $N = L^2$ spins, on a square lattice. This square lattice is described by a perpendicular basis $(a\hat{e}_1, a\hat{e}_2)$. We can convert the sum over all lattice points, to a sum over all points in a $L \times L$ basic unit cell, and a sum over all lattice vectors. The Hamiltonian may then be rewritten as

$$\begin{aligned}\mathcal{H} = \frac{1}{2}\frac{N}{L^2}\mu_{\text{eff}}^2 \sum_{\vec{G}} {\sum_{n,m}}' \sigma_n^\alpha \sigma_m^\beta \lim_{\vec{r}\to 0} \frac{\partial}{\partial r_\alpha} \frac{\partial}{\partial r_\beta} \frac{1}{|\vec{r}_{nm} + \vec{G} - \vec{r}|} + \\ \frac{1}{2}\frac{N}{L^2}\mu_{\text{eff}}^2 \sum_{\vec{G}} {\sum_{n}}' \sigma_n^{\alpha 2} \lim_{\vec{r}\to 0} \frac{\partial^2}{\partial r_\alpha^2} \frac{1}{|\vec{r}_{nn} + \vec{G} - \vec{r}|},\end{aligned} \tag{A.3}$$

where the prime on the sums restricts n and m to those sites in our basic unit cell. The second term will be a constant for any $\{\vec{\mu}\}$, as it is independant of the configuration.

This term contains information on the interaction between a spin and each of its image spins. We refer to this quantity as a self-interaction and define the constant **C** such that:

$$\mathcal{H} = \frac{1}{2}\frac{N}{L^2}\mu_{\rm eff}^2\left[\mathbf{C} + \sum_{\vec{G}}{\sum_{n,m}}' \sigma_n^\alpha \sigma_m^\beta \lim_{\vec{r}\to 0}\frac{\partial}{\partial r_\alpha}\frac{\partial}{\partial r_\beta}\frac{1}{|\vec{r}_{nm}+\vec{G}-\vec{r}|}\right]. \tag{A.4}$$

We now define an effective interaction $\mathcal{W}$,

$$\mathcal{W}^{\alpha\beta}\left(\frac{\vec{r}_{nm}}{a}\right) = a^3 \lim_{\vec{r}\to 0}\frac{\partial}{\partial r_\alpha}\frac{\partial}{\partial r_\beta}\sum_{\vec{G}}\frac{1}{|\vec{r}_{nm}+\vec{G}-\vec{r}|}, \tag{A.5}$$

and rewrite the Hamiltonian as

$$\mathcal{H} = \frac{1}{2}\frac{N}{L^2}\frac{\mu_{\rm eff}^2}{a^3}\left[\mathbf{C}a^3 + {\sum_{n,m}}' \sigma_n^\alpha \mathcal{W}^{\alpha\beta}\left(\frac{\vec{r}_{nm}}{a}\right)\sigma_m^\beta\right]. \tag{A.6}$$

where

$$\frac{1}{|\vec{r}_{nm}+\vec{G}-\vec{r}|} = \frac{2}{\sqrt{\pi}}\int_0^\infty d\rho e^{-(\vec{r}_{nm}+\vec{G}-\vec{r})^2\rho^2}. \tag{A.7}$$

Summing over lattice vectors $\vec{G}$ yields,

$$\sum_{\vec{G}}\frac{1}{|\vec{r}_{nm}+\vec{G}-\vec{r}|} = \frac{2}{\sqrt{\pi}}\int_0^\infty d\rho \sum_{\vec{G}} e^{-(\vec{r}_{nm}+\vec{G}-\vec{r})^2\rho^2} \tag{A.8}$$

$$= \frac{2}{\sqrt{\pi}}\int_0^\infty d\rho \sum_{\vec{G}} e^{-(\vec{G}+\vec{r}_{nm}-\vec{r})^2\rho^2} \tag{A.9}$$

$$= \frac{2}{\sqrt{\pi}}\int_0^\infty d\rho \sum_{\vec{G}} e^{-[G^2+(\vec{r}_{nm}-\vec{r})^2+2\vec{G}\cdot(\vec{r}_{nm}-\vec{r})]\rho^2} \tag{A.10}$$

$$= \frac{2}{\sqrt{\pi}}\int_0^\infty d\rho e^{-(\vec{r}_{nm}-\vec{r})^2\rho^2}\sum_{\vec{G}} e^{-[G^2+2\vec{G}\cdot(\vec{r}_{nm}-\vec{r})]\rho^2}. \tag{A.11}$$

Now, since we have a square lattice with lattice constant a and L sites on an edge, we may write,

$$\vec{G} = La(n_1\hat{e}_1 + n_2\hat{e}_2). \tag{A.12}$$

Therefore substituting equation A.12 in to equation A.11 and rescaling $\vec{r} = \vec{x}a$:

$$\sum_{\vec{G}}\frac{1}{|\vec{r}_{nm}+\vec{G}-\vec{r}|} = \frac{2}{\sqrt{\pi}}\int_0^\infty d\rho e^{-\rho^2a^2(\vec{r}_{nm}-\vec{r})^2}\prod_\beta\sum_{n_\beta} e^{-\rho^2L^2a^2\left[2n_\beta\frac{(x_{nm}^\beta-x^\beta)}{L}+n_\beta^2\right]} \tag{A.13}$$

Now we rescale $\rho \rightarrow \rho La$. Therefore $d\rho \rightarrow Lad\rho$ giving,

$$\sum_{\vec{G}} \frac{1}{|\vec{r}_{nm} + \vec{G} - \vec{r}|} = \frac{2}{\sqrt{\pi}} \int_0^\infty \frac{d\rho}{La} e^{-\frac{\rho^2}{L^2}(\vec{r}_{nm} - \vec{r})^2} \prod_{\beta} \sum_{u_\beta} e^{-\rho^2 \left[2u_\beta \frac{(r^\beta_{nm} - r^\beta)}{L} + u_\beta^2\right]}. \tag{A.14}$$

This integral will converge quickly for large values of ρ, but not for small ρ. Therefore we divide the integral into two parts: one quickly convergent and one slowly convergent. We rewrite the above as:

$$\sum_{\vec{G}} \frac{1}{|\vec{r}_{nm} + \vec{G} - \vec{r}|} = \frac{2}{\sqrt{\pi} La} [\mathbf{A} + \mathbf{B}] \tag{A.15}$$

with

$$\mathbf{A} = \int_\eta^\infty d\rho e^{-\frac{\rho^2}{L^2}(\vec{r}_{nm} - \vec{r})^2} \prod_{\beta} \sum_{u_\beta} e^{-\rho^2 \left[2u_\beta \frac{(r^\beta_{nm} - r^\beta)}{L} + u_\beta^2\right]} \tag{A.16}$$

and

$$\mathbf{B} = \int_0^\eta d\rho e^{-\frac{\rho^2}{L^2}(\vec{r}_{nm} - \vec{r})^2} \prod_{\beta} \sum_{u_\beta} e^{-\rho^2 \left[2u_\beta \frac{(r^\beta_{nm} - r^\beta)}{L} + u_\beta^2\right]} \tag{A.17}$$

The value of η is chosen such that **A** will be quickly convergent and therefore we work on writing **B** in a more managable manner.

If we take the Jacobi Theta function:

$$\Theta_3(Z; X) = \sum_{l=-\infty}^{\infty} e^{-\pi(2lZ + l^2 X)}, \tag{A.18}$$

and the Imaginary Transform

$$\Theta_3(Z; X) = \frac{e^{\pi \frac{Z^2}{X}}}{\sqrt{X}} \Theta_3\left(\frac{Z}{iX}; \frac{1}{X}\right) \tag{A.19}$$

and let

$$l = u_\beta$$
$$Z = \frac{(\vec{x}^\beta_{nm} - \vec{x}^\beta)\rho^2}{\pi L}$$
$$X = \frac{\rho^2}{\pi},$$

we may write **B** as

$$\mathbf{B} = \int_0^\eta d\rho\, e^{-\frac{L^2}{L^2}(\vec{r}_{nm}-\vec{r})^2} \prod_\beta \Theta_3\left(\frac{(\vec{r}^\beta_{nm}-\vec{r}^\beta)\rho^2}{\pi L}; \frac{\rho^2}{\pi}\right) \tag{A.20}$$

$$= \int_0^\eta d\rho\, e^{-\frac{L^2}{L^2}(\vec{r}_{nm}-\vec{r})^2} \prod_\beta \frac{1}{\sqrt{\frac{L^2}{\pi}}} e^{+\frac{L^2}{L^2}(\vec{r}^\beta_{nm}-\vec{r}^\beta)^2} \Theta_3\left(\frac{(\vec{r}^\beta_{nm}-\vec{r}^\beta)}{iL}; \frac{\pi}{\rho^2}\right) \tag{A.21}$$

$$= \int_0^\eta \frac{d\rho\pi}{\rho^2} \prod_\beta \Theta_3\left(\frac{(\vec{r}^\beta_{nm}-\vec{r}^\beta)}{iL}; \frac{\pi}{\rho^2}\right). \tag{A.22}$$

To simplify we let $\rho \to \frac{1}{\rho}$ and rewrite equation A.22 as

$$\mathbf{B} = \int_\infty^{\frac{1}{\eta}} -d\rho\pi \prod_\beta \Theta_3\left(\frac{(\vec{r}^\beta_{nm}-\vec{r}^\beta)}{iL}; \pi\rho^2\right) \tag{A.23}$$

$$= \pi \int_{\frac{1}{\eta}}^\infty d\rho \prod_\beta \Theta_3\left(\frac{(\vec{r}^\beta_{nm}-\vec{r}^\beta)}{iL}; \pi\rho^2\right) \tag{A.24}$$

$$= \pi \int_{\frac{1}{\eta}}^\infty d\rho \prod_\beta \sum_{n_\beta} e^{-2\pi\frac{(r^\beta_{nm}-r^\beta)}{iL}n_\beta - \pi^2 n_\beta^2 \rho^2}. \tag{A.25}$$

In this form **B** will converge quickly. There is a small problem with the $n_\beta = 0$ term, but we may show that $\partial_\alpha\partial_\beta$ of this term is zero. Therefore if we let the $n_\beta = 0$ term be removed from the sum and referred to as **D**, we may rewrite **B** as below, where the prime on the sum indicates that we have removed the $n_\beta = 0$ term.

$$\mathbf{B} = \frac{\sqrt{\pi}}{2}\mathbf{D} + \pi \int_{\frac{1}{\eta}}^\infty d\rho \prod_\beta {\sum_{n_\beta}}' e^{-2\pi\frac{(r^\beta_{nm}-r^\beta)}{iL}n_\beta - \pi^2 n_\beta^2 \rho^2} \tag{A.26}$$

$$= \frac{\sqrt{\pi}}{2}\mathbf{D} + \int_{\frac{1}{\eta}}^\infty d\rho {\sum_{\vec{G}}}' e^{-2\pi\frac{(\vec{r}_{nm}-\vec{r})\cdot\vec{G}}{iL} - \pi^2 G^2 \rho^2}, \tag{A.27}$$

where we have used the general definition of a lattice vector, given in equation A.12.

Now if we make use the definition of the complementary error function, as in equation A.28, we may simplify our expression for **B** in equation A.27 even more.

$$\mathrm{Erfc}(X) = \frac{2}{\sqrt{\pi}} \int_X^\infty e^{-t^2} dt \tag{A.28}$$

and defining,

$$l = \pi|G|\rho \tag{A.29}$$

$$N = \frac{\pi|G|}{\eta}. \tag{A.30}$$

Now **B** may be written as:

$$\mathbf{B} = \frac{\sqrt{\pi}}{2}\mathbf{D} + \frac{\sqrt{\pi}}{2}\sum_{\vec{G}}{}' \frac{e^{2\pi i\frac{(\vec{r}_{nm}-\vec{r})\cdot\vec{G}}{L}}}{|G|}\mathrm{Erfc}\left(\frac{\pi|G|}{\eta}\right). \tag{A.31}$$

Returning to equation A.15, we see that **A** may be written,

$$\mathbf{A} = \int_\eta^\infty d\rho e^{-\frac{\rho^2}{L^2}(\vec{r}_{nm}-\vec{r})^2}\prod_{\alpha}\sum_{n_\alpha} e^{-\rho^2\left[2n_\alpha\frac{(\vec{r}^\alpha_{nm}-r^\alpha)}{l}+n_\alpha{}^2\right]} \tag{A.32}$$

$$= \frac{\sqrt{\pi}}{2}\sum_{\vec{G}}\frac{\mathrm{Erfc}(\eta\left|\frac{(\vec{r}_{mn}-\vec{r})}{L}+|G|\right|)}{\left|\frac{(\vec{r}_{mn}-\vec{r})}{L}+|G|\right|}. \tag{A.33}$$

Now if we substitute eqns A.33 and A.31 into eqn A.15 we have

$$\frac{1}{|\vec{r}_{nm}+\vec{G}-\vec{r}|} = \frac{2}{\sqrt{\pi}La}\left[\frac{\sqrt{\pi}}{2}\sum_{\vec{G}}\frac{\mathrm{Erfc}(\eta\left|\frac{(\vec{r}_{mn}-\vec{r})}{L}+|G|\right|)}{\left|\frac{(\vec{r}_{mn}-\vec{r})}{L}+|G|\right|}+\right.$$
$$\left.\frac{\sqrt{\pi}}{2}\mathbf{D}+\frac{\sqrt{\pi}}{2}\sum_{\vec{G}}{}'\frac{e^{2\pi i\frac{(\vec{r}_{nm}-\vec{r})\cdot\vec{G}}{L}}}{|G|}\mathrm{Erfc}\left(\frac{\pi|G|}{\eta}\right)\right] \tag{A.34}$$

$$= \frac{1}{La}\left[\mathbf{D}+\sum_{\vec{G}}{}'\frac{e^{2\pi i\frac{(\vec{r}_{nm}-\vec{r})\cdot\vec{G}}{L}}}{|G|}+\sum_{\vec{G}}\frac{\mathrm{Erfc}(\eta\left|\frac{(\vec{r}_{mn}-\vec{r})}{L}+|G|\right|)}{\left|\frac{(\vec{r}_{mn}-\vec{r})}{L}+|G|\right|}\right] \tag{A.35}$$

Further substituting eqn. A.35 into eqn. A.5 we arrive at

$$\mathcal{W}^{\alpha\beta}\left(\frac{\vec{r}_{nm}}{a}\right) = \frac{a^3}{La}\lim_{\vec{r}\to 0}\frac{\partial}{\partial r_\alpha}\frac{\partial}{\partial r_\beta}\left[\mathbf{D}+\sum_{\vec{G}}{}'\frac{e^{2\pi i\frac{(\vec{r}_{nm}-\vec{r})\cdot\vec{G}}{L}}}{|G|}+\right.$$
$$\left.\sum_{\vec{G}}\frac{\mathrm{Erfc}(\eta\left|\frac{(\vec{r}_{mn}-\vec{r})}{L}+|G|\right|)}{\left|\frac{(\vec{r}_{mn}-\vec{r})}{L}+|G|\right|}\right]. \tag{A.36}$$

We must be careful to remember that we have rescaled $\vec{r}$ so that,

$$\frac{\partial}{\partial r_\alpha} = \frac{\partial}{a\partial x_\alpha}$$

As well we must remember that the partial derivative of **D** will be zero so we may write

$$W^{\alpha\beta}\left(\frac{\vec{r}_{nm}}{a}\right) = \lim_{\vec{r}\to 0} L^{-1}\frac{\partial}{\partial x_\alpha}\frac{\partial}{\partial x_\beta}\left[\sum_{\vec{G}}{}' \frac{e^{2\pi i\frac{(\vec{r}_{nm}-\vec{r})\cdot\vec{G}}{L}}}{|G|}\mathrm{Erfc}\left(\frac{\pi|G|}{\eta}\right) + \sum_{\vec{G}} \frac{\mathrm{Erfc}\left(\eta\left|\frac{(\vec{r}_{nm}-\vec{r})}{L}+|G|\right|\right)}{\left|\frac{(\vec{r}_{nm}-\vec{r})}{L}+|G|\right|}.\right] \tag{A.37}$$

This is a form that we can deal with relatively easily, using the mathematical program **MATHEMATICA**. Using W as given in eqn A.37 we may write the Hamiltonian quite simply as,

$$\mathcal{H} = \frac{\mu_{\mathrm{eff}}^2}{2a^3}\frac{N}{L^2}\left[\mathrm{C}a^3 + \sum_{n,m}{}' \sigma_n^\alpha W^{\alpha\beta}(x_{nm})\,\sigma_m^\beta\right]. \tag{A.38}$$

We may calculate the energy per site for an L by L lattice, E(L) as

$$\frac{\mathcal{H}}{N} = \frac{\mu_{\mathrm{eff}}^2}{a^3}\frac{E(L)}{L^2} \tag{A.39}$$

$$E(L) = \frac{1}{2}\left[\mathrm{C}a^3 + \sum_{n,m}{}' \sigma_n^\alpha W^{\alpha\beta}(x_{nm})\,\sigma_m^\beta\right], \tag{A.40}$$

and define an effective field at dipole n in direction α as H_n^α, where

$$H_n^\alpha = \sum_{m=1}^{L^2} W^{\alpha\beta}(x_{nm})\,\sigma_m^\beta. \tag{A.41}$$

Writing the energy in terms of the effective fields gives us

$$E(L) = \frac{1}{2}\left[\mathrm{C}a^3 + \sum_{n,m}{}' \sigma_n^\alpha H_n^\alpha\right]. \tag{A.42}$$

Appendix B

The Program

```
Program ewald
IMPLICIT  none
Integer n, l,  ld, lm1, ldml, l2s
Integer nummc, numint, numruns, time
Character*80 wf, gf,outfile,spinin,spinout
Real*8  tfrom, tto, tstep, temp
parameter( n = 6   )          ! What size lattice 2^n
parameter( tfrom   = 2.38  )  ! starting temperature
parameter(  tto    = 2.42  )  ! final temperature
parameter( tstep   = 0.01  )
parameter( nummc   = 5     )  ! number of MC steps between data taking
parameter( numint  = 2500  )  ! number of inital Monte Carlo steps
parameter( numruns = 4000 )   ! number of runs of "nummc" MC steps
Real*8  ising , Jex
parameter( Jex = 0.0)
parameter(wf='W64.dat')
parameter(gf='energy')
parameter( outfile  = '64x64.dat.3' )
parameter( spinin   = '64x64.spins' )
parameter( spinout  = '64x64.spins.3'  )
```

```
      parameter( l = 2**n )
      parameter( ld = l*l )
      parameter( l2s = (l+2)**2 )
      parameter( lm1 = l-1 )
      parameter( ldml = ld - l )
      Real*8      h(ld),w4(ld), w2(ld),w(ld), Ham
      Integer spin(l2s), inner(ld), place
      Real  RANDOM
      Integer Iseed, i, j
      Integer init , site,run
      Integer flip
      Real*8  energy, order, toto, tote,tote2,toto2 , deltae , deltao
      Real*8  gsener, zero
      REAL*8 Change0
      Integer group
      parameter( group = 16 )
      Character*1 line(0:1)
c-------------------------------------------------------------
      CALL GetInner( inner, l, ld  )
      CALL GetSeed( Iseed )
      CALL RCARGO( Iseed )
      Write(6,*)'The Random Seed Was ', Iseed
c*****************************
c*** INITIALIZE THE SYSTEM ***
c*****************************
      CALL Initialize( inner , spinin, spin, ld,l2s, n, group )
```

```
        CALL SetBorder( spin, l2s, l )
        CALL Draw( spin, l2s, l, line )
c*****************************
c*** READ IN THE W FILE    ***
c*****************************
        Open( 17, file = Wf, status = "OLD" )
        DO i = 1, ld
          Read(17,*)w(i)
          w2(i) = 2.0*w(i)
          w4(ld +1-i) = 4.0*w(i)
        ENDDO
c*********************************************
c*** READ IN THE GROUNDSTATE ENERGY FILE    ***
c*********************************************
        Open( 17, file = gf, status = "OLD" )
        DO i = 1, n-1
          Read(17,*)zero, gsener
        ENDDO
c*************************************************************
c*****   START OF THE BIG TEMPERATURE LOOP ********************
c*************************************************************
        DO temp = tfrom,tto,tstep
          Call CalculateH( inner, h, spin, w2, ld,l2s,lm1, n )
c*****************************
c*** EQUILIBRATE THE SYSTEM ***
c*****************************
```

```
          DO init = 1, numint
            DO j = 1,ld
              site =  INT( RANDOM() * ld ) + 1
              place = inner( site )
              ising=2.00*spin(place)*Jex*(spin(place+l+2)+spin(place-l-2)+
     &                                    spin(place+1)  +spin(place-1))
              Ham =  2.00*spin(place)*h(site) - ising
              IF(( Ham.le. 0.0 ).or.(RANDOM().lt.dexp( -Ham/temp)))THEN
                spin( place ) = -1*spin(place)
                CALL UpDateField(h,w4,site,spin(place),n,l,ld,lm1)
              ENDIF
            ENDDO
            CALL SetBorder( spin, l2s, l )
          ENDDO     ! End of the initialization
c*****************************
c*** START REAL MONTE CARLO ***
c*****************************
          toto  = 0.0
          tote  = 0.0
          toto2 = 0.0
          tote2 = 0.0
          deltae = 0.0
          deltao = 0.0
          flip = 0
          CALL Collect_Data(inner,spin,h,Jex,l,ld,l2s,energy,order,zero,n)
          DO run = 1, numruns
```

```
      DO time = 1, nummc
        DO j = 1,ld
          site = INT( RANDOM() * ld ) + 1
          place = inner( site )
          ising=2.*spin(place)*Jex*(spin(place+l+2)+spin(place-l-2)+
     &                              spin(place+1)  +spin(place-1))
          Ham =  2.00*spin(place)*h(site) - ising
          IF(( Ham.le.0.0).or.(RANDOM().le.dexp(-Ham/temp)))THEN
            flip = flip + 1
            spin( place ) = -1*spin(place)
            deltae = deltae + Ham
            deltao = deltao + ChangeO( site, spin(place ), n )
            CALL UpDateField(h,w4,site,spin(place),n,l,ld,lm1)
            CALL SetBorder( spin, l2s, l )
          ENDIF
        ENDDO
      ENDDO       ! End of the time loop
      order  =  order  + deltao
      energy = energy  + deltae
      tote   = tote    + energy
      toto   = toto    + ABS( order )
      tote2  = tote2   + (energy)**2
      toto2  = toto2   + (order)**2
      deltae = 0.0
      deltao = 0.0
    ENDDO             ! End of the number of runs
```

```
          CALL OutputData(outfile,1,ld,temp,Jex, tote,toto,tote2,
     &                    toto2,flip,numruns)
          CALL Write_Spins(inner,spin,group,ld,l2s,spinout,temp)
        ENDDO                   ! End of the number of temperatures
        STOP "Hey man I'm finished"
END
        Subroutine CalculateH(order,h,spin,w2,ld,l2s,lm1,n)
        Integer ld, lm1, n, spin(l2s )
        Integer order(ld)
        Real*8 h(ld),  w2( ld )
        Integer i, j, si, sj, kw
c*****************************
c*** CALCULATE THE H MATRIX ***
c*****************************
C$DOACROSS LOCAL( j, i, si , sj, kw ) , SHARE( h, spin, w2 )
        DO j = 1,ld
          si = iand(j-1,lm1 )-1
          sj = rshift(j-1,n)
          h(j) = 0.0
          DO i=1,ld
            kw=iand(si+i,lm1)+lshift(iand(sj+rshift(i-1,n),lm1),n)+1
            kw = order(kw)
            h(j)=h(j)+spin(kw)*w2(i)
          ENDDO
        ENDDO
        RETURN
```

```
        END
        Function ChangeO( site, spin,n )
        Integer site , spin , n
        Real*8  ChangeO
        ChangeO  = 2.00 * ((-1.0)**(site))*spin
        Return
        End
        Function ChangeE( spin, h)
        Real*8 h, ChangeE
        Integer spin
        ChangeE = 2.00 * spin*( h )
        return
        End
        Subroutine Collect_Data(inner,spin,h,Jex,l,ld,l2s,energy,
     &                                  order,zero,n)
c*************************************************************************
c This routine takes a spin configuration and the resepctive fields and
c calculates the energy and the order parameter.  It then corrects the
c       energy so that the groundstate energy is zero
c       ( therefore the varible zero has as its value
c the groundstate energy for a lattice of that size
c       with no self interaction included)
c*************************************************************************
        Integer l, ld, n,l2s
        Integer spin(l2s)
        Integer inner(ld), kw
```

```
      Real*8 h(ld)
      Real*8 energy, order, zero, ising, Jex
      energy = 0.0
      order = 0.0
      DO i = 1, ld
        kw = inner(i)
        ising=Jex*(spin(kw+l+2)+spin(kw-l-2)+spin(kw+1)+spin(kw-1))
        energy = energy - spin(kw)*( h(i)/2.0 - ising/2.0 )
        order  =  order + ((-1.0)**(i))*spin(kw)
      ENDDO
      energy = energy - zero*float(ld)
      Return
      END
      Subroutine GetInner( order, l, ld )
c     Get the location of all interior sites
      IMPLICIT NONE
      Integer l,ld
      Integer order( ld)
      Integer j, count , ij , i
      count = 0
      DO i = 1, l
        DO j = 2, l+1
          ij =  i * (l+2) + j
          count = count + 1
          order( count ) = ij
        ENDDO
```

```
        ENDDO
        RETURN
        END
        SUBROUTINE GetSeed( ix )
        integer ix
        Real x
        x = SECNDS( 0.00 )
        ix = INT ( x )
        ix = and( ix, 8191 )
DO WHILE( ix .lt. 10000000 )
          ix = ix * 7
ENDDO
        ix = or( ix, 1 )
        Return
        End
        Subroutine Initialize(inner,spinin,spin,ld,12s,n,group)
        Integer ld, n, 12s
        Integer spin( 12s ), inner(ld)
        Character*50 spinin
        Integer kw, group
        Integer i, number, j
        IF (spinin .eq. "groundstate" ) THEN
          DO i =1, ld
            kw = inner( i )
            spin(kw) = (-1)**(i)
          ENDDO
```

```
      ELSEIF (spinin .eq. "random" ) THEN
        DO i =1, ld
          kw  = inner(i)
          spin(kw) = (-1)**(2* INT( RANDOM()+.5 ))
        ENDDO
      ELSE
        Open( 14, file = spinin, status ="OLD" )
        DO i = 0, ld/group
          READ( 14,300)number
          DO j=1,group
            IF( j+i*group .le. ld ) THEN
              kw  =  inner( j + i*group )
              spin( kw) = (2*ibits( number, j, 1 )-1)
            ENDIF
          ENDDO
        ENDDO
300     format( Z10.2 )
        CLOSE( 14 )
      ENDIF
      Return
      END
      Subroutine OutputData(out,l,ld,temp,Jex,tote,toto,
     &                              tote2,toto2,flip,number)
c  In this routine we calculate the specific heat (spht) and
c  susceptibility (sucp) and write them out to the output file,
c  appropriatly named "out".  We also output the average energy (avee)
```

```
c  and the average of the absolute value of the order parameter (aveo).
c  This subroutine also writes out the temp of the run,
c  the size of the lattice (l), and the number of data points used
c  to create the averages (number).  We also print out the number
c  of spin flips that have taken place.
      Integer l, ld, number,flip
      Real*8 temp, tote, toto, tote2, toto2, Jex
      Real*8 spht, susp, avee, aveo
      Character*30 out
      Open( 10, file = out, status="Unknown", access="append" )
      spht=(1.0/ld)*(tote2/float(number)-(tote/float(number))**2)/temp**2
      susp=(1.0/ld)*(toto2/float(number)-(toto/float(number))**2)/temp**2
      avee = tote/float(number*ld)
      aveo = toto/float(number*ld)
      Write( 10,100)temp, Jex
      Write( 10,101) l,number
      Write( 10,102) avee, aveo
      Write( 10,103) spht, susp
      Write( 10,104)flip
      Write(10,*)' '
      Write(10,*)'---------------------------------------'
100   format(5x,'Temperature...',f6.2,7x,'Jex= ',f9.5 )
101   format(5x,'L= ',i3,7x ,'Number of data...',i10)
102   format(9x,'Average Energy.',f20.9,5x,'Average Order P.',f20.9)
103   format(9x,'Specific Heat. ',f20.7,5x,'Susceptibility..',f20.7)
104   format(9x,'Number of spin flips ', i8 )
```

```
      CLOSE(10)
      Return
      END
      Subroutine SetBorder( lat1, ld, l )
c  This is a cool subroutine that caused a lot of problems.  It takes the
c  bottom row of the lattice we want and moves it in to the top row of the
c  lattice we have.  It does similar things to the top, left, and right, row
c  or column.
      Integer ld,l
      Integer lat1( ld )
      Integer i, count, ij, j , site, one
      data one/ 1/
      DO  i=0,1
        count = (1-i)*( l+2)*l + 1 + i*(l+2)
        DO  j = 1,l
          site = count + j
          ij = i*(l+1)*(l+2) + j + 1
          lat1( ij ) = lat1( site )
        ENDDO
      ENDDO
      DO  i = 0,l+1
        count = i*(l+2) + 2
        DO j =0,1
          site = count + j*(l-1)
          ij = i*(l+2) + 1+(1-j)*(l+1)
          lat1( ij ) = lat1( site )
```

```
          ENDDO
        ENDDO
        RETURN
        END
        Subroutine UpDateField(h,w4,site,spin,n,l,ld,lm1)
c  This is probably the routine that takes up the most time
c  during a run. It updates the fields at each lattice point,
c  h(i), given that the spin at lattice point "site" has flipped
c  such that it is now in the state "spin".  The varible "w4
c  contains "4.0 * w" in an inverted order.  We calculate the
c  varible "kw" in order to
c  update the fields in the proper order relative to "site" and w4(i).
        Integer n,l,  ld, lm1, site
        Real*8 h(ld), w4(ld)
        Integer spin
        Integer  si, sj, kw ,i
        si = iand(site-1,lm1 )
        sj = ibits(site-1,n,n)+1
C$DOACROSS LOCAL( i, kw ), SHARE( si, sj, ss, h, w4 )
        DO i= 1, ld
          kw = iand(si+i,lm1)+l*(iand(sj+ibits(i-1,n,n), lm1))+1
          h(kw)=h(kw)+spin*w4(i)
        ENDDO
        RETURN
        END
        Subroutine Write_Spins(order,spin,group,ld,lp2,spinout,temp)
```

```
c  In this routine we take "group" spins and create a binary
c  number from them.  If say spin(1) is -1 we make bit 1
c  in our binary number 0, if spin(10) is 1 then we
c  make bit 10 in our binary number 1.  We then write out this
c  binary number in hexadecimal form in order to save space in
c  the file.  This way we may write 16 states as 5 alpha-numerics.
        Integer ld, group, 12s
        Integer spin(lp2), order(ld)
        Character*50 spinout
        Integer i, j
        Real*8 temp
        Open( 19, file = spinout, status='Unknown', access='append' )
        Write(19,*)'Temp ', temp
        DO i = 0, INT( ld/group )
          number = 0
          DO j=1,group
            IF( j+i*group .le. ld ) THEN
              kw = order( j+i*group)
              number = number + ((spin( kw )+1)/2)*2**(j)
            ENDIF
          ENDDO
          Write(19,300)number
 300      format( Z10.2 )
        ENDDO
        CLOSE(19)
        RETURN
```

```
END
```

Acknowledgements

I would like to offer my sincerest thanks to Dr. J. P. Whitehead, without whom this thesis would not be. His teaching, patience, enthusiasm and critical eye, although at moments not fully appreciated, have made this work more enjoyable and of much higher quality than would have been the case without his participation. As well, I wish to thank Dr. K. De'Bell, who contributed significantly to the completion of this work, for his guidance and for allowing me to the opportunity to visit Trent University, to work with him and his colleagues.

As well I would like to thank a number of people who have given of their time and knowledge. In particular I would like to thank Dr. Naeem Jan for help with the Monte Carlo simulation work, and Dr. B. Birgensen and Haung-Jian Xu for sharing some of their initial results on the data collapse in dipolar systems. I would further like to offer special thanks to Michael Robinson, who contributed to the calculation of the phase diagrams, by running many simulations for me during my stay at Trent University.

I would like to thank the Oceanography Group in the Department of Physics at Memorial University of Newfoundland for the use of their Silicon Graphics workstation, *Crosby*. The larger systems used in this study were simulated using a parallel version of our program on this six processor workstation.

For financial support I would like to thank the Natural Science and Engineering Research Council of Canada (NSERC) for their generous support, as well as, Dr. J.P. Whitehead, Dr. K. De'Bell and Memorial University of Newfoundland.

Bibliography

[1] Robert J. Cava. Superconductors beyond 1-2-3. *Scientific American*, pages 42–49, August 1990.

[2] A. B. MacIsaac, J. P. Whitehead, K. De'Bell, and K. Sowmya Natayanan. Monte Carlo study of two-dimensional Ising dipolar antiferromagnets as a model for rare-earth ordering in the R-BA-Cu-O compounds (R = rare earth). *Phys. Rev. B.*, **46**:6387 6394, 1992.

[3] J.P. Whitehead, K. De'Bell, and A.B. MacIsaac. Magnetism in superconducting compounds. Preprint, 1992.

[4] Robert M. Hazen. Perovskites. *Scientific American*, pages 74–81, June 1988.

[5] M. B. Maple, Y. Dalichaouch, J. M. Ferreira, R. R. Hake, B. W. Lee, J. J. Neumeier, M. S. Torikachvili, K. N. Yang, and H. Zhou. $RBa_2Cu_3O_{7-\delta}$ (R=rare earth) high-T_c magnetic superconductors. *Physica B*, **148**:155–162, 1987.

[6] O. Fischer and M.B. Maple, editors. *Superconductivity in ternary compounds Vol. I and II.* Springer-Verlag, 1982.

[7] R. N. Shelton, R. W. McCallum, M. A. Damento, K. A. Gschneidner Jr., H. C. Ku, H. D. Yang, J. W. Lynn, W.-H. Li, and Q. Li. Effects of crystal anisotropy on magnetization and magnetic order in superconducting $RBa_2Cu_3O_{7-\delta}$. *Physica B*, **148**:285 288, 1987.

[8] J. W. Lynn, W-H. Li, Q. Li, H. C. Ku, H. D. Yang, and R. N. Shelton. Magnetic fluctuations and two-dimensional ordering in $ErBa_2Cu_3O_7$. *Phy. Rev. B*, **36**:2374, 1987.

[9] D. McK. Paul, H. A. Mook, L. A. Boatner, B. C. Sales, J. O. Ramey, and L. Cussen. Magnetic ordering in the high-temperature superconductor $ErBa_2Cu_3O_{7-\delta}$. *Phys. Rev. B*, **39**:4291, 1988.

[10] T. Chattopadhyay, P. J. Brown, B. C. Sales, L. A.Boatner, H. A. Mook, and H. Maletta. Single-crystal neutron-diffraction investigation of the magnetic ordering of the high-temperature superconductor $ErBa_2Cu_3O_{7-\delta}$. *Phys. Rev. B*, **40**:2624, 1989.

[11] J. W. Lynn and W-H. Li. Magnetic order in $RBa_2Cu_3O_{6+x}$. *J. Appl. Phys.*, **64**:6065, 1988.

[12] J. W. Lynn, T. W. Clinton, W-H. Li, R. W. Erwin, J. Z. Liu, K. Vandervoort, and R. N. Shelton. 2d and 3d magnetic behavior of Er in $ErBa_2Cu_3O_7$. *Phys. Rev. Lett.*, **63**:2606, 1989.

[13] S. E. Brown, J. D. Thompson, J. O. Willis, R. M. Aikin, E. Zirngiebl, J. L. Smith, Z. Fisk, and R. B. Schwarz. Magnetic and superconducting properties of $RBa_2Cu_3O_x$. *Phys. Rev. B*, **36**:2298, 1987.

[14] S. Simizu, S. A. Friedberg, E.A. Hayri, and M. Greenblatt. Low-dimensional magnetism in the high-Tc superconductor $LBa_2Cu_3O_{7-\delta}$ (L=Gd,Ho,Er):heat-capacity study. *Phys. Rev. B*, **36**:7129, 1987.

[15] Y. Nakazawa, M. Ishikawa, and T. Takabatake. Low-temperature specific heat of orthorhombic and tetragonal phases of $Ba_2(RE)Cu_3O_{7-\delta}$ (RE=Gd,Dy,Ho,Er and

Tm). *Physica*, **148B**:404, 1987.

[16] B. W. Lee, J. M. Ferreira, Y. Dalichaouch, M. S. Torikachvili, K. N. Yang, and M. B. Maple. Long-range magnetic ordering in the high T_c superconductors $RBa_2Cu_3O_{7-\delta}$ (R = Nd, Sm, Gd, Dy and Er). *Phys. Rev. B.*, **37**:2368, 1988.

[17] Neil W. Ashcroft and N. David Mermin. *Solid State Physics*. Holt, Rinehart and Winston, 1976.

[18] A. I. Goldman, B. X. Yang, J. Tranquada, J. E. Crow, and Chan-Soo Jee. Antiferromagnetic order in $DyBa_2Cu_3O_7$. *Phys. Rev. B*, **36**:7234, 1987.

[19] P. Fischer, K. Kakurai, M. Steiner, K. N. Clausen, B. Lebech, P. Brüesch, and P. Unternährer. Neutron diffraction evidence for 3-D long-range antiferromagetic ordering in $DyBa_2Cu_3O_{6.95}$ and for antiferomagnetic correlations in $HoBa_2Cu_3O_{6.8}$. *Physica C*, **152**:145-152, 1988.

[20] T. W. Clinton and J. W. Lynn. Magnetic order of Dy in $DyBa_2Cu_3O_7$. *J. Appl. Phys*, **70**:5751, 1991.

[21] J.C. Ho, P. H. Hor, R. L. Meng, C. W. Chu, and C. Y. Huang. Calormetric evidence of antiferromagnetism in $GdBa_2Cu_3O_{6+\delta}$. *Solid State Communications*, **63**:711–712, 1987.

[22] K. Kadowaki, H. P. van der Meulen, J. C. P. Klaasse, M. van Sprang, J. Q. A. Koster, L. W. Roeland, F. R. de Boer, Y. K. Huang, and A. A. Menovsky. Coexistance of magnetism and high-Tc superconductivity in $GdBa_2Cu_3O_7$. *Physica*, **145B**:260, 1987.

[23] D. McK. Paul, H. A. Mook, A. W. Hewat, B. C. Sales, L. A. Boatner, Thompson J,

R, and Mark Mostoller. Magnetic ordering in the high-temperature superconductor $GdBa_2Cu_3O_7$. *Phys. Rev. B*, **37**:2341, 1988.

[24] K. De'Bell and J.P. Whitehead. The dipole-dipole contribution to the magnetic propagator in the $REBa_2Cu_3O_{7-\delta}$ compounds. *J. Phys.:Condens. Matter*, **3**:2431 2439, 1991.

[25] Joshua Felsteiner. Nature of the magnetic order of Gd in superconducting and nonsuperconducting $GdBa_2Cu_3O_{7-\delta}$. *Phys. Rev. B*, **39**:7248, 1989.

[26] C. Meyer, H-J Bornemann, H. Schmidt, R. Ahrens, D. Ewert, B. Renker, and G. Czjzek. Magnetism and superconductivity in $GdBa_2Cu_3O_{7-x}$. *J. Phys. F:Met. Phys.*, **17**:L345, 1987.

[27] H. Eugene Stanley. *Introduction to Phase Transitions and Critical Phenomena*. Oxford University Press, 1971.

[28] J. van den Berg, C. J. van der Beek, P. H. Kes, J. A. Mydosh, G. L. Niewenuys, and L. J. de Jongh. Superconductivity and 2-dimensional magnetism in orthorhombic and tetragonal $GdBa_2Cu_3O_{7-\delta}$. *Solid State Comm.*, **64**:699, 1987.

[29] J. M. Ferreira, B. W. Lee, Y. Dalichaouch, M. S. Torikachvili, K. N. Yang, and M. B. Maple. Low-temperature specific heat of the the high-Tc superconductors $La_{1.8}Sr_{0.2}CuO_{4-\delta}$ and $RBa_2Cu_3O_{7-\delta}$ (R=Y, Eu, Ho, Tm and Yb). *Phys. Rev. B.*, **37**:1580, 1988.

[30] H. Zhang, J. W. Lynn, W-H Li, T. W. Clinton, and D. E. Morris. Two- and three-dimensional magnetic order of the rare-earth ions in $RBa_2Cu_4O_8$. *Phys. Rev. B*, **41**:11229, 1990.

[31] Jens Als-Nielsen. Neutron scattering and spatial correlation near the critical point. In C. Domb and M. S. Green, editors, *Phase Transitions and Critical Phenomena*, volume 5a, pages 88 -164. Academic Press, 1976.

[32] F. Nakamura, T. Fukuda, M. Akisue, T. Uchiyama, Y. Ochiai, A. Tominaga, and Y. Narahara. The gadolinium ordering in superconducting and non-superconducting $Gd_xY_{1-x}Ba_2Cu_3O_y$ compounds. *Solid State Communications*, **65**:1339–1341, 1988.

[33] Zhao Guo-meng, Wang Rui-lan, and Dong Zi-wen. Magnetism and superconductivity in $Ba_2GdCu_3O_{7-\delta}$. *Solid State Communications*, **65**:1395–1398, 1988.

[34] B. D. Dunlap, M. Slaski, Z. Sungaila, D. G. Hinks, K. Zhang, C. Segre, S. K. Malik, and E. E. Alp. Magnetic ordering of Gd and Cu in the superconducting and nonsuperconducting $GdBa_2Cu_3O_{7-\delta}$. *Phys. Rev. B*, **37**:592, 1988.

[35] K. Binder. Introduction:Theory and "technical" aspects of Monte Carlo simulations. In K. Binder, editor, *Monte Carlo Methods in Statistical Physics*, pages 1–46. Springer-Verlag, 1979.

[36] N. Metroplis, A. W. Rosenbluth, M. N. Rosenbluth, A. H. Teller, and E. Teller. *J. Chem. Phys.*, **27**:1087, 1953.

[37] R. J. Elliot. *Magnetism*, page 396. Academic, 1965.

[38] R. M. White and T. H. Geballe. *Long range order in Solids*. Academic, 1979.

[39] K. Binder. Monte carlo investigations of phase transtitions and critical phenomena. In C. Domb and M. S. Green, editors, *Phase Transitions and Critical Phenomena*, volume 5b, pages 37 -44. Academic Press, 1976.

[40] Stephen G. Brush. *Statistical physics and the atomic theory of matter, from Boyle and Newton to Landau and Onsager*. Princeon University Press, 1983.

[41] R. Kretschmer and K. Binder. Ordering and phase transitions in Ising systems with competing short range and dipolar interactions. *Z. Physik B.*, 34:375 392, 1979.

[42] J. P. Valleau. The problem of coulombic forces in computer simulation. Proceedings No. 9, National Resource for Computation in Chemistry. Lawerence Berkeley Laboratory, University of California.

[43] This method of dealing with periodic boundary conditions was related to the author by Naeem Jan, who attributed the original idea to D. Stauffer.

[44] The authors would like to thank the Oceanography group at Memorial University of Newfoundland for the use of their Silicon Graphics workstation, *Crosby*.

[45] P. N. Vorontsov-Velýaminov and I. A. Favorskii. Phase transition in the Ising model with a pure dipole interaction. *Sov. Phys. Solid State*, 15:1937 1941, 1974.

[46] Haung-Jian Xu, personal communication.

[47] Huang-Jian Xu, Birger Bergersen, and Zoltán Rácz. Monte Carlo simulations on Ising dipoles:finite size scaling and logarithmic corrections. *J. Phys.: Condens. Matter*, 4:2035–2042, 1992.

[48] Huang-Jian Xu, Birger Bergersen, F. Niedermayer, and Z. Rácz. Ordering of ising dipoles. *J. Phys.: Condens. Matter*, 3:4999 5012, 1991.

[49] A. P. Ramirez, L. F. Schneemeyer, and J. V. Waszczak. Specific heat near Tn in (Pr, Nd, Sm, Gd, and Dy)$Ba_2Cu_3O_7$: Evidence for spin-exchange-driven ordering. *Phys. Rev. B*, 36:7145, 1987.

[50] R. Kretschmer and K. Binder. Surface effects on phase transitions in ferroelectrics and dipolar magnets. *Phys. Rev. B.*, 20:1065–1076, 1979.